Quantitative Assessment of Magnetic Resonance Spectroscopy Data Reconstruction Methods: Region-of-Interest Averaging and Spectral Localization by Imaging

By

Sean Ellis
B.Sc., Brigham Young University, 2013

Submitted to the graduate degree program in Bioengineering and the Graduate Faculty of the University of Kansas in partial fulfillment of the requirements for the degree of Master of Science.

_____

Chair: In-Young Choi

_____

Co-Chair: Phil Lee

_____

Xinmai Yang

_____

Kenneth Fischer

Date Defended: 1 May 2019

The thesis committee for Sean Ellis certifies that this is the approved version of the following thesis:

Quantitative Assessment of Magnetic Resonance Spectroscopy Data Reconstruction Methods: Region-of-Interest Averaging and Spectral Localization by Imaging

_____

Chair: In-Young Choi

_____

Co-Chair: Phil Lee

Date Approved: 5 June 2019

Abstract

The aim of this dissertation was to compare two magnetic resonance spectroscopy (MRS) localization techniques: Fourier based region-of-interest (ROI) averaging, and the non-Fourier based spectral localization by imaging (SLIM). Unlike ROI-averaging, SLIM provides a technique for calculating the metabolite spectra of a compartmental region without the need for averaging voxels of spectral data to estimate that region. Because of this, SLIM has the potential to greatly reduce the acquisition time needed to acquire compartmental spectra.

SLIM was processed over multiple k-space sizes and over an assortment of brain regions and then these results were compared to their equivalent ROI-averaged regions. The assorted k-space sizes were used to demonstrate SLIM operating with different amounts of available data, which was used to compare the process to ROI-averaging. The results of this study validate SLIM as a valuable localization tool that will shorten scan times and improve accuracy in spectral localization.

The dissertation is divided into five main chapters: (1) Introduction, which addresses magnetic resonance background concepts and applications of MRS techniques; (2) Methods, which describes the processes involved in developing a programming pipeline designed to produce metabolite data for the localization techniques; (3) Results, which provides statistical measures of the localization methods; (4) Discussion, where comparisons were drawn from the datasets based on the results section; (5) Conclusions, which evaluates the thesis work and addresses possible research directions for the future.

Acknowledgments

I would like to thank Dr. In-Young Choi and Dr. Phil Lee for mentoring me and for their help and guidance on this thesis project for the past few years. I would also like to thank Dr. Peter Adany for his assistance in helping me learn the MATLAB scripting language, his knowledge and work in developing several essential components of the pipeline that I utilized in this thesis work. I would also like to thank my parents David and Andrea Ellis for their support over the years while developing this thesis. I couldn't have done this without the support of all these individuals.

Table of Contents

List of Figures

List of Tables

Glossary

B_0: The main (static) magnetic field (in T). For atoms that possess spin angular momentum, B_0 is used to produce the magnetization moment in the direction of B_0.

B_1: The magnetic field oscillating at the Larmor radio frequency produced by the transmitter (in T). The direction of the B_1 magnetic field is perpendicular to that of the B_0 field.

Cho: Choline / choline containing compounds. A vitamin-like essential nutrient that provides structural integrity and signaling roles in cell membranes and plays a role in cholinergic neurotransmission.

Cr: Creatine. A nitrogenous organic acid that serves a role in facilitating the recycling of adenosine triphosphate (ATP) in muscle and brain tissue.

CRLB: Cramér–Rao Lower Bound. The lower bound on the variance of any unbiased estimator. CRLB is used in LCModel to estimate the confidence that the model is correct and is expressed as the standard deviation value of the metabolite fit being estimated.

CSF: Cerebral spinal fluid. A clear, colorless fluid in the brain and spinal cord that provides mechanical and immunological protection to the brain inside the skull.

CSI: Chemical Shift Imaging. See also MRSI.

Echo: A signal produced by creating a phase coherence of the spins.

EMF: Electromotive force. Electric pressure that causes a current to flow in a circuit and is the source of the signal detected on receiver coils.

FID: Free induction decay. A damped oscillation of the observable NMR signal excited by a RF pulse. The object's FID can be detected by creating a change in the electromagnetic field, thereby inducing a current in receiver coils that are placed perpendicular to the primary magnetic field. The transverse magnetization is a function of time, which are given by:

$$M_x(t) = M_0 cos[(\omega_0 - \omega)t + \phi]e^{-t/T_2^*} \quad (1)$$

$$M_y(t) = M_0 sin[(\omega_0 - \omega)t + \phi]e^{-t/T_2^*} \quad (2)$$

where ϕ is the phase at $t = 0$, and $M_x(t)$ and $M_y(t)$ are the real and imaginary FID components respectively.

FOV: Field of view. The distance (in mm) over which an MR image is acquired or displayed.

FT: Fourier transformation. A mathematical function for converting a signal in the time domain s(t) to a complex number in the frequency domain s(ω) using the equation:

$$s(\omega) = \int_{-\infty}^{\infty} s(t)e^{-i\omega t}dt \quad (3)$$

while the inverse Fourier transformation for converting a signal in the frequency domain to a signal in the time domain is described using the equation:

$$s(t) = \frac{1}{2\pi}\int_{-\infty}^{\infty} s(\omega)e^{+i\omega t}d\omega \quad (4)$$

FWHM: Full width at half maximum. The width of a line shape at half of its maximum amplitude. Used for quantifying the spectral linewidth. Spectral peaks with a small FWHM are easy to resolve and reduce the chance of overlapping with other peaks.

GABA: gamma-Aminobutyric acid. The primary inhibitory neurotransmitter in the central nervous system.

GRE: Gradient echo. A signal generated at echo time by applying de-phasing and re-phasing gradients following a RF pulse. The gradient echo is a T_2^*-weighed signal.

IR: Inversion recovery. A pulse sequence utilizing a 180° excitation pulse. Inversion recovery sequences provide increased T1 contrast and can be used to selectively nullify tissue signals.

LCModel: Linear Combination of Model Spectra. A metabolite quantification program that estimates the individual contributions of metabolites in a spectra by using a basis set library of individual spectra and estimating the individual contributions of each metabolite to the overall spectra. Additionally, the program also applies a baseline correction to the spectra to account for signal drift.

mI: *Myo*-Inositol. A carbocyclic sugar that serves as the structural basis for several secondary messengers including gene expression, cytoskeleton assembly, and cell membrane potential maintenance.

MIDAS: Metabolite Imaging and Data Analysis System. A package of software programs for processing MRI and MRSI datasets. Included in this software package is MRSI Data reconstruction, B0 / Eddy Current Correction, lipid removal, spatial registration and ROI-averaged signal reconstruction.

MINT: Map INTegrated spectrum. A MIDAS program that estimates compartmental spectra by using ROI-averaging for the region(s). In this paper, MINT also refers to the ROI-averaged dataset that was produced by MIDAS in the results section.

MPRAGE: Magnetization Prepared Rapid Acquisition Gradient Echo. A fast 3D gradient echo pulse sequence with a T1 weighted dominance. MPRAGE is used to obtain an MRI with a high signal intensity by acquiring the echo during T1 relaxation.

MRI: Magnetic resonance imaging. A medical imaging technique that uses principles of nuclear magnetic resonance to generate an image whose signal reflects bulk properties of tissue. By applying a gradient of the magnetic field, spatial information about the object can be encoded as phase and frequency data, which can be used to reconstruct an image of the object.

MRS: Magnetic resonance spectroscopy. A technique for acquiring metabolic information in tissues. Magnetic resonance spectroscopy is acquired in the same way as MRI, except that spatial frequency gradients are not played during signal readout because frequency changes cannot be used for spatial encoding. Spectroscopic techniques can be either single voxel or multi-voxel.

MRSI: MR spectroscopic imaging, which is also known as chemical shift imaging (CSI). A multi-voxel MRS acquisition method utilizes phase encoding gradients applied in 1, 2, or 3 dimensions to segment larger stimulated volumes into multiple smaller voxels.

NAA: N-Acetyl aspartate. A derivative of aspartic acid found predominantly in neuronal cell bodies. NAA is commonly used as a marker for detecting neuronal damage.

NMR: Nuclear magnetic resonance. The process of recording the stimulated absorption and emission of RF energy from nuclei placed within a magnetic field. NMR typically refers to the physical phenomenon of nuclear resonance.

OVS: Outer volume saturation. A technique that uses spatially localized saturation bands to remove unwanted signal (e.g., Lipids).

PCr: Phosphocreatine. A phosphorylated creatine that recycles adenosine trisphosphate in the brain and muscles.

PRESS: Point resolved spectroscopy. A pulse sequence that utilizes three slice-selective RF-pulses (90° - 180° - 180°) and three orthogonal gradients (x, y, and z) to produce a spin echo at the region where the three planes intersect.

PSF: Point spread function. The point spread function describes the response of an imaging system to a point source or a point object.

RF Pulse: Radiofrequency pulse. A short burst of an electromagnetic wave oscillating at the radio frequency used to excite protons in a B_0 magnetic field.

ROI: Region of interest.

ROIS: ROI-averaged dataset produced by programs that were developed in-house. This dataset was developed using the same processes utilized by the in-house SLIM program to compare the two processes in a more direct manner.

SE: Spin echo. A signal generated at echo time by applying a RF pulse in addition to those used in GRE to eliminate phase shifts resulting from magnetic field inhomogeneities. The spin echo is a T2-weighted signal.

SLIM: Spectral Localization by Imaging. A spectral reconstruction technique for acquiring spectral data from arbitrary shapes by utilizing a non-Fourier over-determined system to solve for the reconstructed spectra. The arbitrary shaped compartments are obtained from an MRI using segmentation software and are customizable to obtain spectral reconstructions of any region of interest in the brain.

SNR: Signal-to-Noise Ratio. The ratio of the signal intensity to the baseline / residual noise level of the signal.

Spectroscopy: The study of the interactions between matter and electromagnetic radiation.

STEAM: Stimulated echo acquisition mode. A pulse sequence that utilizes three slice-selective RF-pulses (90° - 90° - 90°) concurrently with three orthogonal gradients (x, y, and z) to produce a spin echo at the region where the three planes intersect to produce a stimulated echo.

SVS: Single voxel spectroscopy. A spectroscopy acquisition method for acquiring the spectra from a single voxel using applied RF-pulses coupled with gradients in three orthogonal planes. The most common method of acquiring SVS is PRESS.

T_1: Longitudinal relaxation time constant (in seconds). Describes the return of longitudinal magnetization after a perturbation.

T_2: Transverse relaxation time constant (in seconds) for the decay/dephasing of transverse magnetization. T2 describes the rate of attenuation for the transverse magnetization signal.

T_2* : Apparent transverse relaxation time constant (in seconds) for the decay/dephasing of transverse magnetization. T_2* accounts for inhomogeneities of the main magnetic field, and is always shorter than T_2 as described by:

$$\frac{1}{T_2^*} = \frac{1}{T_2} + \frac{1}{T_{2i}} \tag{5}$$

where $1/T_{2i} = \gamma \Delta B_i$, and is the relaxation rate contribution caused by magnetic field inhomogeneities across a voxel.

TE: Echo time (in seconds). The time from the center of the excitation pulse to the center of the echo in seconds.

TI: Inversion time (in seconds). In inversion recovery pulse sequences, the TI is the time in seconds between the first 180° pulse and excitation pulse of the main sequence.

TR: Repetition time (in seconds). The length of time between corresponding consecutive points on a series of pulses and echoes. TR signifies the total amount of time a pulse cycle takes.

δ: Chemical shift (in ppm). A measure of the differences in resonance frequency of nuclei. Chemical shift is caused by differences in electron cloud distribution due to differences in their local molecular structure. Chemical shift is defined as

$$\delta = \frac{v - v_{ref}}{v_{ref}} \times 10^6 \quad (6)$$

where v and v_{ref} are the frequencies of the compound under investigation and of a reference compound, respectively.

γ: Gyromagnetic ratio (in rad T^{-1} s^{-1}). The ratio of a particle's magnetic moment to its angular momentum.

ϕ: Phase (in rad). The position of a point in time on a waveform cycle.

ω: Larmor frequency (in rad s^{-1}). The rate of precession of a particle possessing a magnetic moment in the presence of a magnetic field.

Chapter 1: Introduction

This report evaluates and characterizes an emerging advanced magnetic resonance spectroscopy (MRS) localization method: spectral localization by imaging (SLIM) based MRS. The SLIM localization method is evaluated in comparison with conventional Fourier transformation-based localization methods, with the report having a focus on data reconstruction and analysis strategies.

MRS imaging (MRSI) is a clinical and research imaging tool that can map the absolute concentrations of metabolites in living organs, including the brain. MRSI when combined with anatomical magnetic resonance imaging (MRI) can offer valuable information about the brain in an assortment of physiological states and for diseases in general. MRSI can be used to evaluate the effectiveness of a cancer treatment by examining the concentration of metabolites before and after treatment. It can be used to study how metabolic concentrations change over time or over the progression of a disease. The technique can enhance information gleaned from MRI by showing metabolic concentration differences in regions that would otherwise appear identical in anatomical MRI.

While MRSI has many valuable uses in medical and research fields, the technique has limitations that impede its widespread utilization. The prolonged scan time required for MRSI data acquisition can be quite long due to the relatively low concentration of endogenous brain chemicals. These concentrations, which can be $1/10^4$ the strength of the water signal in the brain, can result in significantly lower signal-to-noise ratios (SNR) and restricted spatial resolution. A low spatial resolution in MRSI obscures important spatial anatomical information by the point spread function effect, resulting from the truncated Fourier series representation

obtained by phase encoding. Similarly, a large voxel size is prone to substantial partial volume effects, requiring careful and difficult corrections for accurate quantification.

SLIM provides a solution that addresses some of limitations of MRSI techniques. SLIM takes advantage of structural information from MRI as a means of reducing the required phase-encoding steps needed to acquire MR spectra from homogeneous tissue compartments. Unlike MRSI, which utilizes a Fourier transformation, SLIM utilizes a non-Fourier, overdetermined linear system to reconstruct compartment-based spectra. Thus, the metabolic imaging team at KUMC has developed SLIM-based techniques and new data analysis strategies for acquiring localized spectra (Adany, Choi, & Lee, 2016; Lee, Adany, & Choi, 2017). Because SLIM reconstructs spectra through localization instead of voxel averaging, the technique resolves the partial volume effect and point spread function artifacts, requiring fewer signal acquisitions to derive spectra that represent the same region.

In this report, two region-of-interest (ROI) averaging methods were utilized: ROI averaging using the Metabolite Imaging and Data Analysis System (MIDAS) software suite and an in-house ROI-averaging program developed at KUMC. Although MIDAS is a well-established software suite that produces quality spectra outputs with ROI averaging, the in-house software that was utilized offered multiple advantages to the MIDAS software for this study. Using the in-house suite, spectral scale of the ROI averaged regions would be identical to the SLIM counterparts, allowing metabolic concentrations to be compared without the need of transforming them to ratios of creatine. In addition, most processing steps would be handled between SLIM and ROI averaging in an identical manner, including co-registration, lipid handling, and B_0-correction, enabling a more accurate representation of the differences between the two processing techniques.

The aim for this MS thesis is to evaluate SLIM over multiple k-space sizes and over an assortment of brain regions and then have these results compared to equivalent ROI-averaged regions. This study aims to validate SLIM as a valuable localization method that will shorten scan times and improve accuracy in spectral localization. To clarify the techniques that were used in the methods and results section later in the thesis, the following relevant concepts are described in the section below: Nuclear Magnetic Resonance (NMR), Magnetic Resonance Image (MRI), Magnetic Resonance Spectroscopic Imaging (MRSI), Quantification of MRS signals, Echo-Planar Spectroscopic Imaging (EPSI), and Spectral Localization by IMaging (SLIM).

Background Concepts

Nuclear Magnetic Resonance

Nuclear magnetic resonance (NMR) is a physical phenomenon where nuclei in a magnetic field emit an electromagnetic signal after being perturbed by a weak oscillating magnetic field. Nuclei have an intrinsic form of angular momentum known as nuclear spin, which produces a spin magnetic moment for the particle. Nuclei with an imbalance of protons and/or neutrons will have a non-zero dipole moment and will reside in discrete energy states determined by their spin angular momentum. These nuclei can transition between states by absorbing or emitting electromagnetic radiation in the 10-800 MHz energy range. While NMR is used to analyze compounds containing nitrogen, carbon, or phosphorus (Andrade et al., 2014; Lambert, Binsch, & Roberts, 1964; Park et al., 2014), studies performed on ^{1}H have been the most valuable due to the abundance of ^{1}H in water and organic tissue.

Due to the random alignment of protons in the absence of a magnetic field, the net dipole moment of ^{1}H protons is zero. In presence of a static magnetic field (B_0), a torque is exerted on the magnetic moment by the larger magnetic B_0 field, where the direction of the B_0 field by convention is chosen as the z-axis. The angular momentum L of all elementary particles is limited to discrete values, whose amplitude is given by:

$$L = \left(\frac{h}{2\pi}\right)\sqrt{I(I+1)}\ \text{J·s} \tag{7}$$

In this formula, I is the spin quantum number of the nucleus, and h is Planck's constant (6.626×10^{-34} J·s). The precession angle between μ and B_0 for elementary particles is given by:

$$\cos\theta = \frac{m}{\sqrt{I(I+1)}} \tag{8}$$

where m = +1/2 or -1/2 and θ yielding an angle of = 54.74° relative to the +z or -z axis. Nuclei of spin I = 1/2 are distributed on the surface of two cones and rotate about B_0 at the Larmor frequency. The small energy difference between the spin states will cause a small difference in the population of the two spin states. This creates a net magnetic moment vector in parallel with the B_0 field. This net magnetization is very weak, but this difference in population of these spin states of parallel to antiparallel nuclei can be increased by using a stronger B_0 field which increases the difference in energy between the two energy states and thus creates a larger signal. The nuclei's resonating frequency (ω_0) can be calculated using the Larmor equation:

$$\omega_0 = \gamma B_0 \qquad or \qquad v_0 = \left(\frac{\gamma}{2\pi}\right)B_0\ \text{Mhz} \tag{9}$$

where γ is the gyromagnetic ratio of a particle's magnetic moment to its angular momentum, and B_0 is the strength of the magnetic field. By applying a radiofrequency pulse at the right resonating frequency, the nuclei will emit a signal that can be captured on receiver coils to produce information about the chemical being observed in the magnetic field.

Magnetic Resonance Imaging

Magnetic resonance imaging (MRI) is a medical imaging technique that uses NMR techniques to form images of the organs in the body. This technique has been used in the field of medicine to identify white matter lesions in patients with multiple sclerosis, to locate brain tumors, and for visualizing other brain abnormalities. A typical MRI takes 5 minutes to acquire and is a regular component of a MR scanning session.

MRI acquires spatial information about the object of interest by using frequency and phase encoding to store spatial information into the signal. Since there is a direct relationship between magnetic field strength and the resonating frequency of nuclei, the expected resonance frequency can be changed by adjusting the static B_0 magnetic field. A small readout gradient of frequencies is applied to the B_0 field over a spatial area, which allows a single dimension of resonance data to be acquired instantaneously in a single RF pulse. Phase information can be acquired as a 2nd dimension by applying short magnetic field gradients between the readout gradients. This causes a small shift in phase by temporarily increasing the resonating frequency of the nuclei while the gradient is applied.

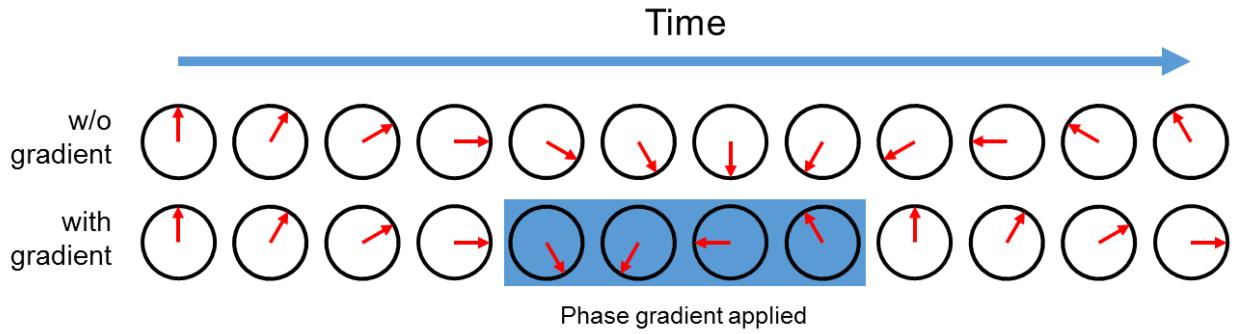

Figure 1: Phase encoding using a phase gradient pulse.
During the application of a phase gradient, the precession frequency is increased for the duration of the pulse. After removing the phase gradient, the precession frequency is restored to its original rate, but a change in phase has occurred which can be used to encode information into the signal.

MRI image contrast comes in the form of signal intensity that is caused by a couple of factors. The first factor is the concentration of the nuclei being excited in the first place. Both water and lipids have high concentrations of ^{1}H and will form most of the signal in a typical MRI. The second factor involves relaxation times that are affected by tissue properties. For example, nuclei in a liquid have long relaxation times compared to nuclei in lipids. Different tissue signals can be selectively suppressed or emphasized by adjusting pulse sequence timing, using spin echo refocusing pulses or using a gradient pulse echo.

Magnetic Resonance Spectroscopy

Magnetic resonance spectroscopy (MRS) is a spectroscopic technique used for observing local magnetic fields around nuclei. Given a strong magnetic field, the same nuclei on different compounds are observed to resonate at different frequencies, even between nuclei on the same molecule. These slight resonance deviations can be used to describe structural characteristics of chemicals and is a useful property for identifying compounds from chemical reactions. Water suppression is usually performed when acquiring metabolic spectra as the metabolite signal is as low as $1/10^{4}$ times that of the water signal. Strong lipid signals can either be suppressed during MRS acquisition through outer volume saturation techniques, or through lipid removal algorithms during post processing.

Using linear recombination and a database of individual spectra that were obtained previously *in vitro*, it is possible to fit a lineshape to raw spectra and estimate the metabolite concentrations of the original spectra. Because of this, MRS is used as a non-invasive assessment of the metabolic activity of the region of interest. For example, an MRS could be used to determine if a brain tumor is benign or malignant through its observed metabolic activity

by observing the differences in spectra (Bruhn et al., 1989). Metabolites could be observed over the course of a disease progression, or to monitor changes during disease treatment to determine how effective a treatment is. MRS has already been used to study the metabolic processes that occur after strokes, brain tumors, multiple sclerosis lesions, and has also been used to study an assortment of neural abnormalities such as depression and seizures (Brandao & Castillo, 2013; Fazekas, Ropele, Enzinger, Seifert, & Strasser-Fuchs, 2002; Rincon et al., 2016; S. Y. Wang et al., 2017; Zhang & Sui, 2017).

Signal deviations at the molecular environment depend on small changes to the larger magnetic B_0 field. The major source of this signal deviation comes from electrons, whose negative electric charge produces a tiny local magnetic field that is oriented antiparallel to the much larger B_0 magnetic field. The small opposing magnetic field reduces the net strength of the total magnetic field at that location. The effect that electrons have on the perceived magnetic field can be calculated by this formula:

$$B_{eff} = B_0(1 - \sigma) \tag{10}$$

where B_{eff} is the magnetic field experienced by the nuclei and σ is the shielding constant. The new NMR resonance frequency could be calculated then as:

$$v = \gamma B_0(1 - \sigma) = v_o(1 - \sigma) \tag{11}$$

In quantum mechanics, electrons are modeled as an electron cloud. The position of the electron cannot be known at any given time, but instead is estimated as a cloud-like region surrounding the nuclei that represents the probability of where the electron lies. On most molecules, the electron cloud will not be evenly distributed, but will distribute near nuclei with a high electron affinity like fluorine, oxygen and nitrogen instead. To standardize values across MR scanners and other studies, a highly shielded reference molecule such as tetramethylsilane

(TMS) is chosen as the reference for 1H-MRS. Any chemical shift away from that resonance peak is recorded in parts per million (ppm) to that peak:

$$\delta = (v_0 - v) \cdot 10^6 / v_o \quad (12)$$

Nuclei that possess a low electron density will experience a greater percentage of the total B_0 field, compared to nuclei with a greater electron density, and experience a strong downshift in resonance frequency, known as a chemical shift (CS). By using a reference molecule, this process is standardized across MR scanners. *In vivo* scans lack TMS, so N-acetyl aspartate (NAA) is commonly used to determine chemical shift positioning because of its well-defined peak.

In addition to electron shielding, another localized effect that can be observed is the indirect (scalar) spin-spin coupling between neighboring nuclei. This effect is responsible for splitting spectroscopic lines into multiplets. Nuclei attached to a carbon backbone are affected by nuclei attached to neighboring carbons. The multiplet split is the result of different combinations of nuclei oriented in parallel and antiparallel orientations to the B_0 field. Nuclei with antiparallel orientations behave similarly to electrons as they reduce the effective influence of the B_0 field; an effect that is felt on their neighboring nuclei. The signal is split into n + 1 peaks, where n is the number of nuclei on neighboring carbons.

Combining these two effects, all compounds can be identified solely on their local spin-spin coupling effects and their electron shielding properties. There have been libraries of compounds catalogued by their NMR spectra. Programs like "Linear Combination of Model Spectra" (LCModel) use NMR spectral libraries for automating the metabolic quantification process of *in vivo* spectra.

Quantification of MRS signals

In vivo MR spectral signals represent the concentration and the variety of the metabolites within the region being observed. The chemicals vary both in their spectral fingerprint and the total quantity of the chemical itself but can be estimated using a metabolite quantification program. These programs will estimate the individual contributions of each metabolite by using a library of individual spectra called a "basis set" and will then estimate the individual contributions of each spectra. One widely used program is LCModel, which estimates metabolite concentrations using maximum-likelihood estimates of the metabolite concentrations and their uncertainties using Cramér–Rao lower bounds on the metabolite spectra. The Cramér–Rao lower bound (CRLB) represents the lowest possible standard deviation of all unbiased model estimates that were obtained from the spectra (Cavassila, Deval, Huegen, van Ormondt, & Graveron-Demilly, 2000). It is generally accepted that CRLB values < 10% indicate that metabolite concentrations are measured with enough precession that they are considered reliable, while values greater than 30% are not considered reliable. These values show up in LCModel as the standard deviations of the metabolites fitted in the spectra.

Spectral Localization

Much of the technical challenge for acquiring *in vivo* MRS involves localization of the signal to the ROI. The simplest MRS localization method is single voxel spectroscopy (SVS), which uses three orthogonal slice-selective pulses to acquire a single metabolic signal from the region/voxel at the intersection with no further localization steps involved. Signals outside the voxel are destroyed using crusher field gradient pulses or outer-volume saturation pulses (Felmlee & Ehman, 1987). High SNR is achieved by selecting a large voxel area, usually in the

4 - 8 cm^3 range, which is necessary due to the lower strength of metabolic signals in the brain compared to the strength of the water and lipid signals. There are two widely-used methods for localizing the signal using a Fourier-based approach: Point REsolved SpectroScopy (PRESS) (Bottomley, 1987) and Stimulated Echo Acquisition Mode (STEAM) (Haase et al., 1986). PRESS uses a 90° excitation pulse combined with two refocusing pulses, while STEAM uses 3 slice-selective RF pulses with 90° flip angles.

Magnetic Resonance Spectroscopic Imaging (MRSI) is a multi-voxel acquisition of *in vivo* spectral data. MRSI datasets are often acquired using a PRESS or STEAM localization process but require a much larger volume to acquire signals across a 2D or 3D ROI. Row and column localization of the signal within the PRESS or STEAM localization pulse is done using phase-encoding only, since frequency encoding cannot be used to store spectral frequency information. Phase-encoding applied by incrementally adjusting the strength of the applied magnetic gradient field for each datapoint in the grid to create a spectral image that spatially spans the excited region.

Due to the large ROI, MRSI can suffer from magnetic field inhomogeneity problems and is prone to spectral degradation from intervoxel contamination. The low resolution of MRSI datasets cause voxel size deviations from the expected size, which is a byproduct of Fourier encoding processes. This deviation in expected values is caused by point spread function (PSF) effects, which describes the response of an imaging system to a point source. The low number of phase-encoding steps causes the reconstructed signal to have strong side lobes from finite discrete sampling, which results in signal contamination between neighboring voxels. Because frequency encoding cannot be used, acquisition times can be quite long. While a 2D MRSI with

16 x 16 matrix dataset can take 5-6 minutes to acquire the ROI, each slice takes that amount of time, meaning a 16 x 16 x 8 3D dataset will take 8 times the scan time of the 2D dataset.

Echo Planar Spectroscopic Imaging

There have been several attempts to reduce the acquisition times of MRSI. One of the best currently available pulse sequences is an MRSI sequence known as Echo Planar Spectroscopic imaging (EPSI). This sequence is currently used to reduce the scan time it takes to acquire MRSI datasets. EPSI uses an oscillating readout gradient that is applied during the data acquisition to collect spatial and spectral information simultaneously (Posse, Tedeschi, Risinger, Ogg, & Le Bihan, 1995). The oscillating readout gradient repeatedly collects one line of k-space at different time points, with conventional phase encoding being applied before the oscillating readout gradient to encode the other spatial dimensions.

In the most commonly used EPSI pulse sequence, three radiofrequency pulses (RF) are used: two for acquiring the metabolite signal and one for the water reference signal. The water reference and metabolite signal are acquired in the same repetition time by exciting the water signal immediately after the metabolite signal acquisition. The region of interest is selected by a slice selective excitation pulse and a slice selective refocusing pulse for the metabolite signal and by a slice selective excitation pulse for the water signal. One line of k-space data is acquired by the oscillating readout gradient following phase encoding.

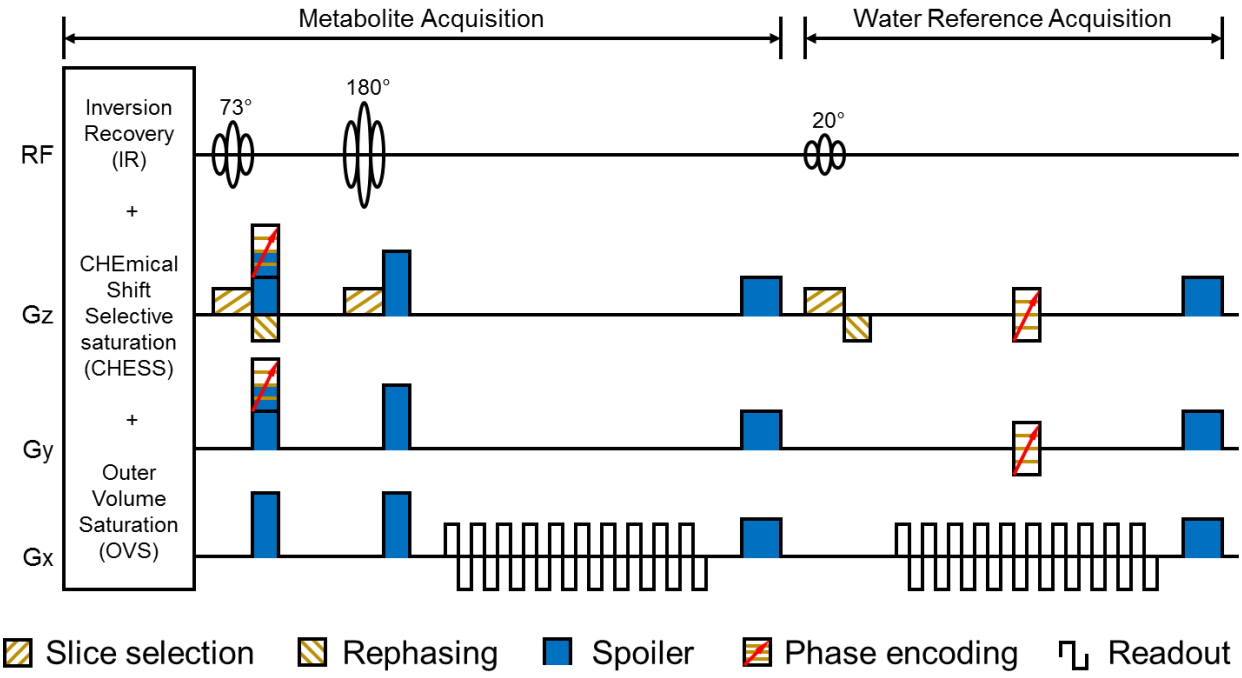

Figure 2: EPSI pulse sequence.
Volumetric proton EPSI acquisition that incorporates an interleaved water reference acquisition. The sequence includes inversion recovery (IR), CHEmical Shift Selective saturation (CHESS) water suppression and Outer Volume Saturation (OVS) to reduce water and lipid contamination during the metabolite acquisition. An oscillating readout gradient is applied to acquire a single dimension of k-space information in a single pulse. The water reference is acquired following a low flip angle excitation applied after metabolite acquisition.

The benefit of using oscillating readout gradient in EPSI is a significant reduced scan time that is an order of magnitude shorter than traditional MRSI. This acceleration of spatial encoding in EPSI enabled three dimensional MRSI, which was not feasible using conventional MRSI due prohibitive scan time requirement.

Spectral Localization by Imaging

Spectral localization by Imaging (SLIM) is a non-Fourier transformation MRSI localization method that uses generalized matrix inversion approaches to calculate the signal for each compartmental region (Hu, Levin, Lauterbur, & Spraggins, 1988). Compartmental region estimates are obtained from an MRI scan of the same region. SLIM operates by dividing the k

space data into several highly customizable compartments that can be defined through binary maps. These compartmental maps are a spectral function given by:

$$\rho_{slim}(r,f) = \sum_{m=1}^{M} \hat{\rho}_m(f) \tag{13}$$

where the estimate of the desired average compartmental spectrum can be represented by the formula:

$$\hat{\rho}_m(f) \approx \rho_m(f) = \begin{cases} \frac{1}{V_m}\int_{D_m} \rho(r,f)dr, & for\ r \in D_m \\ 0, & otherwise \end{cases} \tag{14}$$

D_m in this formula represents the compartmental geometry that was defined by the original anatomical image and V_m is the volume of those compartments. This reconstruction can be solved using least-squares and can be represented as a vector:

$$s_n(t) = G_{nm}c_m(t) \tag{15}$$

In this formula, $s_n(t)$ is the nth phase-encoded signal, $c_m(t)$ is the signal from the mth compartment without phase encoding, and G_{nm} is the SLIM geometry matrix that can be represented as:

$$G_{nm} = \sum_r (\xi_m(r) e^{-j2\pi k_n \cdot r}) \tag{16}$$

In Equation 17, ξ_m is a binary compartment which is used to identify the spatial distribution of the compartment(s) of interest, k_n is the serialized k-space vector, and r is a spatial coordinate vector. Using the least-squares fitting method to solve for $c_m(t)$, the SLIM reconstructed

compartmental signals-encoding vector are obtained for the compartments of interest. Solving for $c_m(t)$ simply involves transforming the dataset using a complex conjugate transformation.

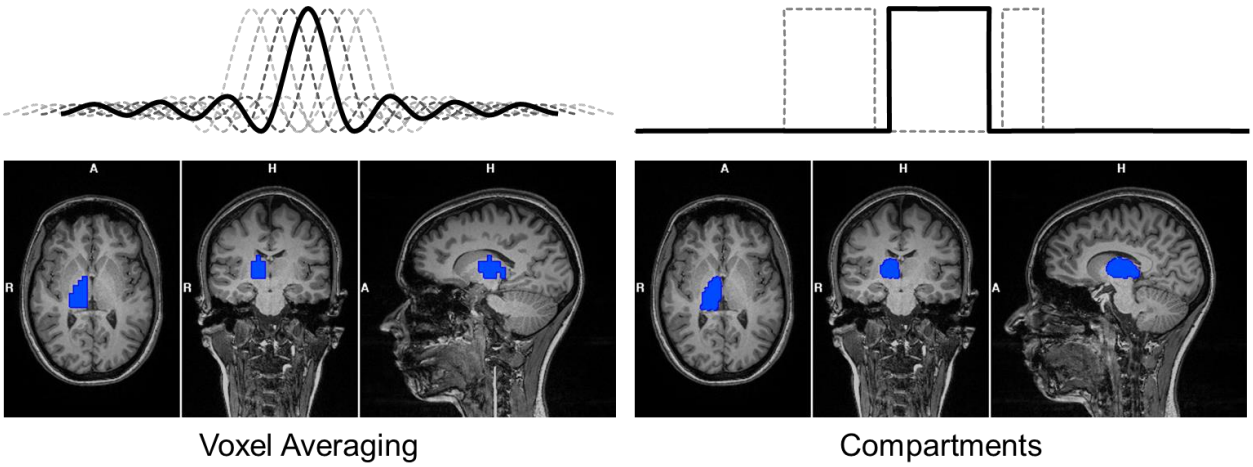

Figure 3: Comparison of Fourier based ROI-averaging vs non-Fourier based SLIM reconstruction.
In Fourier based ROI-averaging, the signal from each voxel used in reconstructing the compartment signal "bleeds" into neighboring voxels due to sidelobe effects as seen by the waveform in the top left image. Reconstructing the signal using SLIM results in a spectra reconstruction that describes the exact shape of the compartment.

The result of SLIM processing is spectra that describe regions defined by the binary compartment maps. This framework allows us to overcome several limitations of current MRSI techniques, the biggest one being its limitation to rectangular voxel shapes for metabolite spectra. SLIM is non-Fourier based, so the spectra are exact recreations of the compartmental areas instead of a Fourier based estimation. Using SLIM, one could acquire the metabolic fingerprint of the thalamus, the hippocampus, and other gray and white matter regions easily by using a compartment shape that matches the exact region the object of interest occupies in the MRI. Early phantom studies on SLIM have demonstrated that spectral reconstruction of water and fat signals originating from cylindrical bottles of oil and water can be retrieved with as few as two phase-encoding steps used as inputs, showing that the main benefit of SLIM is its capability in reconstructing compartmental signal from k space data without the need for acquiring large MRS datasets (Hu et al., 1988).

Currently, there are only a few reports that utilize non-FT based approaches for processing MR spectra. Most papers that utilize MRS employ FT based voxel averaging. Non-FT based approaches reconstruct spectra from spatially well-defined compartments that would eliminate the need for accounting for partial volume fractions, various chemical shift issues, and point spread function effects. The most promising fix is the reduced acquisition time needed, which makes SLIM a valuable tool in clinical studies. Using an EPSI pulse acquisition sequence, a 4x - 8x reduction in k-space acquisitions is possible using a SLIM reconstruction instead of using ROI-averaging. SLIM is an untapped resource that provides another method for how metabolite concentrations are analyzed in specific brain regions.

Applications of MRS Techniques

MRS has been used as a tool for studying the brains of individuals that encompass a wide range of phenotypical differences. The MRS technique has been utilized in studying differences in the brain attributed to age, sex, and race, with some of the most notable discoveries stemming from studying damaged and diseased brains. Increased spatial resolution has enabled researchers with the ability to study localized regions of the brain to observe spatial differences between brain regions. These studies are a window to the metabolic processes in the living brain that is generally not observable using other techniques. There have been many studies already done on the brain with MRS, and the following sections detail MRS research that has been done to study different brain tissue types and various regions of the brain.

Tissue Type specific MRS measurements: GM and WM

White matter MRS studies have uncovered interesting observations about the tissue type. For men, intelligence was associated with higher myelination and a higher number of axons, while intelligence in women was more closely associated with gray matter density (Dunst, Benedek, Koschutnig, Jauk, & Neubauer, 2014). The synapses on axons are dynamically modifiable and may be a source mechanism of learning and memory (Catani et al., 2012). Synapse modification has been shown to occur in subjects learning a musical instrument (Ullen, 2009) and also has been shown in adults learning to read (Carreiras et al., 2009). Aging affects white matter density, where white matter increases in volume and maturity up until age 40, then declining at 3.1 ± 0.4 cm^3 of white matter per year (Resnick et al., 2003; Sowell et al., 2003). Degradation of white matter neural tracts have strong correlations to decreased cognitive function problems in an assortment of neurological disorders (Damasio, 1984). White matter lesions affect cognitive performance in arithmetic and the myelin damage is visible in an MRI through water accumulation at the location of the damage (Anderson et al., 2014; Matejko & Ansari, 2015). In addition, degradation can be detected through reduced NAA concentrations, as macromolecular change in pre-lesion WM occur before a lesion becomes visible on conventional MRI (Fazekas et al., 2002). Abnormal white matter connections in the uncinated fasciculus, frontal, and temporal thalamic projections can be found in subjects with autism spectrum disorders as well as in patients with cerebral palsy (Ameis & Catani, 2015; Pannek, Boyd, Fiori, Guzzetta, & Rose, 2014).

In addition, gray matter MRI and MRS studies have uncovered several interesting details about the tissue type as well. When factoring in differences in brain size, women have a higher proportion of gray matter compared to men, and there is more asymmetry in cortex tissue

volumes of men compared to women (Gur et al., 1999). Longitudinal aging studies have shown that gray matter follows a pattern of buildup and decline, with the gray matter decline beginning at age 30 at a rate of 2.4 ± 0.4 cm^3 per year (Resnick, Pham, Kraut, Zonderman, & Davatzikos, 2003). On a metabolic level, MRS studies on children diagnosed with autism spectrum disorder have been shown to have decreased choline, creatine & phosphocholine, *myo*-inositol, and NAA in gray matter (Friedman et al., 2006). Gray and white matter have also been shown to differ in GABA concentrations, with gray matter having a concentration of 1.30 ± 0.36 µmol/g and white matter having a concentration of 0.16 ± 0.16 µmol/g (Choi, Lee, Merkle, & Shen, 2006).

Region specific MRS measurements

The brain can be divided into functional groups as well as gray and white matter regions, and these smaller regions are often the preferred target of MRS studies. The organ can be characterized as three major functional regions: the brainstem, the cerebellum, and the cerebrum. The largest of these is the cerebrum and consists of two hemispheres that can be further divided into the frontal, parietal, occipital and temporal lobe. There is also a fifth region called the cingulate which has been referred to as the "limbic lobe" by some groups. At the very core of the brain is the basal ganglia that is comprised of the thalamus and the striatum. These regions are all areas that have been previously studied using MRS.

The brainstem is the smallest of these three main regions and plays a role in many autonomic processes including sleep, hearing, equilibrium, eye movement, vomiting, facial expressions, emotion, cardiac and respiratory processes. Parkinson's disease is associated with a loss of dopaminergic neurons in this region, reductions in NAA/Cr in the substantia nigra, and an increase in gamma-Aminobutyric acid in the pons and putamen (Ciurleo, Di Lorenzo, Bramanti,

& Marino, 2014; Duguid, De La Paz, & DeGroot, 1986; Pyatigorskaya, Gallea, Garcia-Lorenzo, Vidailhet, & Lehericy, 2014). The pons has a higher choline and *myo*-inositol concentration compared to other regions, but a much lower creatine concentration (Jacobs, Horska, van Zijl, & Barker, 2001; Minati, Aquino, Bruzzone, & Erbetta, 2010). Lower NAA/Cr ratios have been shown to correlate with more intense and frequent migraines and has been found to be lowered in diseased states such as Wilson's disease and amyotrophic lateral sclerosis (ALS) (Algin et al., 2010; Foerster et al., 2013; Lai, Fuh, Lirng, Lin, & Wang, 2012).

Sitting behind the brainstem are the cerebellum, which are two finely grooved structures that sit just below the cerebrum. The cerebellum serves as a center for motor control and provides some cognitive functions. MRS studies have found higher creatine concentrations in the cerebellum compared to other brain regions (Minati et al., 2010). Metabolic changes in the Cho/Cr ratio of cerebellum lesions are shown to be involved in the development of post-stroke depression (Zhang & Sui, 2017).

The largest region of the brain is the cerebrum, and each hemisphere is divided into four lobes. The largest of these regions is the frontal lobe, and is strongly associated with reward, attention, motivation planning and short-term memory tasks. In addition, the frontal lobe houses Broca's area, which is a region with functions linked to speech production. Broca's area increases in gray matter density in musicians learning an instrument (Abdul-Kareem, Stancak, Parkes, & Sluming, 2011; Sluming et al., 2002). When comparing men and women with identical brain sizes, women had larger gray matter volumes in the left orbitofrontal region, and the primary auditory cortex (Luders, Gaser, Narr, & Toga, 2009). Increased gray matter in the dorsolateral prefrontal cortex has been found to be correlated with higher academic performance (S. Wang et al., 2017). In longitudinal studies, the frontal lobes have been shown to have the

greatest amount of decline in gray matter with age, and this decline correlates with declined cognitive test performances (Sowell et al., 2003; Tisserand et al., 2004). Patients with type 2 diabetes mellitus who had diabetic retinopathy have been shown to have decreased NAA/Cho ratios in frontal white matter (Tong et al., 2014).

The second region is the parietal lobe, which is the main sensory receptive area for spatial navigation and touch. The region is also important for language processing. Substantial metabolic changes in the parietal lobe were observed in children from age 3 to 19 (Horska et al., 2002). Patients with obsessive compulsive disorder showed higher Cho/Cr ratios in the parietal white matter compared to controls (Kitamura et al., 2006).

Beneath the lateral fissure and underneath the parietal and frontal lobe is the temporal lobe, which is involved in processing sensory inputs for retaining visual memory, emotional associations, and language comprehension. The temporal lobe is also home to Wernicke's area, which is involved in the comprehension and understanding of written and spoken language. When comparing men and women with identical brain sizes, women had larger gray matter volumes in the superior temporal gyrus, the primary auditory cortex, and Wernicke's area (Luders et al., 2009). The region is also often a source location for epileptic seizures in adolescents (Tramoni et al., 2011).

The occipital lobe is the smallest lobe of the brain, which lies just above the cerebellum. The region is the visual processing center of the brain where visional information is analyzed for form recognition and object representation, as well as information about motion, color, and object location. In the occipital lobe, NAA, Cr, and Cho concentrations are 20 - 90% higher in the gray matter compared to the white matter (Wang & Li, 1998). Patients with chronic

migraines were found to have reduced or impaired energy metabolisms in the occipital lobe compared to controls (Reyngoudt, Paemeleire, Descamps, De Deene, & Achten, 2011).

This last region of the brain is sometimes referred to as the limbic lobe or cingulate, which is an arc shaped region of cortex that surrounds the corpus callosum and inner organs that sit above the midbrain. The region is vital for memory learning, motivation, and emotional processes, and social skills and empathy are thought to be processed through the limbic lobe. In subjects with Alzheimer's disease, patients had reduced NAA and mI in the limbic lobe (Guo et al., 2015). MRS was also used to detect metabolic changes in the cingulate gyrus (Gardner et al., 2017). In an age-related study, gray matter in the insula declined faster than other regions of the brain (Sowell et al., 2003).

At the core of the brain lies the thalamus, which behaves as a hub for receiving and transmitting signals to other parts of the brain. Made primarily of gray matter, the thalamus plays an important role in the regulation of alertness and sleep states (Steriade & Llinas, 1988). Every sensory system passes through the thalamus for routing to their respective locations for further processing, except for the olfactory system which connects directly to the olfactory bulb. When comparing regions in the brain using MRS, the thalamus was observed to have a higher NAA concentration than the other locations (Minati et al., 2010). In situations where the brain is damaged, the thalamus plays a significant role in neuronal repair after the traumatic brain injury. Patients recovering from a mild traumatic brain injury were observed to have a hyper-connected thalamus during early stages of the injury (Sours, George, Zhuo, Roys, & Gullapalli, 2015). The thalamus has also been observed in many various neurological conditions using MRS. A study done on subjects diagnosed with bipolar disorder found a significantly increased Glx/Cr ratio in the left thalamus compared to control groups (Xu et al., 2013). MRS studies have found a

correlation between individuals with autism spectrum disorder (ASD) and some thalamic abnormalities (Hardan et al., 2008). The thalamus likely plays a role in ALS, as a reduction in NAA and the NAA/Cho ratio in the thalamus was observed in subjects with ALS (Sharma, Saigal, Maudsley, & Govind, 2011). A similar reduction in NAA was found in patients with chronic schizophrenia (Brugger, Davis, Leucht, & Stone, 2011).

Another major brain structure in the center of the brain is the striatum. This structure is comprised of several critical substructures such as the amygdala, putamen, caudate, globus pallidus and hippocampus. These regions facilitate motor and reward systems and coordinate multiple cognitive functions including decision making, reward perception, motivation, and behavioral reinforcement. Posttraumatic stress disorder (PTSD) was also found to be associated with the hippocampus, where affected individuals had significantly lower NAA in the hippocampi and higher Glu and Glu / NAA in the right hippocampus. In addition re-experiencing the symptoms resulted in a negative correlation of NAA in the hippocampi (Rosso, Crowley, Silveri, Rauch, & Jensen, 2017). The caudate is one of several regions of the brain that is significantly reduced in volume of patients with Alzheimer's disease and could be used for early diagnosis (Jiji, Smitha, Gupta, Pillai, & Jayasree, 2013). The globus pallidus plays an important role as a pacemaker for regulating timing of voluntary movements in the body (Surmeier, Mercer, & Chan, 2005). A reduced amygdala volume has been shown to correlate with anxiety, bipolar, and posttraumatic stress disorders, as well as an increase in frequency of anxiety attacks (Thomas et al., 2013; Ziabreva, Poeggel, Schnabel, & Braun, 2003).

Based on the previously mentioned studies, it is evident that there are significant observable differences in brain tissue from that varies greatly by region. The precise roles that these brain regions have make it necessary to have voxels that accurately represent the area being

observed. This is difficult to demonstrate in MRS studies when little consideration is taken of the complex boundaries that define these brain structures. Knowing the important roles that these brain regions have only emphasizes the importance of precise regional measurements in MRS.

MRS observations still depend on the limited spatial resolution of MRSI, which creates a challenge when analyzing functional brain regions. Here, a case for SLIM is presented in which MRI data is utilized to create compartments for SLIM processing. Several resolutions of MRSI data are run through SLIM processing and the resulting spectra are compared to the HR-MRSI area averaged values provided through MIDAS. Quality of spectra in SNR and accuracy are assessed and compared between the two methods.

Chapter 2: Methods

This section details the pre- and post-processing steps of MRI and MRS data used to compare SLIM and ROI averaging. My work focused on three main areas: 1) creation of a high-resolution compartment map for use in SLIM and ROI averaging, 2) calculation of compartment spectra using SLIM and ROI averaging from MIDAS and in-house programs, 3) quantification of metabolite concentrations from the compartmental spectra using automatic quantification programs, and comparison of SLIM and ROI-averaging using statistical analysis methods. Each of these three main areas was organized into a pipeline represented by Figure 4:

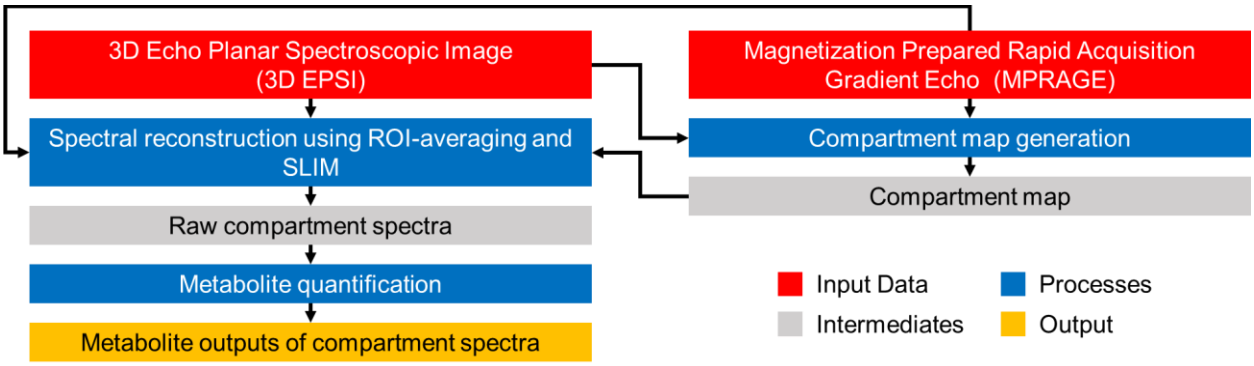

Figure 4: SLIM and ROI-Averaging Processing Pipeline.
3D EPSI and MPRAGE were utilized to create a custom compartment map, which was used to define the compartment boundaries that SLIM and ROI-averaging utilize in their respective spectral reconstruction processes. The 3D EPSI, MPRAGE and compartment maps were processed to generate compartmentally-localized spectra. The metabolic concentrations were quantified and filtered using post processing filtration parameters to produce the datasets found in the Results section.

In Figure 4, the input data represented in red were raw datasets imported directly from MRI scanners. Intermediates were the main forms of semi-processed data that were utilized for processes later in the pipeline and were represented in gray. Regions in blue were the main processes described in this chapter.

MRI and MRS data were acquired from 20 normal healthy control subjects, aged 35 ± 10 years. All datasets were acquired at 3 T (Skyra, Siemens) with a 16-channel head coil. MRI data was acquired using a T1-weighted Magnetization Prepared Rapid Acquisition Gradient

Echo (MPRAGE) sequence. The voxel resolution was 1 x 1 x 1 mm with a TR = 2000 ms, TE = 3.98 ms, TI = 830 ms. The field-of-view and matrix size was 256 x 256 x 176 with a flip angle of 8 degrees. All MRIs were confirmed to be without any structural abnormalities via visual inspection. The 1H MRSI was acquired using a 3D EPSI sequence (Maudsley et al., 2006). The voxel resolution was 5.6 x 5.6 x 10 mm with a TR1 = 1551 ms, TR2 = 511 ms, TE = 16 ms, and TI = 198 ms. The field-of-view was 280 x 280 x 180 with a data acquisition matrix size of 50 x 50 x 18 with a flip angle of 71 degrees and an interpolated resolution of 5.6 x 5.6 x 5.0 mm.

Construction of the Compartmental Maps

The construction of a unique compartment map for each subject was a necessary step for comparing SLIM and ROI-averaging. The brain segmentation program FreeSurfer generated highly parcellated maps that was used as a starting point for custom compartmental maps. To optimize the compartment map for use in SLIM and ROI-averaging however, a few conditions needed to be met: 1) compartments must be continuous or with little fragmentation, 2) compartments must be relatively uniform in size, and 3) spectral data must be relatively homogeneous in each compartment. The first two criteria were resolved by selective merging of compartments from the existing FreeSurfer map. To address the last criteria, a linewidth threshold map was applied to the FreeSurfer map that passes or fails regions of data so that poor quality data was excluded from the final map. An outline of this pipeline can be seen in the figure below that highlights the three main processes:

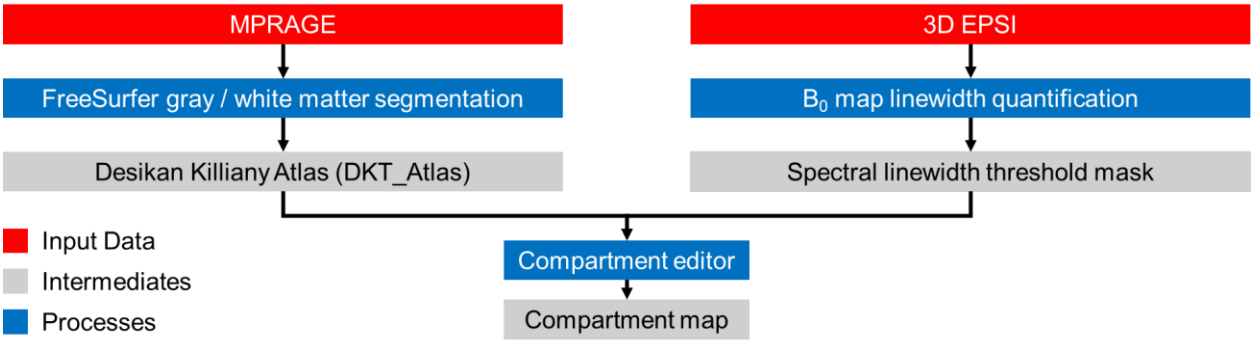

Figure 5: Process 1 – Compartment Map Generation.
MPRAGE was processed in FreeSurfer to produce the brain segmentation map that was resliced according to the Desikan Killiany Atlas. The 3D EPSI data was processed to generate a B_0 linewidth map to separate the poor quality spectral regions. These two maps were combined and compartments were selectively merged together to create the customized compartmental map.

To generate this custom parcellated compartment map, both the MRI and the MRSI scans were required, with the parcellation map being generated from the MRI and the B_0 linewidth map being generated from the MRSI. The resulting compartment map was used for both SLIM and ROI-averaging processes.

FreeSurfer Automatic Gray & White Matter Segmentation

The cortical reconstruction and volumetric segmentation of the MRI was performed with the FreeSurfer image analysis suite (Dale, Fischl, & Sereno, 1999; Dale & Sereno, 1993; Jovicich et al., 2006). FreeSurfer produced a segmentation map that divided up the brain into hundreds of number coded regions that allowed for a high customizability of the compartments used on the brain as seen in the FreeSurfer viewing window below:

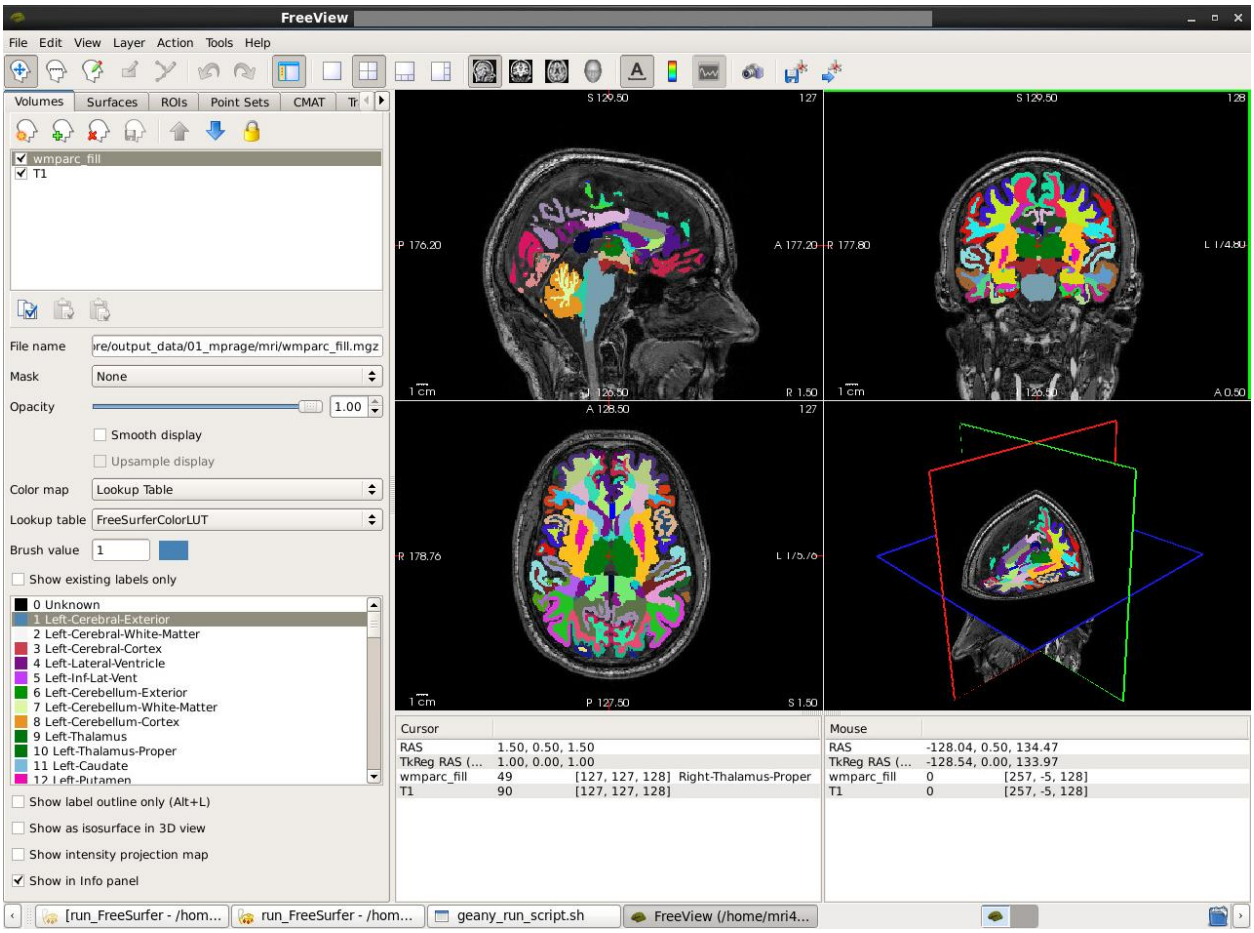

Figure 6: FreeView GUI for showing the results of the FreeSurfer segmentation.
FreeSurfer produces a segmentation map that records an index for each compartment as seen in the lower right corner of the Figure. A lookup table was provided as a .txt file for referencing the numbers to each compartment.

FreeSurfer was run on data for each subject using the default settings, with the only changes to the default settings being that white matter draw distance was increased to minimize the amount of unsegmented white matter found in the resulting segmentation map and unknown regions were removed from the map by incorporating the region into neighboring compartments. FreeSurfer contains two native cortical parcellation atlases: Desikan-Killiany (Desikan et al., 2006) and the Destrieux cortical atlas (Destrieux, Fischl, Dale, & Halgren, 2010; Fischl et al., 2004). Since the Destrieux cortical atlas is a parcellation scheme that segments the brain based on cortex visible on the extremities of the brain, the Desikan-Killiany map was a better choice for retaining compartment uniformity, as the Destrieux map was prone to greater compartment

fragmentation than the Desikan-Killiany map. The final output of FreeSurfer was a 3D .nii file known as the Desikan-Killiany Atlas (DKT_Atlas).

Editing the FreeSurfer compartment map

Because compartments in the DKT_Atlas can vary greatly in size across the ~180 compartments, selective compartment merging was necessary to improve size homogeneity between compartments. Additionally, compartment quality was improved by applying a spectral linewidth threshold mask that excluded regions that exceeded 12 Hz, dividing the DKT_Atlas into two grades of spectral quality. The main regions affected by linewidth filtering were orbitofrontal and temporal regions due to their proximity to the nasal cavities and ear canal which were challenging to acquire quality spectra from. Regions that passed the linewidth threshold were selectively merged based on compartment size, matter type, and functional similarity, while regions outside the threshold were merged based on size only. Unmerged regions retain the same structural characteristics found in the DKT_Atlas.

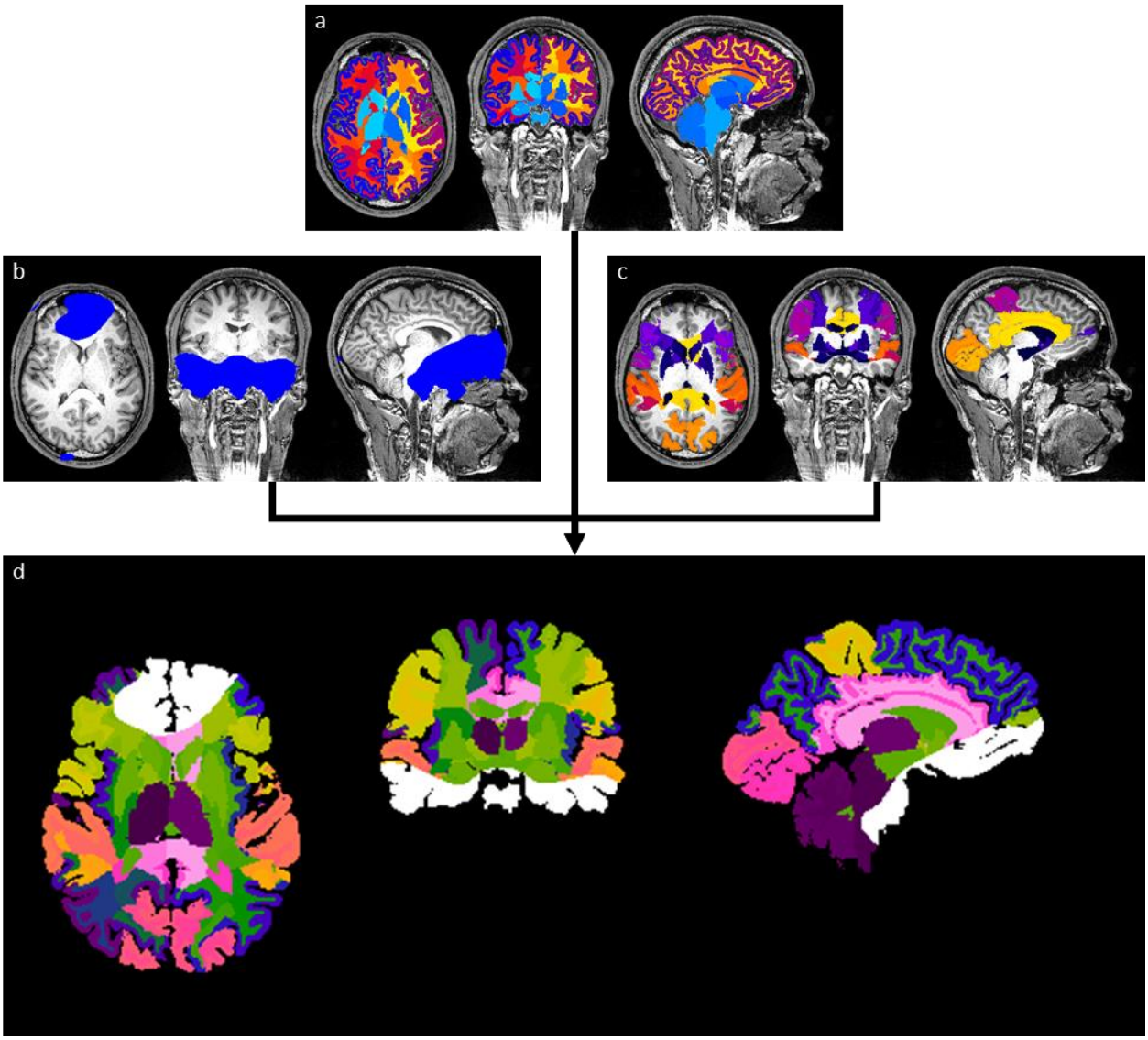

Figure 7: Flow diagram of the construction of the custom compartment map.
a) The DKT_Atlas provides the starting compartmental map that will be edited to generate our final map. b) A binary mask that divides the linewidth map at the 12 Hz threshold was used to segment the DKT_Atlas into good and poor quality spectral regions of the brain. c) Compartmental regions that were selectively merged together based on their functional similarity. d) The final compartment map after applying compartment merging and applying the linewidth threshold mask to the dataset. Each color represents a compartment in the final map.

Figure 7 lays out how the regions were merged together to generate the final compartment map. Image "a" was the original Desikan-Killiany Atlas of the subject. Image "b" was the region of the linewidth map that would be excluded from the final compartment map. Regions that resided in the blue area in image "b" would be merged together to create poor

quality regions. Image "c" was the regions that were selected for merging. Each colored region in image "c" represents two or more areas that were similar enough in function that they were considered equivalent for our purposes and were merged together. Image "d" represents the final compartment map after applying compartment merging where each color represents a compartment.

The following section details the compartments that were merged together: 1) the ventricle region was a combination of the superior and inferior lateral ventricles, the third, fourth and fifth ventricles, CSF, the vessels, the choroid plexus, gray and white matter hypo-intensity regions, as well as the optic chiasm. 2) The ventral diencephalon was a combination of ventral diencephalon regions and unsegmented white matter areas. 3) The Striatum regions were a mixture of the caudate, putamen, pallidum, hippocampus, amygdala, and the accumbens area. The striatum compartment was separated into left and right halves.

For the lobe regions, each compartment was separated into gray and white matter regions as well as left right side info being retained. For the frontal lobe: 1) the Orbital Frontal regions consisted of the caudal middle frontal, lateral orbitofrontal, medial orbitofrontal, and the frontal pole. 2) The pars region consisted of the pars-opercularis, the pars-orbitalis, and the pars-triangularis. 3) The Central region consisted of the para-central and the pre-central regions. No changes were made to the parietal lobe. In the temporal lobe: 1) the inferior temporal region was a combination of the banks of the temporal sulcus, the inferior temporal, and the middle temporal. 2) The fusiform compartments consisted of the entorhinal, fusiform, para-hippocampal, and the temporal pole. 3) The superior temporal region was a combination of the superior temporal and the transverse temporal region. For the occipital lobe: 1) the lateral occipital regions were a combination of the cuneus and the lateral occipital compartments. 2)

The lingual region was a combination of the lingual and pericalcarine regions. The cingulate lobe consists of the caudal-anterior cingulate, the isthmus cingulate, the posterior cingulate, and the rostral-anterior cingulate. The corpus callosum regions were merged with the right cingulate white matter region only, since the corpus callosum was too small of a region to be evaluated properly on its own and the corpus callosum was a central band of white matter.

The original 180 compartments were reduced to 79 compartments, and 8 poor quality regions that fell outside the 12 Hz region. These compartments were further reduced to 12 main compartments that were selected for analysis in the study. After merging, the smallest and largest compartments have a difference in size in the range of 1:4 – 1:15 across the 20 subjects, which was enough of a size similarity that this will not be a major source of errors in SLIM.

Reconstruction of spectra using SLIM and MIDAS

Reconstructing the spectra was done using SLIM and ROI-averaging and the compartment map that was discussed previously. Quantification using ROI-averaging utilized the full k-space dimension of 50 x 50 x 18 and used the Metabolite Imaging and Data Analysis System (MIDAS) as well as a spectral reconstruction program that is currently in development by our laboratory at the KUMC Hoglund Brain Imaging Center. This same in-house program was used to generate compartment spectra using SLIM over 4 decreasing k-space window sizes: 50 x 50 x 12, 40 x 40 x 12, 20 x 20 x 12, and 16 x 16 x 12. The program produced .mat files which needed further processing to be run using LCModel, which was a program used for quantifying metabolites from spectra. A diagram of the process can be seen in the figure below:

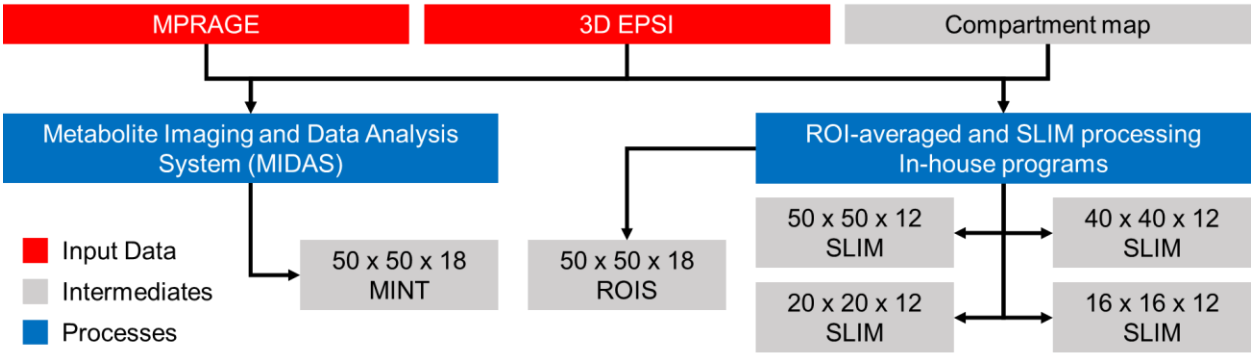

Figure 8: Process 2 – Spectral reconstruction using ROI-averaging and SLIM.
The MPRAGE and 3D EPSI were processed in MIDAS or using in-house programs. The custom compartment map was also provided which produces the six localization methods. The output were spectra that were run on metabolite quantification software later in the pipeline.

In Figure 8, MIDAS processed MPRAGE and 3D EPSI datasets using several built-in programs. After supplying a compartment map to MIDAS, the program generated ROI-averaged spectra of the compartments that were provided. The MPRAGE, 3D EPSI and the compartment map were also processed using in-house software to produce the SLIM and ROI-averaged (ROIS) datasets. Both programs produced the raw compartment spectra that needed to be quantified in later processing steps.

MIDAS Reconstruction

MIDAS is a group of software programs developed at the University of Miami by the research core headed by Dr. Andrew Maudsley (Maudsley et al., 2006). The software was used to take an MRI and MRSI dataset and return high resolution spectroscopic data across the entire brain. Raw MRI and MRSI files were imported into MIDAS and were run through its volumizer program that converts the raw data obtained in the DICOM format into a single file for each data type. The raw EPSI data from the MRI scanner was regridded to produce rectilinear sampled k-space data by incorporating interlaced Fourier transform echo combination with chemical shift correction (Metzger & Hu, 1997). After resampling the EPSI data, the SI data was reconstructed

using a Fourier transform of MRSI k-space data. The MRSI dataset was then co-registered to the MRI dataset using MIDAS Single-Subject Rigid Regristritation (MSREG), which is a program that performs rigid registration between image series for MRI and MRSI 3D volumes. This program was designed to standardize coregistration of patient data between scans, so a subject that has been scanned before and after a treatment will have proper alignment between the two scans. After image registration was performed, the water-reference was used to create B_0 shifts, eddy current corrections, lineshape distortions, and phase correction maps. SI datasets were then Fourier transformed to convert the spectra from the time domain to the frequency domain. A mask was applied to extract the brain from the skull and scalp regions on the MRI and lipid extrapolation was applied to the k-space data.

The final steps of the program involved recovering weaker signals to normalize the signal, and filling "holes" in the SI map by running an intermediate fit of smoothed SI data to help recover some of the weaker spectra in the image. After these processing steps, the data was evaluated using ROI-averaging on the compartment map generated earlier. MIDAS included a built-in program used for importing indexed masks of the subject. The program known as "Mapper" stored the compartments as a mask that was used in MIDAS' ROI-averaging software "Map INTegrated spectrum" (MINT). After running MINT, the files were exported as a collection of reconstructed spectra, with each spectra representing the chemical composition of a region in the brain.

SLIM & ROI-averaging reconstruction

SLIM and ROI-averaging also was done using programs developed in-house. After requesting the MRI and MRSI datasets, the program parsed file ID information, read the datasets

and co-registered the files into the same reference frame. SPM12 was run on the MRI and the lipid layer was used as a mask for later processes. The EPSI data was read, B_0 field was calculated and then the coil data was combined. B_0 correction was applied and produced a linewidth map that was used during the merging of the DKT_Atlas compartments mentioned earlier. After compartment merging has been done, the merged compartment map was loaded into the program and lipid suppression was applied to the EPSI dataset using the PG algorithm. At this point, the data was ready to be processed in ROI-averaging and SLIM. Here, the data was resliced to provide different k-space sizes. The files were exported as MATLAB .mat files which were converted to LCModel format for metabolite quantification later in the pipeline.

Quantification of metabolites and post-processing filtration

Metabolite quantification was run on the compartments using the spectra quantification software LCModel (Provencher, 1993). To assist in processing the large quantity of data, scripts were written for MIDAS and our in-house program to convert their outputs into a format that would be readable in LCModel as a batch process. The script produced a .RAW and .H2O file for each spectra, then edited a preexisting .control file that pointed to those newly created .RAW and .H2O files. The program then ran LCModel by starting a launcher file that ran the program using the .control settings. This process then looped through all the compartments for that run and then over the course of the 20 subjects under all 6 SLIM, MINT and ROIS settings, resulting in thousands of LCModel runs. Upon completion, the program collected the .csv outputs and combined them into a large spreadsheet for easy viewing of the data.

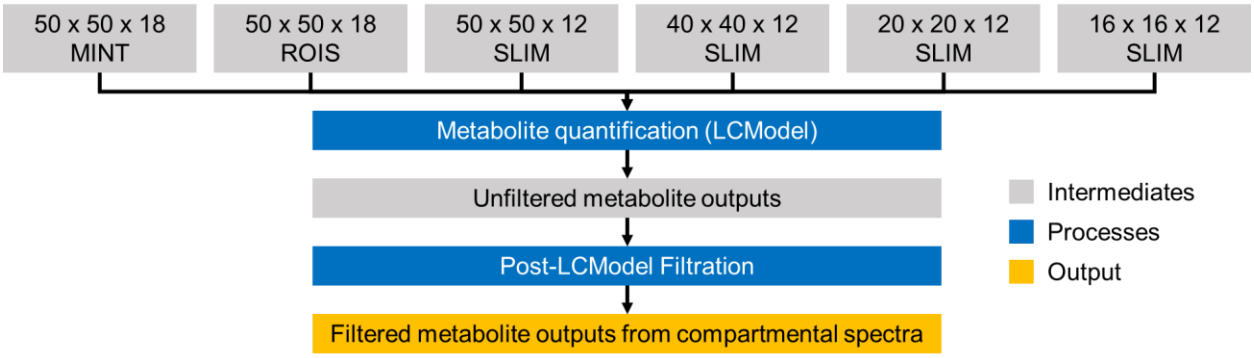

Figure 9: Process 2 – Metabolite Quantification.
Spectra from the six localization methods were processed through metabolite quantification in LCModel to produce metabolite concentrations for the compartments. A post-LCModel filtration step was applied after LCModel quantification to screen out poor quality spectra based on inclusion criteria based on linewidth, SNR, and lipid concentrations in the spectra.

A data quality filter was applied as a post-LCModel analysis processing step. Four parameters were used as metrics for data quality: 1) Linewidth of the fitted compartment spectra, 2) SNR of the LCModel fit, 3) The ratio of lipid and macromolecule signal to creatine near the NAA peak, and 4) The ratio of miscellaneous lipid and macromolecule signals to creatine signal. The data was also filtered to guarantee the existence of an NAA, Cr, and Cho peak. Metabolite data was filtered so that no compartments had a linewidth that exceeded 0.1 ppm, or had a signal-to-noise ratio 5 or less (Kreis, 2004). Compartments were also screened out if the NAA lipid and macromolecule signal exceeded a ratio of 10, or if the miscellaneous lipid and macromolecule signal exceeded a ratio of 27. Lipids were screened out at these ratios because these concentrations were causing wide distortions to the spectral baseline and were destroying any retrievable signal from the spectra.

The MINT dataset concentrations were several magnitudes greater than the in-house ROI and SLIM datasets. This was caused to the differences in the processing methods, so the MINT data was scaled to match the ROIS dataset. The average metabolite concentration of NAA, Creatine and Choline were calculated for MINT and the ROIS datasets creating three possible

scaling factors. The average of these three scaling factors was used to scale every MINT value to preserve local variation in the MINT dataset. By doing this, differences in MINT and ROIS should be minimized to LCModel fitting rather than actual differences in concentration.

Chapter 3: Results

To compare quantification outcomes of the two MRS data reconstruction methods, statistical analysis of the LCModel outputs (.csv files) was applied to the dataset using in-house MATLAB programs. The pipeline produced 6 ways of localizing the metabolite signal to the compartments. Two of these localization datasets were ROI-averaging with one process being ran in MIDAS and the other being ran using our in-house programs. The other four localization datasets were processed in SLIM by cropping the k-space into four sizes: 50 x 50 x 12, 40 x 40 x 12, 20 x 20 x 12, and 16 x 16 x 12. LCModel was run on the six localization methods, across all 79 compartments and across all 20 subjects, which resulted in a total of 9,480 possible LCModel printouts. Of the 9,480 LCModel runs, 465 of these spectra were excluded based on low SNR, high full-width half-maximum (FWHM), or excessive lipid & macromolecule concentrations as described in the Methods section. All data calculations were applied twice, with the first evaluation calculated across all compartments and the second evaluation calculated across a smaller collection of compartments.

Twenty-four regions of the brain were merged with their left or right sided counterpart to create twelve bilaterally symmetrical regions. These compartments were chosen based on their functional roles in the brain, as well as their optimal location in the brain where the quality of B_0 shimming was optimal. Calculations of all the compartments were placed in the appendix section of this report. The regions selected were: the thalamus and striatum, as well as the gray and white matter regions of the central motor strip, cingulate, insula, postcentral, and precuneus. The thalamus acts as an information relay hub that transmits information between areas of the brain. The striatum is a collection of regions that include the hippocampus, globus pallidus and amygdala and this area is involved in memory and emotion. The central motor strip is involved

in executing voluntary motor movements. The postcentral is the region of the brain where sense of touch is processed. The cingulate is the main component of the limbic system which regulates emotion, memory and behavior. The insula is involved in awareness and is involved in processing emotions. The precuneus plays a role in visuospatial imagery and memory. Due to the wide variety of functions of these regions and their optimal position in the brain for B_0 shimming, these regions were optimal candidates for a more detailed inspection.

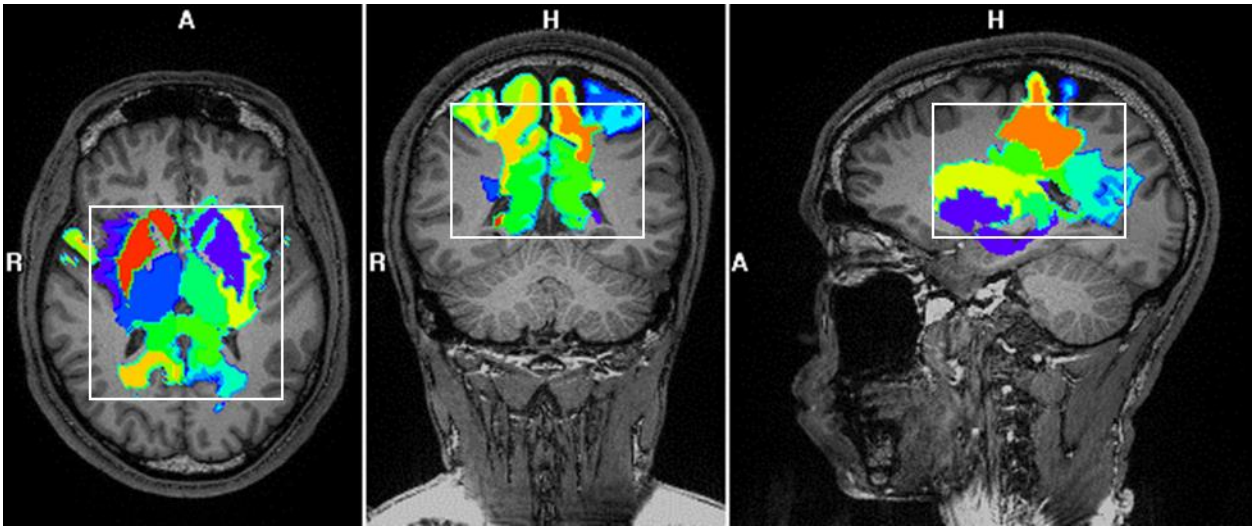

Figure 10: Selection of 24 compartments chosen for data processing.
A selection of the 79 compartments that were chosen for a detailed analysis in the Results section. The regions were selected based on their location within the B_0 shimming window (white rectangle) as well as their functional purpose in the brain as research areas of interest. Regions were merged with their left or right-handed equivalent regions to create 12 functional areas. 10 of these areas have gray and white matter counterparts and include the central motor strip which is involved in executing voluntary motor movements, the postcentral where sense of touch is primarily processed, the cingulate which is the primary component of the limbic system, the insula which is involved in the processing of emotions and environmental awareness, and the precuneus which is involved in processing visuospatial imagery. The thalamus which acts as an information relay hub and the striatum which is involved in memory and emotion were also included in this list as areas of research interest.

Average metabolite concentrations by method

After applying post-LCModel filtration, the average metabolite concentration was calculated for each compartment by averaging the data across the 20 subjects and was repeated to calculate the average creatine ratios for the compartments as well. Table 1 shows the average

metabolite concentrations of the central gray matter motor strip and the striatum across the five metabolites and across the in-house SLIM and ROIS processes.

Table 1: Average metabolite concentrations and standard deviations of the Central Gray Matter (1a) and Striatum (1b).

a		ROIS 50x50x18	SLIM 50x50x12	SLIM 40x40x12	SLIM 20x20x12	SLIM 16x16x12
Central Gray Matter	NAA	33.6 ± 4.8	32.1 ± 4.7	31.9 ± 4.9	29.9 ± 6.8	29.1 ± 5.6
	Cr	24.6 ± 4.1	23.9 ± 4.4	23.2 ± 5.5	21.1 ± 5.7	20.1 ± 5.5
	Cho	4.3 ± 1.0	3.9 ± 0.9	3.8 ± 0.9	3.3 ± 1.3	3.4 ± 1.2
	mI	10.5 ± 4.1	10.0 ± 2.9	9.5 ± 3.5	8.3 ± 3.4	7.7 ± 4.0
	Glx	8.7 ± 8.2	7.6 ± 6.4	9.8 ± 12.5	7.9 ± 6.8	6.3 ± 5.7
	NAA / Cr	1.4 ± 0.1	1.4 ± 0.2	1.4 ± 0.2	1.5 ± 0.3	1.5 ± 0.3
	Cho / Cr	0.2 ± 0.0	0.2 ± 0.0	0.2 ± 0.0	0.2 ± 0.0	0.2 ± 0.0
	mI / Cr	0.4 ± 0.1	0.4 ± 0.1	0.8 ± 2.4	0.4 ± 0.1	0.4 ± 0.2
	Glx / Cr	0.4 ± 0.4	0.3 ± 0.3	9.2 ± 36.5	0.4 ± 0.4	0.4 ± 0.6

b		ROIS 50x50x18	SLIM 50x50x12	SLIM 40x40x12	SLIM 20x20x12	SLIM 16x16x12
Striatum	NAA	25.2 ± 5.9	24.8 ± 5.3	24.8 ± 5.6	22.5 ± 5.1	21.0 ± 6.1
	Cr	23.4 ± 5.2	24.5 ± 5.2	24.6 ± 5.1	25.6 ± 7.0	24.0 ± 7.4
	Cho	6.1 ± 1.5	6.6 ± 1.5	6.7 ± 1.6	6.6 ± 1.7	6.3 ± 1.8
	mI	12.9 ± 3.9	13.9 ± 5.4	14.6 ± 7.5	12.5 ± 6.4	13.8 ± 7.5
	Glx	9.6 ± 4.1	7.1 ± 4.5	7.3 ± 5.3	9.4 ± 5.1	11.5 ± 9.4
	NAA / Cr	1.1 ± 0.1	1.0 ± 0.1	1.0 ± 0.1	0.9 ± 0.1	0.9 ± 0.2
	Cho / Cr	0.3 ± 0.0	0.3 ± 0.0	0.3 ± 0.1	0.3 ± 0.1	0.3 ± 0.1
	mI / Cr	0.6 ± 0.2	0.6 ± 0.1	0.6 ± 0.2	0.5 ± 0.2	0.6 ± 0.3
	Glx / Cr	0.5 ± 0.5	0.3 ± 0.2	0.3 ± 0.2	0.4 ± 0.2	0.6 ± 0.6

Note: Concentrations of NAA, Cr and Cho were stable for both the central gray matter and striatum across the five localization methods that used the in-house programs. Glx had a high amount of standard deviation that caused the Glx results to be unreliable. Metabolite concentrations were shown in Institutional Units (IU).

The concentrations in Table 1 indicate that the differences in concentration between N-acetyl aspartate (NAA), creatine (Cr), choline (Cho), and *myo*-inositol (mI) do not deviate significantly between the five in-house localization methods. This was supported by the similarity in creatine ratios of the respective metabolites. The apparent overestimation of NAA in SLIM disappears when calculated as a creatine ratio, so the processes did not appear to affect concentrations significantly. Of the five metabolites observed, only glutamate (Glx) showed

significant differences between the processes, but this was likely due to poor LCModel fitting of Glx.

A second calculation was applied to the average concentrations by subtracting the difference between ROIS and the four SLIM localization methods, then dividing that result by the ROIS value. This was done to calculate the fractional difference in the metabolite concentrations of the SLIM localization methods using ROIS as the reference localization method. Negative values indicate that SLIM undersampled the concentration compared to ROIS while positive values indicate an oversampling of the concentration (i.e., a -0.10 indicates that the SLIM concentration was 10% less, while 0.05 is 5% greater than the concentration of ROIS).

Table 2: Relative metabolite concentration differences between the four SLIM localization methods and the ROI-averaged method in the Central Gray Matter (2a) and Striatum (2b).

a		SLIM 50x50x12	SLIM 40x40x12	SLIM 20x20x12	SLIM 16x16x12
Central Gray Matter	NAA	0.04	0.05	0.11	0.13
	Cr	0.03	0.06	0.14	0.18
	Cho	0.08	0.13	0.22	0.21
	mI	0.09	0.13	0.24	0.31
	Glx	0.10	-0.33	0.17	0.28
	NAA / Cr	0.01	0.01	-0.06	-0.10
	Cho / Cr	0.05	0.10	0.09	0.02
	mI / Cr	0.03	-0.80	0.06	0.14
	Glx / Cr	-0.03	-32.99	-0.09	-0.11

b		SLIM 50x50x12	SLIM 40x40x12	SLIM 20x20x12	SLIM 16x16x12
Striatum	NAA	0.01	0.02	0.11	0.16
	Cr	-0.05	-0.05	-0.10	-0.03
	Cho	-0.08	-0.09	-0.08	0.00
	mI	-0.07	-0.13	0.03	-0.08
	Glx	0.29	0.30	0.01	-0.13
	NAA / Cr	0.06	0.06	0.17	0.17
	Cho / Cr	-0.04	-0.05	-0.02	-0.01
	mI / Cr	0.01	-0.03	0.14	-0.10
	Glx / Cr	0.47	0.49	0.28	-0.04

Note: Relative differences between ROI-average and SLIM became greater with smaller k-space sample sizes. The central gray matter region showed an over sampling of the concentrations compared to ROIS, while there was a trend towards under sampling of the metabolites in the striatum.

The average metabolite concentrations of the 12 compartments were plotted into bar graphs to observe local differences in concentrations between the compartments and to observe differences in standard deviation.

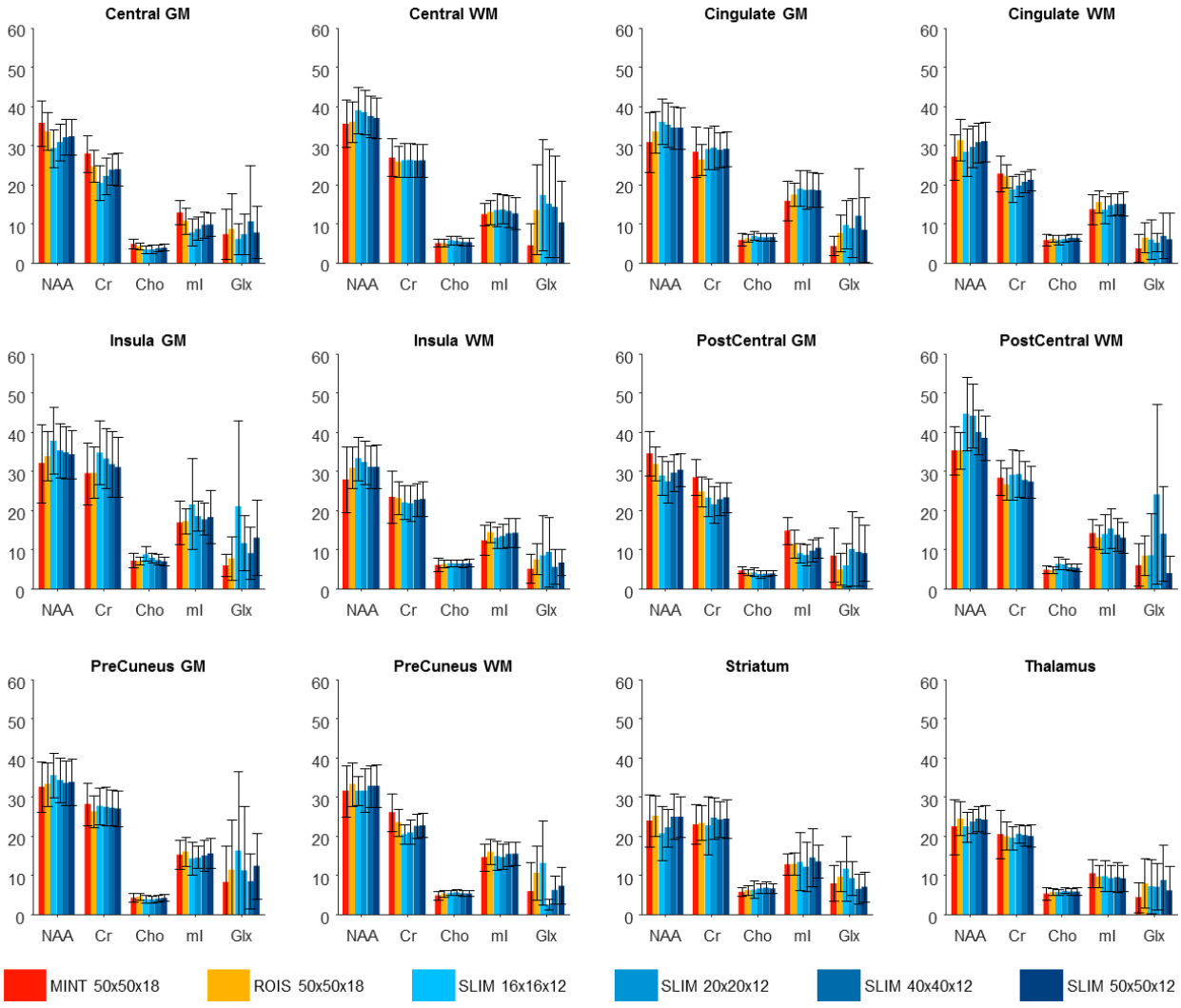

Figure 11: Average concentration and standard deviation for all five metabolites across all six localization methods and across the 12 compartments.

The average concentration and standard deviation of each metabolite was averaged across the twenty subjects and were compared with their localization method equivalents. Concentrations were expressed in Institutional Units (IU). N-acetyl aspartate, Creatine, and Choline showed stable concentrations across the localization methods, while Glutamate showed larger variation between localization methods due to poor fitting in LCModel.

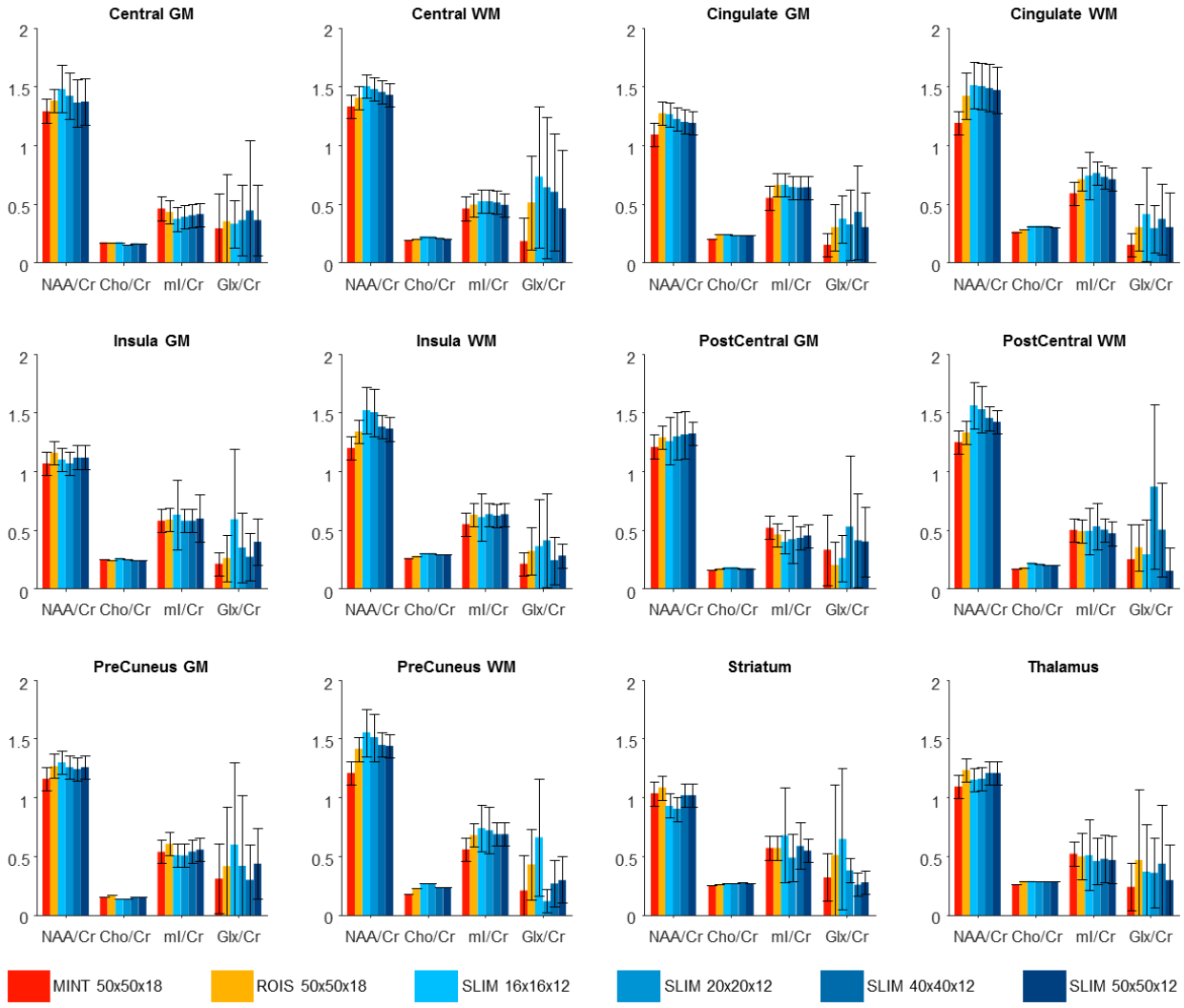

Figure 12: Average concentration ratios of metabolites to creatine and standard deviation for all five metabolites across all six localization methods and across the 12 compartments.
The average creatine ratio and standard deviation of each metabolite was averaged across the twenty subjects and were compared with their localization method equivalents. N-acetyl aspartate, Creatine, and Choline showed stable creatine ratios across the localization methods, while Glutamate showed larger variation between localization methods due to poor fitting in LCModel.

Figure 11 and 12 show that the metabolite concentrations of NAA, Creatine and Choline were found to be relatively consistent between the six localization methods and fall within the standard deviation of the other 5 localization methods, except for in a couple of the compartments where SLIM recorded higher concentrations than in the ROI-averaged runs. The creatine ratios were more stable, except for Glx which was found to be unreliable and had high

standard deviations between the localizations. *Myo*-Inositol was found to be stable in most compartments except for SLIM processes with lower k-space sizes.

In addition to calculating average concentrations, the mean and standard deviation of MINT 50 x 50 x 18 and the four k-space SLIM localization methods were calculated as ratios of ROIS 50 x 50 x 18. Processing the data in this manner inherently normalizes the mean relative to a magnitude of 1.0 and demonstrates similarities between the two methods using ROI-averaging as the standard. Averaging method pairs with values close to 1 and a low standard deviation indicate relative agreement between the methods. This was calculated across all compartments and on a compartment basis as well.

Table 3: Mean and standard deviation of the ratios of five different localization methods to ROI-averaging method.

		MINT 50x50x18	SLIM 16x16x12	SLIM 20x20x12	SLIM 40x40x12	SLIM 50x50x12
All Compartments	NAA	0.97 ± 0.2	1.00 ± 0.2	1.00 ± 0.1	1.01 ± 0.1	1.00 ± 0.1
	Cr	1.06 ± 0.2	0.98 ± 0.2	0.99 ± 0.1	1.00 ± 0.1	1.01 ± 0.1
	Cho	0.99 ± 0.2	1.04 ± 0.2	1.03 ± 0.2	1.02 ± 0.2	1.02 ± 0.1
	mI	1.04 ± 0.3	0.99 ± 0.4	0.98 ± 0.3	1.01 ± 0.3	1.00 ± 0.3
	Glx	2.66 ± 8.0	8.01 ± 42.3	5.01 ± 20.8	2.41 ± 6.2	2.46 ± 6.8
	NAA / Cr	0.91 ± 0.1	1.03 ± 0.1	1.01 ± 0.1	1.01 ± 0.1	1.00 ± 0.1
	Cho / Cr	0.94 ± 0.1	1.06 ± 0.2	1.04 ± 0.2	1.02 ± 0.2	1.02 ± 0.1
	mI / Cr	0.98 ± 0.3	1.03 ± 0.4	0.99 ± 0.3	1.00 ± 0.3	1.00 ± 0.3
	Glx / Cr	2.91 ± 9.8	7.99 ± 40.1	5.03 ± 18.4	2.48 ± 6.9	2.56 ± 7.1

Note: Mean values near 1.0 with a small standard deviation (e.g., ~0.1) indicate relative agreement. NAA, Cr, Cho, and mI show strong levels of relative agreement with ROIS and the five other localization methods. Only Glx showed little correlation between the methods.

In Table 3, NAA, Cr, Cho, and mI had mean ratios within 0.06 units of 1 for all points in the dataset with a low standard deviation. Only Glx did not have a mean ratio close to 1 which was likely caused by the poor LCModel fitting of Glx.

Signal-to-Noise Ratio & Full-Width Half-Maximum of compartmental spectra

Table 4: Average SNR across all compartments and the 12 selected compartments.

	MINT 50x50x18	ROIS 50x50x18	SLIM 50x50x12	SLIM 40x40x12	SLIM 20x20x12	SLIM 16x16x12
All Compartments	21.2	14.8	13.2	12.8	10.9	10.1
Central GM	24.2	17.0	15.4	14.6	10.6	9.5
Central WM	23.5	14.5	13.9	14.1	13.3	12.9
Cingulate GM	16.7	14.7	12.9	12.9	11.2	10.4
Cingulate WM	18.5	15.6	14.3	14.0	13.0	12.2
Insula GM	18.8	13.3	12.7	12.1	10.2	9.2
Insula WM	21.6	17.3	15.5	15.1	13.3	12.5
Post-Central GM	24.0	16.7	13.2	12.2	10.4	10.6
Post-Central WM	23.9	16.1	13.0	12.6	11.0	8.8
Pre-Cuneus GM	20.4	15.5	14.1	13.2	11.3	9.9
Pre-Cuneus WM	22.0	15.2	14.3	13.9	10.7	10.4
Striatum	24.4	12.1	10.6	10.3	7.7	7.2
Thalamus	16.2	9.7	8.5	8.6	8.1	7.4

Note: The SNR was retrieved from LCModel outputs where the value was calculated as the ratio of the maximum in the spectrum-minus-baseline to twice the root mean square (RMS) residuals. RMS refers to the square root of the mean square. These values were averaged across the subjects to produce the average SNR across all compartments and the average SNR across the 12 selected compartments.

SNR values were retrieved from the LCModel printouts and their values were averaged across the 20 subjects. The SNR was calculated as the ratio of the maximum in the baseline subtracted spectrum to twice the rms residuals. The results in Table 3 indicated that the SNR decreases as the k-space was reduced in SLIM, as k-space points were being removed from the final SLIM reconstruction of the compartments. Because MIDAS applies spatial smoothing to their spectral data, they obtain higher SNR values than the in-house processes, which do not apply spatial smoothing to the datasets. Generally, compartments saw a ~30% reduction in SNR between the 50 x 50 x 12 and the 16 x 16 x 12.

Another area of interest was the differences in FWHM of the spectra across the localization methods. FWHM values were retrieved from LCModel and were averaged across the 20 subjects to identify any trends in the data for the 12 compartments and for all the compartments overall.

Table 5: Average FWHM across all compartments and the select compartments.

Compartment	MINT 50x50x18	ROIS 50x50x18	SLIM 50x50x12	SLIM 40x40x12	SLIM 20x20x12	SLIM 16x16x12
All	0.046 ppm (5.9 Hz)	0.045 ppm (5.7 Hz)	0.05 ppm (6.4 Hz)	0.052 ppm (6.6 Hz)	0.054 ppm (6.9 Hz)	0.053 ppm (6.8 Hz)
Central GM	0.057 ppm (7.3 Hz)	0.047 ppm (6.0 Hz)	0.058 ppm (7.4 Hz)	0.061 ppm (7.8 Hz)	0.056 ppm (7.2 Hz)	0.057 ppm (7.3 Hz)
Central WM	0.045 ppm (5.7 Hz)	0.052 ppm (6.6 Hz)	0.052 ppm (6.6 Hz)	0.05 ppm (6.4 Hz)	0.055 ppm (7.0 Hz)	0.04 ppm (5.1 Hz)
Cingulate GM	0.053 ppm (6.8 Hz)	0.052 ppm (6.6 Hz)	0.045 ppm (5.7 Hz)	0.055 ppm (7.0 Hz)	0.048 ppm (6.1 Hz)	0.047 ppm (6.0 Hz)
Cingulate WM	0.048 ppm (6.1 Hz)	0.051 ppm (6.5 Hz)	0.048 ppm (6.1 Hz)	0.048 ppm (6.1 Hz)	0.052 ppm (6.6 Hz)	0.055 ppm (7.0 Hz)
Insula GM	0.055 ppm (7.0 Hz)	0.063 ppm (8.0 Hz)	0.059 ppm (7.5 Hz)	0.055 ppm (7.0 Hz)	0.059 ppm (7.5 Hz)	0.062 ppm (7.9 Hz)
Insula WM	0.053 ppm (6.8 Hz)	0.047 ppm (6.0 Hz)	0.045 ppm (5.7 Hz)	0.055 ppm (7.0 Hz)	0.052 ppm (6.6 Hz)	0.052 ppm (6.6 Hz)
Post-Central GM	0.063 ppm (8.0 Hz)	0.057 ppm (7.3 Hz)	0.058 ppm (7.4 Hz)	0.063 ppm (8.0 Hz)	0.06 ppm (7.7 Hz)	0.056 ppm (7.2 Hz)
Post-Central WM	0.056 ppm (7.2 Hz)	0.051 ppm (6.5 Hz)	0.047 ppm (6.0 Hz)	0.051 ppm (6.5 Hz)	0.055 ppm (7.0 Hz)	0.056 ppm (7.2 Hz)
Pre-Cuneus GM	0.049 ppm (6.3 Hz)	0.052 ppm (6.6 Hz)	0.05 ppm (6.4 Hz)	0.055 ppm (7.0 Hz)	0.054 ppm (6.9 Hz)	0.055 ppm (7.0 Hz)
Pre-Cuneus WM	0.054 ppm (6.9 Hz)	0.048 ppm (6.1 Hz)	0.051 ppm (6.5 Hz)	0.05 ppm (6.4 Hz)	0.045 ppm (5.7 Hz)	0.038 ppm (4.9 Hz)
Striatum	0.055 ppm (7.0 Hz)	0.058 ppm (7.4 Hz)	0.068 ppm (8.7 Hz)	0.073 ppm (9.3 Hz)	0.069 ppm (8.8 Hz)	0.065 ppm (8.3 Hz)
Thalamus	0.055 ppm (7.0 Hz)	0.058 ppm (7.4 Hz)	0.064 ppm (8.2 Hz)	0.061 ppm (7.8 Hz)	0.063 ppm (8.0 Hz)	0.065 ppm (8.3 Hz)

Note: FWHM was retrieved from LCModel which was an estimation of the linewidth of the *in vivo* spectra. The FWHM was consistent between all datasets indicating that linewidth was not significantly affected by the localization method used.

The regions observed in Table 4 did not show a significant trend in variation between the localization methods or significant differences in the compartments. This suggests that SLIM does significantly affect the resulting FWHM.

Correlation of ROI-averaging and other localization methods

Pearson correlation coefficients were calculated between ROIS 50 x 50 x 18 and the five other averaging methods. This too was calculated on a compartment basis, as well as across all compartments. The results show a high level of correlation between SLIM and ROI-averaging for NAA, Cr, and Cho at 0.81 and higher. Glx showed very weak correlation due to poor fitting in LCModel and cannot be used as a reliable indicator of correlation. mI showed a fair amount of correlation between SLIM and ROI-averaging using in-house programs, but became less reliable at lower SLIM k-space sizes. Correlation results between MINT and ROI-averaging

using in-house programs indicate that the processing methods were different enough that a direct comparison between MINT and SLIM would not be meaningful.

Table 6: Pearson Correlation Coefficients across all compartments.

		MINT 50x50x18	SLIM 50x50x12	SLIM 40x40x12	SLIM 20x20x12	SLIM 16x16x12
All Compartments	NAA	0.72	0.95	0.92	0.86	0.81
	Cr	0.69	0.92	0.92	0.86	0.83
	Cho	0.70	0.91	0.87	0.86	0.81
	mI	0.58	0.75	0.76	0.74	0.54
	Glx	0.14	0.34	0.47	0.25	0.24
	NAA / Cr	0.66	0.90	0.88	0.82	0.79
	Cho / Cr	0.82	0.91	0.86	0.86	0.83
	mI / Cr	0.54	0.74	0.79	0.71	0.56
	Glx / Cr	0.15	0.27	0.40	0.21	0.36

Note: Pearson correlation coefficients were calculated for the five localization methods against the ROI-averaged localization method using in-house tools. Correlation of SLIM performed better against the in-house ROI-averaged set than the MINT correlation, indicating that a direct comparison with SLIM and MINT would not be an accurate comparison due to the differences in processing methods of the two programs. SLIM and ROI-averaged datasets correlate quite well at high SLIM resolutions for NAA, Cr, and Cho and have a fair correlation for mI. Glx does not correlate well because of poor fitting in LCModel.

The correlation data of metabolite concentrations were plotted as scatterplots as pairs of data between the five localization methods and ROI averaging. Similar plots were also created for metabolite ratios to creatine. The 95% confidence and predictive intervals were also calculated, and a linear regression with one degree of freedom (slope) was calculated, i.e., the regression line y-intercept was constrained to zero.

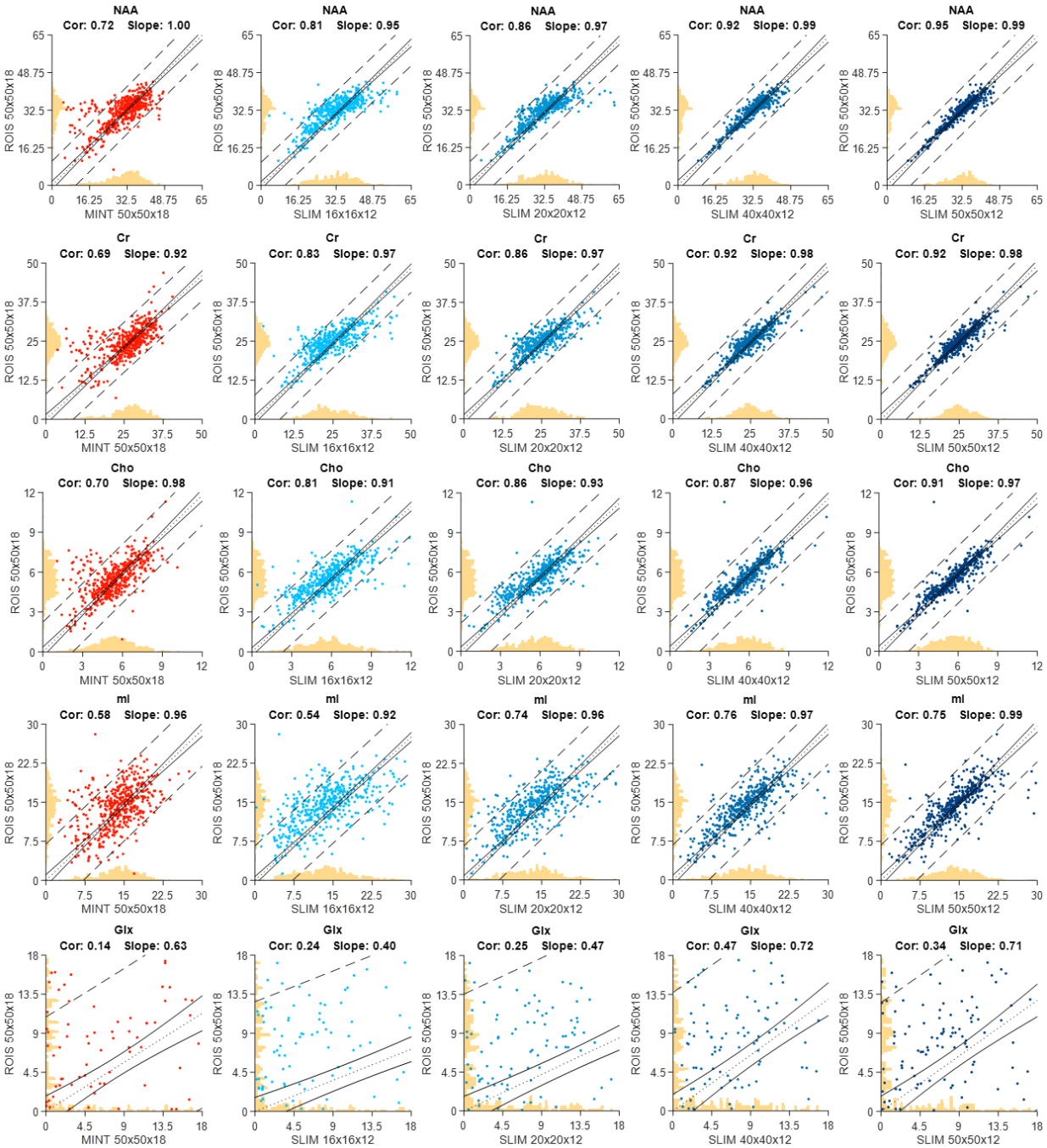

Figure 13: Correlation scatterplots of metabolite concentrations for five localization methods vs ROI averaging. Correlation scatterplots were calculated across all five metabolites and all five localization methods. The dotted line was the linear regression of the dataset, the solid lines were the confidence interval of the linear regression at the 95th percentile, and the dashed lines were the prediction intervals of the data at the 95th percentile. Slope indicates the slope of the linear regression while the Pearson correlation coefficient (Cor) indicates the measure of correlation between ROIS 50 x 50 x 18 and the other localization methods. The orange histograms on the x and y axes demonstrate data distribution for the SLIM and ROI-averaged data. All concentrations were expressed in Institutional Units (IU).

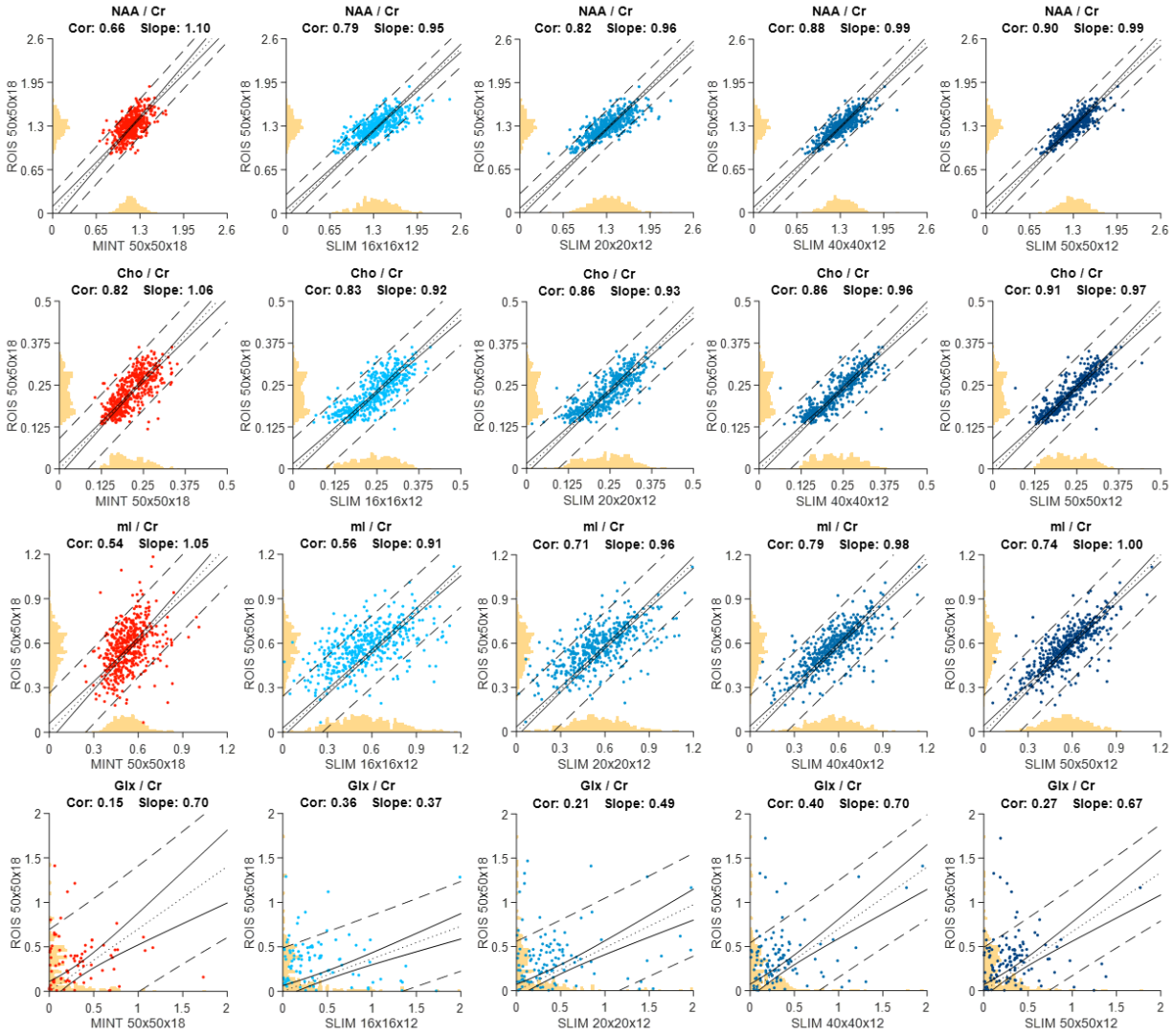

Figure 14: Correlation scatterplots of metabolite creatine ratios for five localization methods vs ROI averaging. Correlation scatterplots were calculated across all four metabolites and all five localization methods. The dotted line was the linear regression of the dataset, the solid lines were the confidence interval of the linear regression at the 95th percentile, and the dashed lines were the prediction intervals of the data at the 95th percentile. Slope indicates the slope of the linear regression while the Pearson correlation coefficient (Cor) indicates the measure of correlation between ROIS 50 x 50 x 18 and the other localization methods. The orange histograms on the x and y axes demonstrate data distribution for the SLIM and ROI-averaged data.

The SLIM localization methods with high k-space sizes showed higher correlation coefficients and the slope closer to 1.0 than the ROIS 50 x 50 x 18 localization method for NAA, Cr, and Cho. Glx showed little to no correlation for both the absolute metabolite concentrations and the creatine ratios for all localization method. The SLIM localization methods at higher k-space sizes had better correlation with ROIS than SLIM at low k-space sizes.

Spectral Quality Inclusion Criteria

As a method of filtering out poor-quality spectra, LCModel outputs were screened based on metabolite FWHM, SNR and lipid concentration. First, spectra with a FWHM of 0.1 ppm or greater, or spectra with a SNR of 3 or less were filtered out of the final dataset. Second, lipid-creatine ratios were calculated for the lipid macromolecules near the NAA peak and for miscellaneous lipid signals in the spectra. Spectra with a lipid NAA creatine ratio greater than 10 or spectra with a miscellaneous lipid creatine ratio greater than 27 were filtered out of the final dataset.

The filtered dataset was then collected and calculated to identify where data were being excluded from the results. Percentages of included data were calculated by compartment, metabolite, averaging system, and by subject to assist in determining the quality of the dataset overall. Each calculation was done as a ratio of data that passed the inclusion criteria divided by total data possible for each set. For example, the calculation for central gray matter region was a ratio of all the central gray matter data points that passed the inclusion criteria divided by the total data possible for the central gray matter across the metabolites, the subject and the localization method.

Table 7: Percentage of MRS data that passed inclusion criteria based on linewidth, SNR, and lipid signals.

% data obtained by compartment							
Central GM	94%	Central WM	91%	Cingulate GM	92%	Cingulate WM	90%
Insula GM	90%	Insula WM	89%	Post-Central GM	92%	Post-Central WM	92%
Pre-Cuneus GM	91%	Pre-Cuneus WM	84%	Striatum	96%	Thalamus	88%
All	91%						
% data obtained by metabolite							
NAA	99%	NAA / Cr	99%	Cho	99%	Cho / Cr	99%
mI	99%	mI / Cr	99%	Glx	61%	Glx / Cr	61%
Cr	99%						
% data obtained by localization method							
SLIM 16x16x12	91%	SLIM 20x20x12	91%	SLIM 40x40x12	91%	SLIM 50x50x12	91%
MINT 50x50x18	90%	ROIS 50x50x18	91%				
% data obtained by subject							
Subject 008	94%	Subject 009	91%	Subject 010	89%	Subject 012	90%
Subject 013	84%	Subject 014	92%	Subject 015	91%	Subject 016	93%
Subject 017	93%	Subject 018	92%	Subject 019	90%	Subject 020	92%
Subject 021	86%	Subject 022	92%	Subject 023	92%	Subject 024	96%
Subject 025	88%	Subject 026	94%	Subject 027	89%	Subject 028	91%

Note: Percentages were calculated as total data that passed the inclusion criteria over total data. Compartment selection played a minor role in the percentage of data that failed to pass the inclusion criteria as the precuneus white matter and the thalamus were poorer quality than regions like the striatum. Of the five metabolites, Glx was the main metabolite that consistently failed to pass the inclusion criteria. Localization method did not play a significant factor in the inclusion criteria. Subject variation played a small role in the inclusion of data, but only in a couple of the subjects observed in this study.

When examining Table 10, it was interesting to note that the percent of included data calculated by-localization-method showed the least variance out of the four ways of percent data calculation. This indicates that t spectral quality did not significantly differ among localization methods. Among metabolites, Glx showed the lowest percent of data passing the inclusion criteria, which was caused by poor metabolite fitting in LCModel. Among compartments, the region with the highest percentage of data that passed the inclusion criteria was the striatum, while the precuneus white matter, thalamus, and the white matter of the insula had the lowest percentage of data that passed the inclusion criteria. These differences indicate that spectral quality was dependent on the compartment.

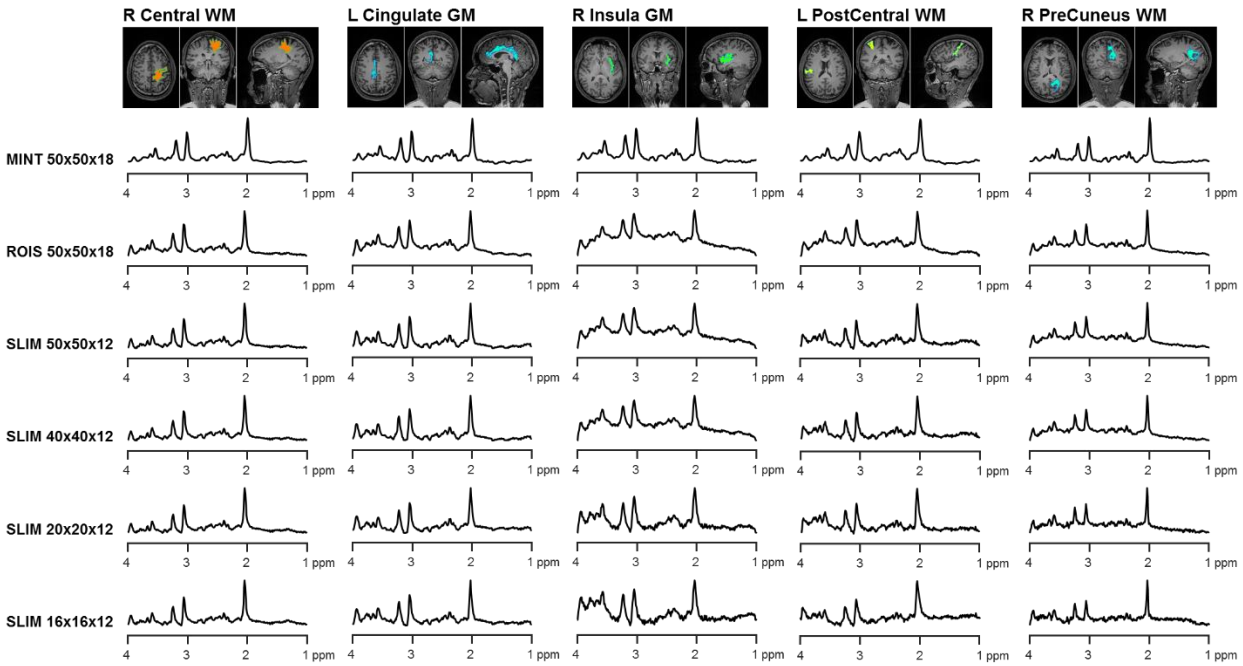

Figure 15: Comparison of compartmental spectra from five regions of the brain across all six localization methods. The metabolite peaks of NAA, Cr, and Cho were visually similar for the six localization methods and were easily quantifiable in LCModel. Unlike MINT which automatically corrects for baseline distortion, baseline correction in the in-house programs used to process SLIM and ROI-averaging was not applied to the spectra since LCModel automatically corrects for this when calculating metabolite quantification. This can be seen especially in the right insular gray matter compartment.

As an initial examination of the metabolite spectra, several compartments of the brain were visually compared for similarity. One of the twenty subjects was chosen and the spectra from the six localization methods were graphed and evaluated across five compartments: right central white matter, left cingulate gray matter, right insula gray matter, left postcentral white matter, and the right precuneus white matter. A visual inspection of the spectra verifies that the two processes provide comparable results. In Figure 15, we see that reductions in the k-space dimensions for the SLIM localization methods resulted in no immediately visible differences between the datasets across a wide range of brain regions, with the main difference between MIDAS' MINT process and our in-house programs was our inclusion of the uncorrected baseline.

Chapter 4: Discussion

Overall this study demonstrates that the SLIM localization methods could provide reliable quantification of compartmental spectra over varying k-space sample sizes. The SLIM reconstruction method with the full k-space data showed highly comparable outcomes to the ROI averaged data in terms of SNR, spectral quality, and metabolite concentrations. A reduction in k-space size in SLIM reconstruction methods showed a correlation with a reduction of SNR, which was the result of reduced effective averaging. Despite this observation, we saw no significant difference in metabolite concentrations for NAA, Cr, and Cho between SLIM and the FT-based reconstruction methods. Therefore, these results suggest that the SLIM localization method can provide reliable quantification of compartmental spectra without requiring acquisition of large resolution k-space data, resulting in shorter scan time by a factor of 4 – 8 times compared with ROI averaging.

Our metabolite creatine ratios matched the results of other studies that have been published. A recent study using MIDAS provided choline creatine ratios observed for the gray and white matter of the frontal, parietal, occipital, temporal and the cerebellum (Goryawala, Sheriff, Stoyanova, & Maudsley, 2018). In addition, the same study observed the choline creatine ratios of the thalamus and putamen. The MINT choline creatine ratios from the study of the regions range from 0.18 - 0.30, which match the results obtained by SLIM, which fall within a range of 0.20 - 0.30 for their respective compartments. The study observed NAA creatine ratios for the Thalamus and Putamen as well at ratios of ~1.4, which closely align with the ratios of the Thalamus and striatum (a compartment which contains the putamen) of this study with a ratio of ~1.3.

Another recent study mapped the NAA and choline ratios of creatine from MIDAS where they recorded these ratios from the gray and white matter regions of the four lobes of the cerebrum (Maudsley et al., 2009). They observed gray matter NAA/Cr ratios of ~1.4 for gray matter and ~1.7 for white matter and Cho/Cr ratios of ~0.2 for gray matter and ~0.3 for white matter. Our creatine ratios showed a wider variation in values, with a NAA/Cr ratio of ~1.3 for gray matter and ~1.5 for white matter and Cho/Cr ratios of ~0.2 for gray matter and ~0.3 for white matter. Interestingly, these differences carried over to our MINT run of the same dataset, which indicates that there was likely a difference in processing between their MINT process and the one used in this study.

In this study we used k-space sizes of 40 x 40 x 12, 20 x 20 x 12 and 16 x 16 x 12 to demonstrate the effect of the reduced k-space data. Because 3D EPSI measures a single line of k-space data (i.e., one dimensional k-space) in a single read, reducing the size of k-space samples in the read direction does not reduce scan time. Instead, reducing k-space sizes by acquiring fewer phase encoding steps from the other spatial encoding directions could be translated into an actual reduced scan time. Further study is necessary to investigate the effect of non-isotropic reduction of the k-space size, e.g., 50 x 10 x 10, on the SLIM localization methods.

While the high correlation between SLIM and ROIS showed that SLIM performs comparatively with the ROI-averaged counterpart, there were improvements that can be made to the post-LCModel filtration settings. One post-LCModel filtration setting that would be useful to implement in future studies is the inclusion of a filtration parameter that filters out metabolite data points based on CRLB results. The current iteration of post-LCModel filtration only filtered out poor quality spectra based on FWHM, SNR, and lipid concentrations, but a more refined filtration system could be programmed that filtered metabolic data on a metabolite basis instead

of simply filtering out whole spectra. A metabolite-based filtration system will be added to future studies as this will likely improve the correlation results observed in the results section.

Chapter 5: Conclusions

SLIM offers a way for us to obtain MR spectra from well-defined compartments with complex shapes. In addition, SLIM provides MR spectra without the need for large k-space acquisitions as is the case with ROI-averaging localization methods. SLIM has the potential to reduce the scan time by 4-8 times with comparable spectral quality of conventional FT-based MRS. Thus, SLIM can be utilized in acquiring MRS for patients who struggle with staying still in an MR scanner such as young children and subjects with minor neurological disorders.

References

Abdul-Kareem, I. A., Stancak, A., Parkes, L. M., & Sluming, V. (2011). Increased gray matter volume of left pars opercularis in male orchestral musicians correlate positively with years of musical performance. *J Magn Reson Imaging, 33*(1), 24-32. doi:10.1002/jmri.22391

Adany, P., Choi, I. Y., & Lee, P. (2016). B0-adjusted and sensitivity-encoded spectral localization by imaging (BASE-SLIM) in the human brain in vivo. *Neuroimage, 134*, 355-364. doi:10.1016/j.neuroimage.2016.04.016

Algin, O., Taskapilioglu, O., Hakyemez, B., Ocakoglu, G., Yurtogullari, S., Erer, S., & Parlak, M. (2010). Structural and neurochemical evaluation of the brain and pons in patients with Wilson's disease. *Jpn J Radiol, 28*(9), 663-671. doi:10.1007/s11604-010-0491-4

Ameis, S. H., & Catani, M. (2015). Altered white matter connectivity as a neural substrate for social impairment in Autism Spectrum Disorder. *Cortex, 62*, 158-181. doi:10.1016/j.cortex.2014.10.014

Anderson, V. C., Obayashi, J. T., Kaye, J. A., Quinn, J. F., Berryhill, P., Riccelli, L. P., . . . Rooney, W. D. (2014). Longitudinal relaxographic imaging of white matter hyperintensities in the elderly. *Fluids Barriers CNS, 11*, 24. doi:10.1186/2045-8118-11-24

Andrade, C. S., Otaduy, M. C., Valente, K. D., Park, E. J., Kanas, A. F., Silva Filho, M. R., . . . Leite, C. C. (2014). Widespread pH abnormalities in patients with malformations of cortical development and epilepsy: a phosphorus-31 brain MR spectroscopy study. *Brain Dev, 36*(10), 899-906. doi:10.1016/j.braindev.2013.12.010

Bottomley, P. A. (1987). Spatial localization in NMR spectroscopy in vivo. *Ann N Y Acad Sci, 508*, 333-348.

Brandao, L. A., & Castillo, M. (2013). Adult brain tumors: clinical applications of magnetic resonance spectroscopy. *Neuroimaging Clin N Am, 23*(3), 527-555. doi:10.1016/j.nic.2013.03.002

Brugger, S., Davis, J. M., Leucht, S., & Stone, J. M. (2011). Proton magnetic resonance spectroscopy and illness stage in schizophrenia--a systematic review and meta-analysis. *Biol Psychiatry, 69*(5), 495-503. doi:10.1016/j.biopsych.2010.10.004

Bruhn, H., Frahm, J., Gyngell, M. L., Merboldt, K. D., Hanicke, W., Sauter, R., & Hamburger, C. (1989). Noninvasive differentiation of tumors with use of localized H-1 MR spectroscopy in vivo: initial experience in patients with cerebral tumors. *Radiology, 172*(2), 541-548. doi:10.1148/radiology.172.2.2748837

Carreiras, M., Seghier, M. L., Baquero, S., Estevez, A., Lozano, A., Devlin, J. T., & Price, C. J. (2009). An anatomical signature for literacy. *Nature, 461*(7266), 983-986. doi:10.1038/nature08461

Catani, M., Dell'acqua, F., Bizzi, A., Forkel, S. J., Williams, S. C., Simmons, A., . . . Thiebaut de Schotten, M. (2012). Beyond cortical localization in clinico-anatomical correlation. *Cortex, 48*(10), 1262-1287. doi:10.1016/j.cortex.2012.07.001

Cavassila, S., Deval, S., Huegen, C., van Ormondt, D., & Graveron-Demilly, D. (2000). Cramer-Rao bound expressions for parametric estimation of overlapping peaks: influence of prior knowledge. *J Magn Reson, 143*(2), 311-320. doi:10.1006/jmre.1999.2002

Choi, I. Y., Lee, S. P., Merkle, H., & Shen, J. (2006). In vivo detection of gray and white matter differences in GABA concentration in the human brain. *Neuroimage, 33*(1), 85-93. doi:10.1016/j.neuroimage.2006.06.016

Ciurleo, R., Di Lorenzo, G., Bramanti, P., & Marino, S. (2014). Magnetic resonance spectroscopy: an in vivo molecular imaging biomarker for Parkinson's disease? *Biomed Res Int, 2014*, 519816. doi:10.1155/2014/519816

Dale, A. M., Fischl, B., & Sereno, M. I. (1999). Cortical surface-based analysis. I. Segmentation and surface reconstruction. *Neuroimage, 9*(2), 179-194. doi:10.1006/nimg.1998.0395

Dale, A. M., & Sereno, M. I. (1993). Improved Localizadon of Cortical Activity by Combining EEG and MEG with MRI Cortical Surface Reconstruction: A Linear Approach. *J Cogn Neurosci, 5*(2), 162-176. doi:10.1162/jocn.1993.5.2.162

Damasio, A. R. (1984). Behavioral Neurology - Research and Practice. *Seminars in Neurology, 4*(2), 117-119. doi:DOI 10.1055/s-2008-1041540

Desikan, R. S., Segonne, F., Fischl, B., Quinn, B. T., Dickerson, B. C., Blacker, D., . . . Killiany, R. J. (2006). An automated labeling system for subdividing the human cerebral cortex on MRI scans into gyral based regions of interest. *Neuroimage, 31*(3), 968-980. doi:10.1016/j.neuroimage.2006.01.021

Destrieux, C., Fischl, B., Dale, A., & Halgren, E. (2010). Automatic parcellation of human cortical gyri and sulci using standard anatomical nomenclature. *Neuroimage, 53*(1), 1-15. doi:10.1016/j.neuroimage.2010.06.010

Duguid, J. R., De La Paz, R., & DeGroot, J. (1986). Magnetic resonance imaging of the midbrain in Parkinson's disease. *Ann Neurol, 20*(6), 744-747. doi:10.1002/ana.410200618

Dunst, B., Benedek, M., Koschutnig, K., Jauk, E., & Neubauer, A. C. (2014). Sex differences in the IQ-white matter microstructure relationship: a DTI study. *Brain Cogn, 91*, 71-78. doi:10.1016/j.bandc.2014.08.006

Fazekas, F., Ropele, S., Enzinger, C., Seifert, T., & Strasser-Fuchs, S. (2002). Quantitative magnetization transfer imaging of pre-lesional white-matter changes in multiple sclerosis. *Mult Scler, 8*(6), 479-484. doi:10.1191/1352458502ms860oa

Felmlee, J. P., & Ehman, R. L. (1987). Spatial presaturation: a method for suppressing flow artifacts and improving depiction of vascular anatomy in MR imaging. *Radiology, 164*(2), 559-564. doi:10.1148/radiology.164.2.3602402

Fischl, B., van der Kouwe, A., Destrieux, C., Halgren, E., Segonne, F., Salat, D. H., . . . Dale, A. M. (2004). Automatically parcellating the human cerebral cortex. *Cereb Cortex, 14*(1), 11-22.

Foerster, B. R., Pomper, M. G., Callaghan, B. C., Petrou, M., Edden, R. A., Mohamed, M. A., . . . Feldman, E. L. (2013). An imbalance between excitatory and inhibitory neurotransmitters in amyotrophic lateral sclerosis revealed by use of 3-T proton magnetic resonance spectroscopy. *JAMA Neurol, 70*(8), 1009-1016. doi:10.1001/jamaneurol.2013.234

Friedman, S. D., Shaw, D. W., Artru, A. A., Dawson, G., Petropoulos, H., & Dager, S. R. (2006). Gray and white matter brain chemistry in young children with autism. *Arch Gen Psychiatry, 63*(7), 786-794. doi:10.1001/archpsyc.63.7.786

Gardner, A. J., Iverson, G. L., Wojtowicz, M., Levi, C. R., Kay-Lambkin, F., Schofield, P. W., . . . Stanwell, P. (2017). MR Spectroscopy Findings in Retired Professional Rugby League Players. *Int J Sports Med, 38*(3), 241-252. doi:10.1055/s-0042-120843

Goryawala, M. Z., Sheriff, S., Stoyanova, R., & Maudsley, A. A. (2018). Spectral decomposition for resolving partial volume effects in MRSI. *Magn Reson Med, 79*(6), 2886-2895. doi:10.1002/mrm.26991

Guo, Z., Zhang, J., Liu, X., Hou, H., Cao, Y., Wei, F., . . . Chen, W. (2015). Neurometabolic characteristics in the anterior cingulate gyrus of Alzheimer's disease patients with depression: a (1)H magnetic resonance spectroscopy study. *BMC Psychiatry, 15*, 306. doi:10.1186/s12888-015-0691-7

Gur, R. C., Turetsky, B. I., Matsui, M., Yan, M., Bilker, W., Hughett, P., & Gur, R. E. (1999). Sex differences in brain gray and white matter in healthy young adults: correlations with cognitive performance. *J Neurosci, 19*(10), 4065-4072.

Haase, A., Frahm, J., Matthaei, D., Hanicke, W., Bomsdorf, H., Kunz, D., & Tischler, R. (1986). MR imaging using stimulated echoes (STEAM). *Radiology, 160*(3), 787-790. doi:10.1148/radiology.160.3.3737918

Hardan, A. Y., Minshew, N. J., Melhem, N. M., Srihari, S., Jo, B., Bansal, R., . . . Stanley, J. A. (2008). An MRI and proton spectroscopy study of the thalamus in children with autism. *Psychiatry Res, 163*(2), 97-105. doi:10.1016/j.pscychresns.2007.12.002

Horska, A., Kaufmann, W. E., Brant, L. J., Naidu, S., Harris, J. C., & Barker, P. B. (2002). In vivo quantitative proton MRSI study of brain development from childhood to adolescence. *J Magn Reson Imaging, 15*(2), 137-143.

Hu, X., Levin, D. N., Lauterbur, P. C., & Spraggins, T. (1988). SLIM: spectral localization by imaging. *Magn Reson Med, 8*(3), 314-322.

Jacobs, M. A., Horska, A., van Zijl, P. C., & Barker, P. B. (2001). Quantitative proton MR spectroscopic imaging of normal human cerebellum and brain stem. *Magn Reson Med, 46*(4), 699-705.

Jiji, S., Smitha, K. A., Gupta, A. K., Pillai, V. P., & Jayasree, R. S. (2013). Segmentation and volumetric analysis of the caudate nucleus in Alzheimer's disease. *Eur J Radiol, 82*(9), 1525-1530. doi:10.1016/j.ejrad.2013.03.012

Jovicich, J., Czanner, S., Greve, D., Haley, E., van der Kouwe, A., Gollub, R., . . . Dale, A. (2006). Reliability in multi-site structural MRI studies: effects of gradient non-linearity correction on phantom and human data. *Neuroimage, 30*(2), 436-443. doi:10.1016/j.neuroimage.2005.09.046

Kitamura, H., Shioiri, T., Kimura, T., Ohkubo, M., Nakada, T., & Someya, T. (2006). Parietal white matter abnormalities in obsessive-compulsive disorder: a magnetic resonance spectroscopy study at 3-Tesla. *Acta Psychiatr Scand, 114*(2), 101-108. doi:10.1111/j.1600-0447.2006.00858.x

Kreis, R. (2004). Issues of spectral quality in clinical 1H-magnetic resonance spectroscopy and a gallery of artifacts. *NMR Biomed, 17*(6), 361-381. doi:10.1002/nbm.891

Lai, T. H., Fuh, J. L., Lirng, J. F., Lin, C. P., & Wang, S. J. (2012). Brainstem 1H-MR spectroscopy in episodic and chronic migraine. *J Headache Pain, 13*(8), 645-651. doi:10.1007/s10194-012-0491-0

Lambert, J. B., Binsch, G., & Roberts, J. D. (1964). Nitrogen-15 Magnetic Resonance Spectroscopy. I. Chemical Shifts. *Proc Natl Acad Sci U S A, 51*, 735-737.

Lee, P., Adany, P., & Choi, I. Y. (2017). Imaging based magnetic resonance spectroscopy (MRS) localization for quantitative neurochemical analysis and cerebral metabolism studies. *Anal Biochem, 529*, 40-47. doi:10.1016/j.ab.2017.01.007

Luders, E., Gaser, C., Narr, K. L., & Toga, A. W. (2009). Why sex matters: brain size independent differences in gray matter distributions between men and women. *J Neurosci*, *29*(45), 14265-14270. doi:10.1523/JNEUROSCI.2261-09.2009

Matejko, A. A., & Ansari, D. (2015). Drawing connections between white matter and numerical and mathematical cognition: a literature review. *Neurosci Biobehav Rev, 48*, 35-52. doi:10.1016/j.neubiorev.2014.11.006

Maudsley, A. A., Darkazanli, A., Alger, J. R., Hall, L. O., Schuff, N., Studholme, C., . . . Zhu, X. (2006). Comprehensive processing, display and analysis for in vivo MR spectroscopic imaging. *NMR Biomed, 19*(4), 492-503. doi:10.1002/nbm.1025

Maudsley, A. A., Domenig, C., Govind, V., Darkazanli, A., Studholme, C., Arheart, K., & Bloomer, C. (2009). Mapping of brain metabolite distributions by volumetric proton MR spectroscopic imaging (MRSI). *Magn Reson Med, 61*(3), 548-559. doi:10.1002/mrm.21875

Metzger, G., & Hu, X. (1997). Application of interlaced Fourier transform to echo-planar spectroscopic imaging. *J Magn Reson, 125*(1), 166-170. doi:10.1006/jmre.1997.1114

Minati, L., Aquino, D., Bruzzone, M. G., & Erbetta, A. (2010). Quantitation of normal metabolite concentrations in six brain regions by in-vivoH-MR spectroscopy. *J Med Phys, 35*(3), 154-163. doi:10.4103/0971-6203.62128

Pannek, K., Boyd, R. N., Fiori, S., Guzzetta, A., & Rose, S. E. (2014). Assessment of the structural brain network reveals altered connectivity in children with unilateral cerebral palsy due to periventricular white matter lesions. *Neuroimage Clin, 5*, 84-92. doi:10.1016/j.nicl.2014.05.018

Park, I., Larson, P. E., Tropp, J. L., Carvajal, L., Reed, G., Bok, R., . . . Nelson, S. J. (2014). Dynamic hyperpolarized carbon-13 MR metabolic imaging of nonhuman primate brain. *Magn Reson Med, 71*(1), 19-25. doi:10.1002/mrm.25003

Posse, S., Tedeschi, G., Risinger, R., Ogg, R., & Le Bihan, D. (1995). High speed 1H spectroscopic imaging in human brain by echo planar spatial-spectral encoding. *Magn Reson Med, 33*(1), 34-40.

Provencher, S. W. (1993). Estimation of metabolite concentrations from localized in vivo proton NMR spectra. *Magn Reson Med, 30*(6), 672-679.

Pyatigorskaya, N., Gallea, C., Garcia-Lorenzo, D., Vidailhet, M., & Lehericy, S. (2014). A review of the use of magnetic resonance imaging in Parkinson's disease. *Ther Adv Neurol Disord, 7*(4), 206-220. doi:10.1177/1756285613511507

Resnick, S. M., Pham, D. L., Kraut, M. A., Zonderman, A. B., & Davatzikos, C. (2003). Longitudinal magnetic resonance imaging studies of older adults: a shrinking brain. *J Neurosci, 23*(8), 3295-3301.

Reyngoudt, H., Paemeleire, K., Descamps, B., De Deene, Y., & Achten, E. (2011). 31P-MRS demonstrates a reduction in high-energy phosphates in the occipital lobe of migraine without aura patients. *Cephalalgia, 31*(12), 1243-1253. doi:10.1177/0333102410394675

Rincon, S. P., Blitstein, M. B., Caruso, P. A., Gonzalez, R. G., Thibert, R. L., & Ratai, E. M. (2016). The Use of Magnetic Resonance Spectroscopy in the Evaluation of Pediatric Patients With Seizures. *Pediatr Neurol, 58*, 57-66. doi:10.1016/j.pediatrneurol.2016.01.013

Rosso, I. M., Crowley, D. J., Silveri, M. M., Rauch, S. L., & Jensen, J. E. (2017). Hippocampus Glutamate and N-Acetyl Aspartate Markers of Excitotoxic Neuronal Compromise in

Posttraumatic Stress Disorder. *Neuropsychopharmacology, 42*(8), 1698-1705. doi:10.1038/npp.2017.32

Sharma, K. R., Saigal, G., Maudsley, A. A., & Govind, V. (2011). 1H MRS of basal ganglia and thalamus in amyotrophic lateral sclerosis. *NMR Biomed, 24*(10), 1270-1276. doi:10.1002/nbm.1687

Sluming, V., Barrick, T., Howard, M., Cezayirli, E., Mayes, A., & Roberts, N. (2002). Voxel-based morphometry reveals increased gray matter density in Broca's area in male symphony orchestra musicians. *Neuroimage, 17*(3), 1613-1622.

Sours, C., George, E. O., Zhuo, J., Roys, S., & Gullapalli, R. P. (2015). Hyper-connectivity of the thalamus during early stages following mild traumatic brain injury. *Brain Imaging Behav, 9*(3), 550-563. doi:10.1007/s11682-015-9424-2

Sowell, E. R., Peterson, B. S., Thompson, P. M., Welcome, S. E., Henkenius, A. L., & Toga, A. W. (2003). Mapping cortical change across the human life span. *Nat Neurosci, 6*(3), 309-315. doi:10.1038/nn1008

Steriade, M., & Llinas, R. R. (1988). The Functional-States of the Thalamus and the Associated Neuronal Interplay. *Physiological Reviews, 68*(3), 649-742.

Surmeier, D. J., Mercer, J. N., & Chan, C. S. (2005). Autonomous pacemakers in the basal ganglia: who needs excitatory synapses anyway? *Curr Opin Neurobiol, 15*(3), 312-318. doi:10.1016/j.conb.2005.05.007

Thomas, L. A., Kim, P., Bones, B. L., Hinton, K. E., Milch, H. S., Reynolds, R. C., . . . Leibenluft, E. (2013). Elevated amygdala responses to emotional faces in youths with chronic irritability or bipolar disorder. *Neuroimage Clin, 2*, 637-645. doi:10.1016/j.nicl.2013.04.007

Tisserand, D. J., van Boxtel, M. P., Pruessner, J. C., Hofman, P., Evans, A. C., & Jolles, J. (2004). A voxel-based morphometric study to determine individual differences in gray matter density associated with age and cognitive change over time. *Cereb Cortex, 14*(9), 966-973. doi:10.1093/cercor/bhh057

Tong, J., Geng, H., Zhang, Z., Zhu, X., Meng, Q., Sun, X., . . . Liang, Q. (2014). Brain metabolite alterations demonstrated by proton magnetic resonance spectroscopy in diabetic patients with retinopathy. *Magn Reson Imaging, 32*(8), 1037-1042. doi:10.1016/j.mri.2014.04.020

Tramoni, E., Felician, O., Barbeau, E. J., Guedj, E., Guye, M., Bartolomei, F., & Ceccaldi, M. (2011). Long-term consolidation of declarative memory: insight from temporal lobe epilepsy. *Brain, 134*(Pt 3), 816-831. doi:10.1093/brain/awr002

Ullen, F. (2009). Is activity regulation of late myelination a plastic mechanism in the human nervous system? *Neuron Glia Biol, 5*(1-2), 29-34. doi:10.1017/S1740925X09990330

Wang, S., Zhou, M., Chen, T., Yang, X., Chen, G., Wang, M., & Gong, Q. (2017). Examining gray matter structure associated with academic performance in a large sample of Chinese high school students. *Sci Rep, 7*(1), 893. doi:10.1038/s41598-017-00677-9

Wang, S. Y., Wang, M., Wang, X. X., Chen, W., Sheng, C., & Gong, Z. K. (2017). Study on the clinical application of the MRS in the cognitive assessment after stroke. *Eur Rev Med Pharmacol Sci, 21*(10), 2437-2442.

Wang, Y., & Li, S. J. (1998). Differentiation of metabolic concentrations between gray matter and white matter of human brain by in vivo 1H magnetic resonance spectroscopy. *Magn Reson Med, 39*(1), 28-33.

Xu, J., Dydak, U., Harezlak, J., Nixon, J., Dzemidzic, M., Gunn, A. D., . . . Anand, A. (2013). Neurochemical abnormalities in unmedicated bipolar depression and mania: a 2D 1H MRS investigation. *Psychiatry Res, 213*(3), 235-241. doi:10.1016/j.pscychresns.2013.02.008

Zhang, L., & Sui, R. B. (2017). Proton Magnetic Resonance Spectroscopy Study on the Metabolism Changes of Cerebellum in Patients with Post-Stroke Depression. *Cell Physiol Biochem, 41*(4), 1393-1402. doi:10.1159/000467907

Ziabreva, I., Poeggel, G., Schnabel, R., & Braun, K. (2003). Separation-induced receptor changes in the hippocampus and amygdala of Octodon degus: influence of maternal vocalizations. *J Neurosci, 23*(12), 5329-5336.

Appendix

Table 8: Metabolite concentrations averaged across all compartments.

		MINT 50x50x18	ROIS 50x50x18	SLIM 50x50x12	SLIM 40x40x12	SLIM 20x20x12	SLIM 16x16x12
All	NAA	31.2	32.5	32.9	32.8	33.5	33.8
	Cr	26.8	26.0	26.3	26.2	26.7	26.9
	Cho	5.5	5.7	5.8	5.8	5.9	6.0
	ml	15.1	15.5	15.3	15.2	15.3	15.5
	Glx	9.8	9.6	9.8	10.0	11.4	12.4
	NAA / Cr	1.2	1.3	1.3	1.3	1.3	1.3
	Cho / Cr	0.2	0.2	0.2	0.2	0.2	0.2
	ml / Cr	0.6	0.6	0.6	0.6	0.6	0.6
	Glx / Cr	0.4	0.4	0.4	0.4	0.4	0.5
L. Central GM	NAA	35.6	33.5	31.7	31.2	28.5	27.3
	Cr	27.3	24.4	23.7	23.6	20.7	19.0
	Cho	4.8	4.4	4.1	3.9	3.3	3.5
	ml	12.7	11.4	10.2	10.2	8.3	7.9
	Glx	7.5	10.0	6.3	11.7	7.7	4.1
	NAA / Cr	1.3	1.4	1.4	1.3	1.4	1.5
	Cho / Cr	0.2	0.2	0.2	0.2	0.2	0.2
	ml / Cr	0.5	0.5	0.4	0.4	0.4	0.4
	Glx / Cr	0.3	0.4	0.3	0.5	0.4	0.2
L. Cerebellum GM	NAA	21.8	26.3	27.1	27.8	28.7	28.3
	Cr	30.5	38.4	38.5	38.5	39.5	38.0
	Cho	5.8	8.5	8.2	8.3	8.3	7.8
	ml	15.7	18.1	18.5	18.0	19.8	17.8
	Glx	14.5	14.7	12.5	14.1	12.4	12.7
	NAA / Cr	0.7	0.7	0.7	0.8	0.7	0.8
	Cho / Cr	0.2	0.2	0.2	0.2	0.2	0.2
	ml / Cr	0.5	0.5	0.5	0.5	0.5	0.5
	Glx / Cr	0.5	0.4	0.3	0.5	0.3	0.4
L. Cingulate GM	NAA	30.2	34.2	34.8	34.5	36.9	38.1
	Cr	27.6	27.3	29.8	29.4	31.5	30.9
	Cho	5.8	6.5	6.6	6.4	6.8	7.1
	ml	15.6	17.3	18.3	18.2	18.9	18.4
	Glx	4.2	4.3	7.2	10.6	8.3	11.5
	NAA / Cr	1.1	1.3	1.2	1.2	1.2	1.3
	Cho / Cr	0.2	0.2	0.2	0.2	0.2	0.2
	ml / Cr	0.6	0.6	0.6	0.6	0.6	0.6
	Glx / Cr	0.2	0.2	0.3	0.4	0.3	0.4
L. Fusiform GM	NAA	24.1	29.7	29.9	29.3	31.4	28.6
	Cr	21.8	26.8	26.6	26.4	29.4	27.9
	Cho	4.9	6.2	6.4	6.4	6.9	6.6
	ml	13.9	16.1	15.9	16.0	18.6	17.1
	Glx	8.9	10.7	11.6	9.2	14.8	16.4
	NAA / Cr	1.1	1.1	1.1	1.1	1.1	1.0
	Cho / Cr	0.2	0.2	0.2	0.3	0.2	0.2
	ml / Cr	0.7	0.6	0.6	0.6	0.6	0.8
	Glx / Cr	0.4	0.4	0.4	0.3	0.5	1.5

		MINT 50x50x18	ROIS 50x50x18	SLIM 50x50x12	SLIM 40x40x12	SLIM 20x20x12	SLIM 16x16x12
Brain Stem	NAA	12.7	17.6	18.2	18.1	18.0	18.2
	Cr	17.1	20.0	20.6	20.5	21.4	22.4
	Cho	5.2	6.0	6.3	6.6	6.5	6.5
	ml	13.1	12.7	13.6	13.6	12.5	15.1
	Glx	4.4	6.6	6.9	4.7	3.4	2.7
	NAA / Cr	0.8	0.9	0.9	0.9	0.9	0.9
	Cho / Cr	0.3	0.3	0.3	0.4	0.3	0.3
	ml / Cr	0.8	0.7	0.7	0.7	0.6	0.7
	Glx / Cr	0.3	0.3	0.3	0.3	0.2	0.2
L. Central WM	NAA	34.8	36.6	37.9	38.3	40.4	41.4
	Cr	25.8	26.3	26.9	26.9	27.7	27.5
	Cho	4.9	5.3	5.7	5.7	6.1	6.2
	ml	11.8	13.2	13.9	13.4	13.8	14.1
	Glx	6.3	9.3	8.3	6.5	6.4	12.5
	NAA / Cr	1.4	1.4	1.4	1.4	1.5	1.5
	Cho / Cr	0.2	0.2	0.2	0.2	0.2	0.2
	ml / Cr	0.5	0.5	0.5	0.5	0.5	0.5
	Glx / Cr	0.3	0.4	0.3	0.3	0.2	0.4
L. Cerebellum WM	NAA	20.8	24.6	26.2	26.2	27.2	28.6
	Cr	31.4	36.6	38.4	38.4	41.2	44.1
	Cho	6.5	8.5	9.0	9.3	9.5	10.2
	ml	16.4	20.8	20.8	19.9	20.3	20.6
	Glx	9.7	11.5	14.1	12.1	9.0	13.7
	NAA / Cr	0.7	0.7	0.7	0.7	0.7	0.7
	Cho / Cr	0.2	0.2	0.2	0.2	0.2	0.2
	ml / Cr	0.5	0.6	0.6	0.5	0.5	0.5
	Glx / Cr	0.3	0.3	0.4	0.3	0.3	0.3
L. Cingulate WM	NAA	26.4	32.7	32.3	32.1	30.7	29.3
	Cr	22.2	23.0	22.1	21.8	20.3	19.4
	Cho	5.8	6.3	6.6	6.6	6.3	6.0
	ml	13.4	15.4	15.2	15.2	15.3	13.5
	Glx	2.8	7.8	8.3	10.2	6.7	6.8
	NAA / Cr	1.2	1.4	1.5	1.5	1.5	1.5
	Cho / Cr	0.3	0.3	0.3	0.3	0.3	0.3
	ml / Cr	0.6	0.7	0.7	0.7	0.8	0.7
	Glx / Cr	0.1	0.4	0.4	0.5	0.4	0.4
L. Fusiform WM	NAA	24.4	30.2	29.5	30.2	30.4	38.8
	Cr	20.9	25.1	23.9	24.2	22.7	32.5
	Cho	5.2	6.2	7.1	7.2	7.1	9.5
	ml	13.1	16.3	15.6	15.8	18.6	25.3
	Glx	8.0	7.6	4.3	6.7	2.8	9.2
	NAA / Cr	1.2	1.2	1.3	1.3	1.4	1.3
	Cho / Cr	0.3	0.3	0.3	0.3	0.3	0.3
	ml / Cr	0.7	0.7	0.7	0.7	0.8	0.9
	Glx / Cr	0.4	0.3	0.2	0.2	0.1	0.4

		MINT 50x50x18	ROIS 50x50x18	SLIM 50x50x12	SLIM 40x40x12	SLIM 20x20x12	SLIM 16x16x12
Ventral Diencephalon	NAA	20.3	20.9	19.2	19.0	19.7	19.1
	Cr	18.4	17.9	17.5	17.7	18.1	17.4
	Cho	5.4	5.8	5.6	5.7	5.5	5.6
	ml	11.8	12.0	12.4	12.3	13.7	11.9
	Glx	6.8	8.0	7.0	8.0	12.5	5.5
	NAA / Cr	1.1	1.2	1.1	1.1	1.1	1.1
	Cho / Cr	0.3	0.3	0.3	0.3	0.3	0.3
	ml / Cr	0.7	0.7	0.7	0.7	0.8	0.7
	Glx / Cr	0.4	0.5	0.4	0.4	0.6	0.3
R. Central GM	NAA	35.8	33.6	32.5	32.8	33.1	31.6
	Cr	28.5	24.9	24.0	24.2	23.3	22.3
	Cho	4.9	4.2	3.8	3.6	3.6	3.5
	ml	13.1	10.7	9.9	9.5	8.9	8.0
	Glx	7.1	6.9	8.1	7.1	7.6	7.7
	NAA / Cr	1.3	1.4	1.4	1.4	1.5	1.5
	Cho / Cr	0.2	0.2	0.2	0.2	0.2	0.2
	ml / Cr	0.5	0.4	0.4	0.4	0.4	0.4
	Glx / Cr	0.3	0.3	0.4	0.3	0.4	0.4
R. Cerebellum GM	NAA	25.6	23.6	25.5	25.4	26.3	24.5
	Cr	36.5	34.0	33.8	33.8	33.7	32.4
	Cho	7.4	7.5	6.8	6.8	7.0	6.7
	ml	19.6	16.4	16.8	16.6	16.0	15.4
	Glx	18.1	10.0	14.3	12.1	11.6	11.9
	NAA / Cr	0.7	0.7	0.7	0.7	0.8	0.8
	Cho / Cr	0.2	0.2	0.2	0.2	0.2	0.2
	ml / Cr	0.5	0.5	0.5	0.5	0.5	0.5
	Glx / Cr	0.6	0.3	0.4	0.4	0.3	0.4
R. Cingulate GM	NAA	31.3	32.7	34.0	34.3	33.6	34.1
	Cr	28.9	25.4	28.2	28.2	27.3	27.4
	Cho	5.9	6.1	6.6	6.7	6.5	6.7
	ml	16.0	17.5	18.7	19.0	18.4	19.6
	Glx	3.7	12.6	12.7	14.0	9.5	6.5
	NAA / Cr	1.1	1.3	1.2	1.2	1.3	1.3
	Cho / Cr	0.2	0.2	0.2	0.2	0.2	0.3
	ml / Cr	0.6	0.7	0.7	0.7	0.7	0.7
	Glx / Cr	0.1	0.5	0.5	0.5	0.4	0.3
R. Fusiform GM	NAA	28.7	25.5	26.2	25.9	27.6	28.9
	Cr	26.8	23.2	23.3	24.0	27.1	27.3
	Cho	5.9	5.7	5.8	5.7	6.3	6.3
	ml	16.8	14.0	14.4	14.4	16.2	20.2
	Glx	11.1	7.2	7.5	8.3	7.4	13.7
	NAA / Cr	1.1	1.1	1.1	1.1	1.0	1.1
	Cho / Cr	0.2	0.3	0.3	0.2	0.2	0.2
	ml / Cr	0.6	0.6	0.6	0.6	0.6	0.8
	Glx / Cr	0.4	0.3	0.4	0.4	0.3	0.6

		MINT 50x50x18	ROIS 50x50x18	SLIM 50x50x12	SLIM 40x40x12	SLIM 20x20x12	SLIM 16x16x12
Ventricles	NAA	22.9	25.8	23.9	24.3	23.5	24.6
	Cr	19.1	18.7	16.8	16.7	16.4	17.3
	Cho	6.0	5.6	5.5	5.6	5.7	5.9
	ml	12.2	14.5	13.7	14.4	13.0	14.6
	Glx	3.9	6.2	4.2	5.0	3.2	5.6
	NAA / Cr	1.2	1.4	1.4	1.5	1.5	1.4
	Cho / Cr	0.3	0.3	0.3	0.3	0.4	0.4
	ml / Cr	0.6	0.8	0.8	0.9	0.8	0.8
	Glx / Cr	0.2	0.3	0.2	0.3	0.2	0.3
R. Central WM	NAA	36.2	35.3	35.8	36.3	36.4	36.4
	Cr	27.9	25.4	25.3	25.3	24.8	24.9
	Cho	5.3	4.9	5.0	5.1	5.2	5.3
	ml	13.1	12.4	11.4	12.7	13.6	13.2
	Glx	3.4	17.2	13.3	20.5	21.3	19.6
	NAA / Cr	1.3	1.4	1.4	1.5	1.5	1.5
	Cho / Cr	0.2	0.2	0.2	0.2	0.2	0.2
	ml / Cr	0.5	0.5	0.5	0.5	0.6	0.5
	Glx / Cr	0.1	0.7	0.7	0.9	1.0	1.0
R. Cerebellum WM	NAA	24.6	23.7	23.5	23.6	23.6	24.8
	Cr	36.9	33.9	36.0	36.0	38.3	37.7
	Cho	7.8	7.8	8.6	8.6	8.5	9.0
	ml	17.9	18.3	19.0	19.2	20.2	21.9
	Glx	10.9	10.4	8.9	9.8	11.2	9.1
	NAA / Cr	0.7	0.7	0.7	0.7	0.6	0.6
	Cho / Cr	0.2	0.2	0.2	0.3	0.3	0.2
	ml / Cr	0.5	0.6	0.6	0.6	0.6	0.6
	Glx / Cr	0.3	0.3	0.3	0.4	0.4	0.3
R. Cingulate WM	NAA	27.6	29.8	29.5	29.2	28.6	27.2
	Cr	23.3	21.2	20.1	19.4	19.2	18.1
	Cho	5.9	6.0	6.2	6.2	6.0	5.7
	ml	13.8	15.7	14.7	14.7	14.4	13.5
	Glx	4.3	6.0	5.2	6.0	4.4	6.3
	NAA / Cr	1.2	1.4	1.5	1.5	1.5	1.5
	Cho / Cr	0.3	0.3	0.3	0.3	0.3	0.3
	ml / Cr	0.6	0.8	0.7	0.8	0.8	0.8
	Glx / Cr	0.2	0.3	0.3	0.3	0.3	0.5
R. Fusiform WM	NAA	28.0	27.2	25.2	25.3	26.6	30.7
	Cr	23.6	22.3	20.9	20.9	21.4	25.6
	Cho	6.2	5.6	5.5	5.7	5.9	7.1
	ml	15.3	14.3	14.9	15.0	15.9	21.8
	Glx	9.2	6.1	6.0	5.5	6.3	15.3
	NAA / Cr	1.2	1.2	1.2	1.2	1.3	1.3
	Cho / Cr	0.3	0.3	0.3	0.3	0.3	0.3
	ml / Cr	0.7	0.7	0.7	0.8	0.8	0.9
	Glx / Cr	0.4	0.3	0.3	0.3	0.3	0.7

		MINT 50x50x18	ROIS 50x50x18	SLIM 50x50x12	SLIM 40x40x12	SLIM 20x20x12	SLIM 16x16x12
L. Inferior Parietal GM	NAA	37.3	38.4	38.6	39.1	41.0	40.5
	Cr	30.0	28.0	29.8	30.2	32.5	32.3
	Cho	5.3	5.4	5.3	5.4	5.4	5.2
	ml	16.7	19.7	19.8	19.6	20.6	20.7
	Glx	12.7	10.5	11.4	11.6	17.7	18.2
	NAA / Cr	1.2	1.4	1.3	1.3	1.3	1.3
	Cho / Cr	0.2	0.2	0.2	0.2	0.2	0.2
	ml / Cr	0.6	0.7	0.7	0.7	0.6	0.6
	Glx / Cr	0.4	0.4	0.4	0.4	0.6	0.6
L. Inferior Temporal GM	NAA	28.5	30.3	32.9	32.8	32.4	30.8
	Cr	24.2	23.2	26.0	26.0	25.9	25.1
	Cho	4.8	5.4	5.6	5.5	5.5	5.4
	ml	15.2	14.7	15.0	15.1	13.9	13.2
	Glx	12.8	11.2	13.5	13.6	10.0	8.5
	NAA / Cr	1.2	1.3	1.3	1.3	1.3	1.3
	Cho / Cr	0.2	0.2	0.2	0.2	0.2	0.2
	ml / Cr	0.6	0.6	0.6	0.6	0.6	0.6
	Glx / Cr	0.5	0.5	0.5	0.5	0.4	0.3
L. Insula GM	NAA	31.1	34.2	35.0	35.2	36.9	39.3
	Cr	29.0	29.2	30.5	30.5	33.0	35.3
	Cho	7.0	7.1	7.1	7.4	8.1	8.8
	ml	16.6	17.1	19.1	17.3	17.9	18.8
	Glx	6.1	4.9	15.4	9.4	6.9	25.2
	NAA / Cr	1.1	1.2	1.2	1.2	1.1	1.1
	Cho / Cr	0.2	0.3	0.2	0.3	0.3	0.3
	ml / Cr	0.6	0.6	0.6	0.6	0.6	0.5
	Glx / Cr	0.2	0.2	0.5	0.3	0.2	0.7
L. Lateral Occipital GM	NAA	29.0	35.1	35.7	36.2	37.7	40.0
	Cr	23.1	27.3	27.5	27.6	27.9	28.9
	Cho	3.8	4.9	4.8	4.9	4.8	5.1
	ml	14.1	16.3	15.7	15.5	15.3	16.2
	Glx	14.1	13.9	10.8	11.2	18.6	17.9
	NAA / Cr	1.3	1.3	1.3	1.3	1.4	1.4
	Cho / Cr	0.2	0.2	0.2	0.2	0.2	0.2
	ml / Cr	0.6	0.6	0.6	0.6	0.6	0.6
	Glx / Cr	0.7	0.5	0.4	0.4	0.7	0.6
L. Lingual GM	NAA	28.2	34.0	33.0	32.9	33.1	30.8
	Cr	23.8	28.7	27.6	27.5	28.9	27.5
	Cho	3.7	4.7	4.4	4.4	4.0	4.2
	ml	14.6	18.9	17.0	16.8	15.2	15.2
	Glx	7.0	12.1	9.6	7.6	5.3	6.4
	NAA / Cr	1.2	1.2	1.2	1.2	1.2	1.2
	Cho / Cr	0.2	0.2	0.2	0.2	0.1	0.1
	ml / Cr	0.6	0.7	0.6	0.6	0.5	0.6
	Glx / Cr	0.3	0.5	0.4	0.3	0.2	0.2

		MINT 50x50x18	ROIS 50x50x18	SLIM 50x50x12	SLIM 40x40x12	SLIM 20x20x12	SLIM 16x16x12
L. Inferior Parietal WM	NAA	34.0	38.0	38.5	38.2	37.8	38.3
	Cr	27.8	25.9	26.0	25.9	24.4	24.4
	Cho	5.0	5.7	5.8	5.8	6.2	6.6
	ml	15.7	18.1	17.5	17.1	15.6	14.7
	Glx	12.4	7.3	4.4	6.8	5.7	32.1
	NAA / Cr	1.2	1.5	1.5	1.5	1.6	1.6
	Cho / Cr	0.2	0.2	0.2	0.2	0.3	0.3
	ml / Cr	0.6	0.7	0.7	0.7	0.7	0.6
	Glx / Cr	0.4	0.3	0.2	0.2	0.3	1.3
L. Inferior Temporal WM	NAA	27.3	30.2	29.6	29.7	31.0	31.2
	Cr	22.8	21.9	21.3	21.2	22.1	22.5
	Cho	4.9	6.0	6.1	6.1	6.4	6.2
	ml	14.7	15.0	14.8	15.0	16.1	15.1
	Glx	9.2	6.8	9.2	8.0	6.5	2.6
	NAA / Cr	1.2	1.4	1.4	1.4	1.4	1.4
	Cho / Cr	0.2	0.3	0.3	0.3	0.3	0.3
	ml / Cr	0.6	0.7	0.7	0.7	0.7	0.7
	Glx / Cr	0.4	0.3	0.4	0.4	0.4	0.1
L. Insula WM	NAA	27.3	31.6	31.9	31.7	33.0	34.3
	Cr	22.8	23.1	22.7	22.3	21.9	22.1
	Cho	6.1	6.4	6.6	6.6	6.6	6.8
	ml	12.7	13.8	13.8	13.5	12.9	13.0
	Glx	6.3	7.1	4.4	3.9	6.5	10.5
	NAA / Cr	1.2	1.4	1.4	1.4	1.5	1.6
	Cho / Cr	0.3	0.3	0.3	0.3	0.3	0.3
	ml / Cr	0.6	0.6	0.6	0.6	0.6	0.6
	Glx / Cr	0.3	0.3	0.2	0.2	0.3	0.4
L. Lateral Occipital WM	NAA	30.2	36.3	38.7	38.5	43.9	44.7
	Cr	23.5	27.1	27.4	27.7	30.4	30.3
	Cho	3.9	5.4	5.6	5.5	5.7	5.3
	ml	14.7	18.0	17.5	17.6	18.4	16.7
	Glx	7.5	8.3	8.1	8.8	19.7	4.4
	NAA / Cr	1.3	1.3	1.4	1.4	1.5	1.5
	Cho / Cr	0.2	0.2	0.2	0.2	0.2	0.2
	ml / Cr	0.6	0.7	0.7	0.7	0.6	0.6
	Glx / Cr	0.3	0.3	0.3	0.3	0.6	0.1
L. Lingual WM	NAA	28.1	34.7	38.3	38.7	40.4	38.5
	Cr	22.9	26.6	26.5	26.9	27.2	26.5
	Cho	4.1	5.1	5.7	5.7	6.3	6.6
	ml	14.7	17.6	18.7	17.8	19.8	17.3
	Glx	5.1	9.8	16.6	11.8	23.0	4.1
	NAA / Cr	1.2	1.3	1.5	1.4	1.5	1.5
	Cho / Cr	0.2	0.2	0.2	0.2	0.2	0.3
	ml / Cr	0.7	0.7	0.7	0.7	0.7	0.7
	Glx / Cr	0.2	0.4	0.6	0.5	0.9	0.1

		MINT 50x50x18	ROIS 50x50x18	SLIM 50x50x12	SLIM 40x40x12	SLIM 20x20x12	SLIM 16x16x12
R. Inferior Parietal GM	NAA	36.2	36.3	36.6	36.4	40.2	36.3
	Cr	29.5	27.4	29.7	30.4	30.4	30.5
	Cho	5.5	5.4	5.6	5.4	5.1	5.2
	ml	17.3	17.9	17.0	16.3	16.1	16.2
	Glx	15.4	12.0	8.8	8.3	21.9	20.9
	NAA / Cr	1.2	1.3	1.3	1.3	1.3	1.3
	Cho / Cr	0.2	0.2	0.2	0.2	0.2	0.2
	ml / Cr	0.6	0.7	0.6	0.6	0.5	0.5
	Glx / Cr	0.6	0.5	0.3	0.3	0.7	0.5
R. Inferior Temporal GM	NAA	31.5	29.8	30.1	30.2	29.7	30.6
	Cr	25.9	23.5	24.5	25.4	25.1	24.8
	Cho	5.5	5.4	4.8	4.7	4.9	5.3
	ml	16.7	13.7	12.4	13.0	14.3	14.2
	Glx	17.6	12.1	13.6	13.6	15.9	14.2
	NAA / Cr	1.2	1.3	1.3	1.2	1.3	1.3
	Cho / Cr	0.2	0.2	0.2	0.2	0.2	0.2
	ml / Cr	0.7	0.6	0.5	0.5	0.6	0.6
	Glx / Cr	0.7	0.5	0.6	0.6	0.5	0.5
R. Insula GM	NAA	32.7	33.3	33.6	33.9	33.7	35.3
	Cr	29.7	29.6	31.6	32.2	33.5	33.7
	Cho	7.3	7.1	7.0	7.2	7.7	8.6
	ml	17.2	17.6	17.4	17.6	19.2	21.8
	Glx	5.6	11.4	13.8	9.8	15.7	16.7
	NAA / Cr	1.1	1.1	1.1	1.1	1.0	1.1
	Cho / Cr	0.3	0.2	0.2	0.2	0.2	0.3
	ml / Cr	0.6	0.6	0.6	0.6	0.6	0.7
	Glx / Cr	0.2	0.4	0.4	0.3	0.5	0.5
R. Lateral Occipital GM	NAA	30.2	34.0	33.1	32.2	31.6	31.4
	Cr	25.2	26.2	25.8	25.1	23.2	23.2
	Cho	4.3	4.5	4.1	4.1	4.5	3.9
	ml	14.2	14.8	13.3	13.5	13.3	11.0
	Glx	15.8	9.9	10.5	8.3	8.0	12.2
	NAA / Cr	1.3	1.3	1.3	1.3	1.4	1.4
	Cho / Cr	0.2	0.2	0.2	0.2	0.2	0.2
	ml / Cr	0.6	0.6	0.5	0.5	0.6	0.5
	Glx / Cr	0.6	0.4	0.4	0.4	0.4	0.6
R. Lingual GM	NAA	33.4	30.5	29.9	29.9	30.0	30.2
	Cr	28.7	25.1	25.3	25.0	25.8	25.9
	Cho	4.2	4.4	4.0	4.0	4.0	4.2
	ml	16.8	17.1	15.4	15.1	15.6	14.8
	Glx	14.6	8.2	7.9	7.8	9.9	6.4
	NAA / Cr	1.2	1.2	1.2	1.2	1.2	1.2
	Cho / Cr	0.2	0.2	0.2	0.2	0.2	0.2
	ml / Cr	0.6	0.7	0.6	0.6	0.6	0.6
	Glx / Cr	0.5	0.3	0.3	0.3	0.4	0.3

		MINT 50x50x18	ROIS 50x50x18	SLIM 50x50x12	SLIM 40x40x12	SLIM 20x20x12	SLIM 16x16x12
R. Inferior Parietal WM	NAA	35.8	35.1	35.4	35.6	35.1	35.6
	Cr	29.1	24.8	25.4	24.9	24.3	24.8
	Cho	5.2	5.6	5.7	5.7	5.8	6.0
	ml	16.6	17.4	17.9	17.7	17.1	16.8
	Glx	7.3	6.5	7.5	14.0	12.9	14.6
	NAA / Cr	1.2	1.4	1.4	1.4	1.5	1.4
	Cho / Cr	0.2	0.2	0.2	0.2	0.2	0.2
	ml / Cr	0.6	0.7	0.7	0.7	0.7	0.7
	Glx / Cr	0.2	0.3	0.3	0.6	0.6	0.6
R. Inferior Temporal WM	NAA	31.5	28.2	27.9	28.0	28.6	29.5
	Cr	25.5	22.0	22.1	21.9	22.2	22.8
	Cho	5.5	5.5	5.4	5.4	5.4	5.6
	ml	16.0	14.3	14.2	14.4	14.3	12.7
	Glx	14.1	9.7	6.1	6.7	6.1	7.7
	NAA / Cr	1.2	1.3	1.3	1.3	1.3	1.3
	Cho / Cr	0.2	0.3	0.3	0.3	0.3	0.3
	ml / Cr	0.6	0.7	0.7	0.7	0.7	0.6
	Glx / Cr	0.5	0.5	0.3	0.3	0.3	0.3
R. Insula WM	NAA	28.3	30.2	30.4	30.4	31.4	32.1
	Cr	24.0	23.2	23.3	23.0	21.6	22.0
	Cho	6.1	6.2	6.4	6.3	6.3	6.3
	ml	12.0	15.1	14.8	14.7	14.1	13.0
	Glx	5.2	8.2	7.8	7.4	7.8	0.8
	NAA / Cr	1.2	1.3	1.3	1.3	1.5	1.5
	Cho / Cr	0.3	0.3	0.3	0.3	0.3	0.3
	ml / Cr	0.5	0.7	0.6	0.6	0.7	0.6
	Glx / Cr	0.2	0.4	0.3	0.3	0.4	0.0
R. Lateral Occipital WM	NAA	33.9	33.4	35.1	35.1	38.6	40.3
	Cr	26.4	26.2	27.0	26.9	29.4	31.0
	Cho	4.6	4.6	4.8	4.7	4.9	4.7
	ml	15.8	15.0	14.4	14.3	15.0	14.6
	Glx	16.4	10.9	7.9	8.9	8.1	4.8
	NAA / Cr	1.3	1.3	1.3	1.3	1.3	1.3
	Cho / Cr	0.2	0.2	0.2	0.2	0.2	0.2
	ml / Cr	0.6	0.6	0.6	0.6	0.5	0.5
	Glx / Cr	0.6	0.4	0.3	0.3	0.3	0.2
R. Lingual WM	NAA	32.6	31.5	32.3	32.3	35.6	38.0
	Cr	27.2	24.2	22.9	22.7	24.2	25.3
	Cho	4.5	4.7	5.1	5.1	5.5	5.7
	ml	16.0	16.7	16.9	16.4	15.8	18.0
	Glx	9.2	7.5	4.7	8.3	3.4	8.3
	NAA / Cr	1.2	1.3	1.4	1.4	1.5	1.5
	Cho / Cr	0.2	0.2	0.2	0.2	0.2	0.2
	ml / Cr	0.6	0.7	0.8	0.7	0.7	0.7
	Glx / Cr	0.3	0.3	0.3	0.4	0.1	0.3

		MINT 50x50x18	ROIS 50x50x18	SLIM 50x50x12	SLIM 40x40x12	SLIM 20x20x12	SLIM 16x16x12
L. Orbito-Frontal GM	NAA	34.2	34.4	35.4	35.4	39.7	40.7
	Cr	27.4	25.1	25.7	26.0	29.1	30.0
	Cho	5.3	5.5	5.2	5.2	5.1	5.1
	ml	14.7	12.3	13.3	12.6	15.5	17.1
	Glx	7.0	10.7	16.4	17.2	15.1	17.8
	NAA / Cr	1.3	1.4	1.4	1.4	1.4	1.5
	Cho / Cr	0.2	0.2	0.2	0.2	0.2	0.2
	ml / Cr	0.5	0.5	0.5	0.5	0.6	0.7
	Glx / Cr	0.2	0.5	0.7	0.7	0.6	0.6
L. Pars GM	NAA	35.6	38.4	39.7	39.6	40.3	41.1
	Cr	29.2	28.6	30.2	31.1	32.6	32.5
	Cho	5.9	6.4	6.7	6.7	7.1	6.8
	ml	17.9	18.2	20.8	20.4	19.6	17.7
	Glx	16.5	11.3	6.7	13.9	8.0	11.4
	NAA / Cr	1.2	1.3	1.3	1.3	1.2	1.3
	Cho / Cr	0.2	0.2	0.2	0.2	0.2	0.2
	ml / Cr	0.6	0.6	0.7	0.7	0.6	0.6
	Glx / Cr	0.5	0.4	0.2	0.5	0.3	0.5
L. Post-Central GM	NAA	34.5	31.9	30.0	29.3	26.8	29.1
	Cr	28.0	24.7	23.4	23.1	21.3	24.0
	Cho	4.7	4.3	4.1	4.1	3.9	4.4
	ml	14.5	12.1	11.4	10.8	9.2	10.0
	Glx	11.3	7.0	9.5	8.0	9.4	6.4
	NAA / Cr	1.2	1.3	1.3	1.3	1.3	1.3
	Cho / Cr	0.2	0.2	0.2	0.2	0.2	0.2
	ml / Cr	0.5	0.5	0.5	0.5	0.5	0.4
	Glx / Cr	0.4	0.3	0.4	0.4	0.6	0.3
L. Pre-Cuneus GM	NAA	31.0	33.9	34.6	34.3	35.1	35.0
	Cr	26.7	27.2	27.9	27.9	27.9	27.5
	Cho	4.1	4.6	4.3	4.1	3.9	3.8
	ml	14.4	16.3	16.2	15.5	15.3	14.9
	Glx	9.2	16.1	10.7	7.1	14.6	16.3
	NAA / Cr	1.2	1.3	1.3	1.2	1.3	1.3
	Cho / Cr	0.2	0.2	0.2	0.2	0.1	0.1
	ml / Cr	0.5	0.6	0.6	0.5	0.5	0.5
	Glx / Cr	0.4	0.6	0.4	0.2	0.5	0.6
L. Rostral Middle Frontal GM	NAA	38.3	37.7	38.8	38.4	37.6	39.5
	Cr	31.8	30.0	31.1	30.3	33.0	30.5
	Cho	6.1	6.2	5.8	5.5	4.8	5.3
	ml	19.3	20.0	21.0	19.8	20.5	19.8
	Glx	12.9	10.6	10.6	14.0	11.5	15.1
	NAA / Cr	1.2	1.3	1.3	1.3	1.2	1.4
	Cho / Cr	0.2	0.2	0.2	0.2	0.2	0.2
	ml / Cr	0.6	0.7	0.7	0.7	0.6	0.8
	Glx / Cr	0.4	0.4	0.3	0.6	0.4	1.2

		MINT 50x50x18	ROIS 50x50x18	SLIM 50x50x12	SLIM 40x40x12	SLIM 20x20x12	SLIM 16x16x12
L. Orbito-Frontal WM	NAA	30.8	33.8	32.5	32.8	32.9	33.0
	Cr	24.4	25.2	24.1	23.7	23.9	23.5
	Cho	5.7	6.1	6.4	6.5	6.6	6.6
	ml	12.5	14.4	13.5	13.3	13.0	13.4
	Glx	6.0	10.9	5.5	6.2	3.4	5.2
	NAA / Cr	1.3	1.4	1.4	1.4	1.4	1.4
	Cho / Cr	0.2	0.2	0.3	0.3	0.3	0.3
	ml / Cr	0.5	0.6	0.6	0.6	0.6	0.6
	Glx / Cr	0.2	0.4	0.2	0.3	0.1	0.2
L. Pars WM	NAA	34.0	37.0	36.6	36.9	35.2	36.9
	Cr	27.0	26.0	26.0	25.7	24.1	26.9
	Cho	6.1	6.6	6.7	6.8	6.4	7.0
	ml	16.0	17.3	14.3	14.0	14.1	16.9
	Glx	8.8	8.5	2.9	4.7	5.0	3.6
	NAA / Cr	1.3	1.4	1.4	1.5	1.5	1.4
	Cho / Cr	0.2	0.3	0.3	0.3	0.3	0.3
	ml / Cr	0.6	0.7	0.6	0.6	0.7	0.6
	Glx / Cr	0.3	0.3	0.1	0.2	0.2	0.2
L. Post-Central WM	NAA	35.3	35.8	39.0	40.8	46.8	49.0
	Cr	27.7	26.7	27.3	27.9	30.1	30.1
	Cho	4.7	4.8	5.5	5.7	6.7	6.9
	ml	13.7	13.1	13.7	14.4	15.7	14.5
	Glx	6.6	10.3	2.3	15.4	16.4	9.2
	NAA / Cr	1.3	1.4	1.4	1.5	1.6	1.7
	Cho / Cr	0.2	0.2	0.2	0.2	0.2	0.2
	ml / Cr	0.5	0.5	0.5	0.5	0.5	0.5
	Glx / Cr	0.3	0.4	0.1	0.7	0.6	0.3
L. Pre-Cuneus WM	NAA	29.6	34.7	34.7	34.6	34.5	34.2
	Cr	24.3	24.3	23.7	23.6	23.0	22.3
	Cho	4.7	5.5	5.6	5.6	5.9	5.7
	ml	13.8	16.4	15.4	15.2	14.7	15.0
	Glx	3.5	14.2	8.6	7.4	1.9	25.5
	NAA / Cr	1.2	1.4	1.5	1.5	1.5	1.6
	Cho / Cr	0.2	0.2	0.2	0.2	0.3	0.3
	ml / Cr	0.6	0.7	0.7	0.7	0.7	0.7
	Glx / Cr	0.1	0.6	0.3	0.3	0.1	1.1
L. Rostral Middle Frontal WM	NAA	36.5	38.9	38.9	38.9	39.7	37.8
	Cr	29.1	28.6	28.3	28.2	29.4	28.2
	Cho	6.5	7.3	7.7	7.8	8.0	8.3
	ml	17.9	19.6	19.9	19.7	19.0	17.6
	Glx	6.9	11.8	11.3	10.9	12.7	6.4
	NAA / Cr	1.3	1.4	1.4	1.4	1.4	1.4
	Cho / Cr	0.2	0.3	0.3	0.3	0.3	0.3
	ml / Cr	0.6	0.7	0.7	0.7	0.7	0.6
	Glx / Cr	0.2	0.4	0.4	0.4	0.4	0.2

		MINT 50x50x18	ROIS 50x50x18	SLIM 50x50x12	SLIM 40x40x12	SLIM 20x20x12	SLIM 16x16x12
R. Orbito-Frontal GM	NAA	34.3	35.9	38.5	39.7	39.7	41.1
	Cr	27.3	27.5	31.2	31.9	38.4	42.6
	Cho	5.6	5.3	5.7	5.8	5.3	5.8
	ml	15.1	13.7	14.3	14.6	15.9	20.6
	Glx	9.3	10.4	11.9	10.8	17.1	22.7
	NAA / Cr	1.3	1.3	1.3	1.3	1.2	1.1
	Cho / Cr	0.2	0.2	0.2	0.2	0.2	0.2
	ml / Cr	0.5	0.5	0.5	0.5	0.5	0.5
	Glx / Cr	0.3	0.4	0.4	0.4	0.7	0.8
R. Pars GM	NAA	37.6	36.5	36.8	37.4	39.6	40.9
	Cr	30.5	29.0	29.6	30.8	31.3	34.1
	Cho	6.3	6.3	6.3	6.4	6.7	6.6
	ml	17.4	18.5	16.8	17.4	15.3	15.6
	Glx	18.1	12.1	10.0	10.6	15.8	15.1
	NAA / Cr	1.2	1.3	1.2	1.2	1.3	1.2
	Cho / Cr	0.2	0.2	0.2	0.2	0.2	0.2
	ml / Cr	0.6	0.6	0.6	0.6	0.5	0.5
	Glx / Cr	0.6	0.4	0.3	0.3	0.5	0.4
R. Post-Central GM	NAA	34.5	31.7	30.4	30.0	28.4	28.8
	Cr	28.9	24.9	23.5	23.2	22.4	22.9
	Cho	4.6	3.9	3.8	3.7	3.6	4.0
	ml	15.1	10.8	9.6	9.0	8.6	8.5
	Glx	8.7	3.9	12.2	11.7	11.6	6.4
	NAA / Cr	1.2	1.3	1.3	1.3	1.3	1.3
	Cho / Cr	0.2	0.2	0.2	0.2	0.2	0.2
	ml / Cr	0.5	0.4	0.4	0.4	0.4	0.4
	Glx / Cr	0.4	0.2	0.6	0.5	0.6	0.3
R. Pre-Cuneus GM	NAA	34.1	32.5	32.9	32.7	33.7	35.8
	Cr	29.6	25.4	26.1	26.5	27.3	27.7
	Cho	4.5	4.4	4.1	4.0	3.8	3.8
	ml	16.0	15.7	15.6	15.3	13.9	13.6
	Glx	13.3	8.1	15.7	12.0	15.8	16.4
	NAA / Cr	1.2	1.3	1.3	1.2	1.3	1.3
	Cho / Cr	0.2	0.2	0.2	0.2	0.1	0.1
	ml / Cr	0.5	0.6	0.6	0.6	0.5	0.5
	Glx / Cr	0.4	0.3	0.6	0.4	0.6	0.6
R. Rostral Middle Frontal GM	NAA	39.6	39.2	39.4	39.5	41.4	41.8
	Cr	32.1	31.2	31.7	32.0	34.0	34.3
	Cho	6.4	6.5	6.5	6.3	6.4	5.9
	ml	18.9	19.8	20.1	18.9	18.9	17.6
	Glx	9.3	14.7	10.2	11.8	11.3	11.6
	NAA / Cr	1.2	1.3	1.3	1.2	1.2	1.2
	Cho / Cr	0.2	0.2	0.2	0.2	0.2	0.2
	ml / Cr	0.6	0.6	0.6	0.6	0.6	0.5
	Glx / Cr	0.3	0.5	0.3	0.4	0.3	0.3

		MINT 50x50x18	ROIS 50x50x18	SLIM 50x50x12	SLIM 40x40x12	SLIM 20x20x12	SLIM 16x16x12
R. Orbito-Frontal WM	NAA	30.7	34.7	35.2	35.0	35.2	34.6
	Cr	24.6	25.2	24.9	25.1	24.6	23.6
	Cho	5.6	6.0	6.2	6.2	6.4	6.3
	ml	12.5	14.3	14.1	14.1	14.5	14.6
	Glx	10.0	7.8	11.0	6.3	2.3	9.3
	NAA / Cr	1.3	1.4	1.4	1.4	1.4	1.5
	Cho / Cr	0.2	0.2	0.3	0.3	0.3	0.3
	ml / Cr	0.5	0.6	0.6	0.6	0.6	0.6
	Glx / Cr	0.5	0.3	0.4	0.3	0.1	0.4
R. Pars WM	NAA	35.7	35.5	36.6	34.5	35.3	35.6
	Cr	28.7	26.4	26.8	25.1	25.3	24.9
	Cho	6.6	6.5	7.3	6.7	7.4	7.2
	ml	16.3	17.3	17.6	16.0	17.6	15.9
	Glx	8.7	10.4	11.2	12.6	5.0	8.8
	NAA / Cr	1.2	1.3	1.4	1.6	1.4	1.4
	Cho / Cr	0.2	0.3	0.3	0.3	0.3	0.3
	ml / Cr	0.6	0.7	0.7	0.8	0.7	0.7
	Glx / Cr	0.3	0.4	0.4	3.3	0.2	0.3
R. Post-Central WM	NAA	35.2	34.8	37.8	39.1	41.5	40.8
	Cr	28.9	26.6	27.2	27.7	28.5	28.1
	Cho	5.0	4.6	5.2	5.2	5.6	5.8
	ml	14.6	13.1	12.9	13.7	15.4	13.3
	Glx	7.0	7.6	6.4	15.2	32.1	3.7
	NAA / Cr	1.2	1.3	1.4	1.4	1.5	1.5
	Cho / Cr	0.2	0.2	0.2	0.2	0.2	0.2
	ml / Cr	0.5	0.5	0.5	0.5	0.6	0.5
	Glx / Cr	0.3	0.3	0.2	0.5	1.1	0.1
R. Pre-Cuneus WM	NAA	33.4	31.6	31.0	30.9	28.8	29.1
	Cr	27.8	22.6	21.8	21.5	19.0	18.8
	Cho	4.9	5.1	5.2	5.2	5.4	5.3
	ml	15.4	15.5	15.7	15.7	14.7	14.9
	Glx	11.8	8.6	7.2	6.2	3.5	7.0
	NAA / Cr	1.2	1.4	1.4	1.4	1.5	1.6
	Cho / Cr	0.2	0.2	0.2	0.2	0.3	0.3
	ml / Cr	0.6	0.7	0.7	0.7	0.8	0.8
	Glx / Cr	0.4	0.4	0.3	0.3	0.2	0.4
R. Rostral Middle Frontal WM	NAA	36.8	38.1	38.5	37.8	38.5	37.8
	Cr	29.1	28.6	29.0	28.3	29.2	28.6
	Cho	6.8	7.2	7.3	7.3	7.6	7.5
	ml	16.7	19.3	20.2	20.6	21.7	21.1
	Glx	5.0	14.2	11.2	13.5	5.7	8.1
	NAA / Cr	1.3	1.3	1.3	1.4	1.3	1.3
	Cho / Cr	0.2	0.3	0.3	0.3	0.3	0.3
	ml / Cr	0.6	0.7	0.7	0.7	0.7	0.7
	Glx / Cr	0.2	0.5	0.4	0.6	0.2	0.4

		MINT 50x50x18	ROIS 50x50x18	SLIM 50x50x12	SLIM 40x40x12	SLIM 20x20x12	SLIM 16x16x12
L. Superior Frontal GM	NAA	36.1	35.0	35.6	33.9	33.9	32.3
	Cr	29.1	26.4	25.8	25.1	23.9	25.9
	Cho	6.3	5.8	5.6	5.4	5.5	5.0
	ml	14.1	12.1	11.0	10.3	11.7	18.8
	Glx	9.9	13.0	10.7	9.6	15.5	26.7
	NAA / Cr	1.3	1.3	1.4	1.4	1.5	1.3
	Cho / Cr	0.2	0.2	0.2	0.2	0.2	0.2
	ml / Cr	0.5	0.5	0.4	0.4	0.5	0.7
	Glx / Cr	0.3	0.6	0.4	0.4	0.6	0.8
L. Superior Parietal GM	NAA	30.3	32.8	30.6	29.6	26.8	27.0
	Cr	25.3	26.0	24.9	23.8	22.0	18.5
	Cho	3.8	4.2	3.4	3.3	3.3	2.9
	ml	12.6	14.4	11.2	11.1	7.9	7.3
	Glx	4.6	9.6	6.9	7.9	14.0	12.8
	NAA / Cr	1.2	1.3	1.3	1.3	1.3	1.5
	Cho / Cr	0.2	0.2	0.1	0.1	0.2	0.2
	ml / Cr	0.5	0.5	0.4	0.5	0.4	0.4
	Glx / Cr	0.2	0.4	0.3	0.4	0.6	0.8
L. Superior Temporal GM	NAA	31.2	31.3	31.8	31.6	31.9	31.5
	Cr	27.4	25.9	28.4	28.2	28.3	27.7
	Cho	5.5	5.7	5.9	5.9	6.2	5.9
	ml	17.8	15.6	15.8	15.4	15.2	13.9
	Glx	10.2	8.6	9.4	6.1	14.1	8.3
	NAA / Cr	1.1	1.2	1.2	1.1	1.2	1.2
	Cho / Cr	0.2	0.2	0.2	0.2	0.2	0.2
	ml / Cr	0.7	0.6	0.6	0.6	0.5	0.5
	Glx / Cr	0.4	0.3	0.3	0.2	0.5	0.3
L. Supra-Marginal GM	NAA	37.1	36.4	36.3	36.0	36.5	38.3
	Cr	31.5	27.7	27.7	27.5	28.5	30.0
	Cho	5.7	5.2	5.0	4.9	4.8	4.7
	ml	18.1	17.2	17.1	16.7	17.1	17.5
	Glx	13.7	6.8	9.7	8.3	10.1	13.3
	NAA / Cr	1.2	1.3	1.3	1.3	1.3	1.3
	Cho / Cr	0.2	0.2	0.2	0.2	0.2	0.2
	ml / Cr	0.6	0.6	0.6	0.6	0.6	0.6
	Glx / Cr	0.4	0.2	0.3	0.3	0.4	0.4
L. Striatum	NAA	23.4	24.8	24.7	24.8	21.9	21.6
	Cr	22.7	22.4	23.8	24.0	24.1	23.5
	Cho	5.7	6.0	6.7	6.8	6.4	6.6
	ml	13.1	11.6	12.4	13.1	11.6	12.9
	Glx	8.3	10.1	6.7	6.8	8.9	9.0
	NAA / Cr	1.0	1.1	1.0	1.0	0.9	0.9
	Cho / Cr	0.3	0.3	0.3	0.3	0.3	0.3
	ml / Cr	0.6	0.5	0.5	0.5	0.5	0.6
	Glx / Cr	0.4	0.6	0.3	0.3	0.4	0.4

		MINT 50x50x18	ROIS 50x50x18	SLIM 50x50x12	SLIM 40x40x12	SLIM 20x20x12	SLIM 16x16x12
L. Superior Frontal WM	NAA	34.4	36.7	37.5	37.8	39.5	41.6
	Cr	27.2	27.9	29.4	29.4	30.8	32.1
	Cho	6.3	6.4	6.6	6.7	7.2	7.4
	ml	13.3	13.7	14.7	14.8	14.0	18.0
	Glx	7.1	9.5	11.7	8.5	5.4	16.3
	NAA / Cr	1.3	1.3	1.3	1.3	1.3	1.4
	Cho / Cr	0.2	0.2	0.2	0.2	0.2	0.2
	ml / Cr	0.5	0.5	0.5	0.5	0.5	0.6
	Glx / Cr	0.3	0.3	0.4	0.3	0.2	0.5
L. Superior Parietal WM	NAA	31.7	36.4	38.5	38.9	42.5	45.5
	Cr	25.7	26.5	27.9	28.4	31.3	33.9
	Cho	4.4	5.4	5.5	5.6	6.0	6.2
	ml	13.3	16.5	17.4	17.3	17.9	18.2
	Glx	9.0	11.8	21.9	21.6	18.7	26.3
	NAA / Cr	1.2	1.4	1.4	1.4	1.4	1.4
	Cho / Cr	0.2	0.2	0.2	0.2	0.2	0.2
	ml / Cr	0.5	0.6	0.6	0.6	0.6	0.5
	Glx / Cr	0.4	0.5	0.8	0.8	0.6	0.8
L. Superior Temporal WM	NAA	28.6	31.8	34.1	33.2	34.1	37.7
	Cr	25.3	24.1	24.9	24.2	24.3	28.2
	Cho	5.2	6.0	6.1	6.1	6.3	6.6
	ml	15.4	15.9	14.6	14.1	14.4	15.0
	Glx	9.1	9.6	10.3	5.0	21.4	21.6
	NAA / Cr	1.1	1.3	1.4	1.4	1.4	1.4
	Cho / Cr	0.2	0.3	0.2	0.3	0.3	0.3
	ml / Cr	0.6	0.7	0.6	0.6	0.6	0.6
	Glx / Cr	0.4	0.5	0.5	0.3	0.8	0.7
L. Supra-Marginal WM	NAA	35.1	39.2	39.2	39.5	39.0	37.9
	Cr	28.9	27.1	26.1	26.1	24.8	24.0
	Cho	5.6	6.1	6.4	6.4	6.6	6.5
	ml	16.1	17.3	16.1	15.9	16.0	14.8
	Glx	6.7	5.7	4.9	9.6	11.0	3.0
	NAA / Cr	1.2	1.5	1.5	1.5	1.6	1.6
	Cho / Cr	0.2	0.2	0.3	0.3	0.3	0.3
	ml / Cr	0.6	0.6	0.6	0.6	0.7	0.6
	Glx / Cr	0.2	0.2	0.2	0.3	0.4	0.1
L. Thalamus	NAA	21.8	25.1	25.4	25.3	24.9	23.6
	Cr	19.9	20.1	20.7	20.7	21.3	20.1
	Cho	5.0	6.0	6.2	6.1	6.2	5.9
	ml	10.5	9.8	9.2	9.4	9.3	9.7
	Glx	5.0	7.5	6.6	8.4	7.8	10.3
	NAA / Cr	1.1	1.3	1.2	1.2	1.2	1.2
	Cho / Cr	0.3	0.3	0.3	0.3	0.3	0.3
	ml / Cr	0.5	0.5	0.5	0.5	0.5	0.5
	Glx / Cr	0.3	0.5	0.3	0.4	0.4	0.5

		MINT 50x50x18	ROIS 50x50x18	SLIM 50x50x12	SLIM 40x40x12	SLIM 20x20x12	SLIM 16x16x12
R. Superior Frontal GM	NAA	35.7	35.9	35.7	35.5	35.8	33.2
	Cr	29.6	27.6	26.6	26.3	25.5	23.8
	Cho	6.1	5.9	5.8	5.7	5.3	6.0
	ml	14.3	12.7	13.0	13.0	13.0	15.4
	Glx	13.2	8.8	11.9	12.5	11.6	17.4
	NAA / Cr	1.2	1.3	1.4	1.4	1.4	1.4
	Cho / Cr	0.2	0.2	0.2	0.2	0.2	0.3
	ml / Cr	0.5	0.5	0.5	0.5	0.5	0.6
	Glx / Cr	0.5	0.3	0.5	0.5	0.5	0.7
R. Superior Parietal GM	NAA	32.1	31.9	31.9	30.7	32.8	27.4
	Cr	26.9	25.2	25.3	24.1	25.1	23.0
	Cho	4.3	3.9	3.5	3.2	3.7	3.1
	ml	14.4	12.7	9.8	8.2	7.5	6.2
	Glx	11.7	8.5	9.4	12.8	21.7	27.2
	NAA / Cr	1.2	1.3	1.3	1.3	1.3	1.4
	Cho / Cr	0.2	0.2	0.1	0.1	0.2	0.1
	ml / Cr	0.5	0.5	0.4	0.3	0.3	0.3
	Glx / Cr	0.4	0.3	0.4	0.6	0.8	1.2
R. Superior Temporal GM	NAA	34.3	31.5	33.3	32.8	34.1	33.2
	Cr	29.5	26.2	28.3	28.3	27.6	26.3
	Cho	6.3	5.8	6.0	5.9	6.2	5.7
	ml	18.0	14.5	16.2	15.4	14.7	15.0
	Glx	9.7	8.7	9.9	8.6	8.7	9.8
	NAA / Cr	1.2	1.2	1.2	1.2	1.3	1.3
	Cho / Cr	0.2	0.2	0.2	0.2	0.2	0.2
	ml / Cr	0.6	0.6	0.6	0.6	0.5	0.6
	Glx / Cr	0.3	0.3	0.4	0.3	0.3	0.5
R. Supra-Marginal GM	NAA	38.5	35.5	37.6	37.5	39.5	39.8
	Cr	32.5	28.4	30.8	30.5	31.9	31.9
	Cho	5.7	5.4	5.0	5.0	5.1	5.3
	ml	18.7	17.4	17.5	17.7	18.3	18.8
	Glx	10.1	9.1	10.0	10.2	19.4	23.0
	NAA / Cr	1.2	1.3	1.2	1.2	1.3	1.3
	Cho / Cr	0.2	0.2	0.2	0.2	0.2	0.2
	ml / Cr	0.6	0.6	0.6	0.6	0.6	0.6
	Glx / Cr	0.3	0.3	0.3	0.3	0.6	0.7
R. Striatum	NAA	24.6	25.5	24.5	24.5	22.2	20.1
	Cr	23.3	24.4	24.6	24.5	24.4	22.3
	Cho	5.9	6.3	6.5	6.7	6.8	6.3
	ml	12.6	14.2	14.2	14.6	11.6	13.3
	Glx	6.5	9.0	7.5	6.8	9.5	14.3
	NAA / Cr	1.0	1.1	1.0	1.0	0.9	0.9
	Cho / Cr	0.3	0.3	0.3	0.3	0.3	0.3
	ml / Cr	0.6	0.6	0.6	0.6	0.5	0.7
	Glx / Cr	0.3	0.4	0.3	0.3	0.4	0.8

		MINT 50x50x18	ROIS 50x50x18	SLIM 50x50x12	SLIM 40x40x12	SLIM 20x20x12	SLIM 16x16x12
R. Superior Frontal WM	NAA	32.9	36.6	37.2	37.2	38.8	39.8
	Cr	27.2	28.1	27.9	28.1	29.0	29.7
	Cho	6.4	6.4	6.7	6.7	6.9	7.0
	ml	13.8	14.9	15.1	14.5	14.4	13.0
	Glx	10.1	9.8	15.7	9.3	14.4	17.8
	NAA / Cr	1.2	1.3	1.3	1.3	1.4	1.4
	Cho / Cr	0.2	0.2	0.2	0.2	0.2	0.2
	ml / Cr	0.5	0.5	0.5	0.5	0.5	0.4
	Glx / Cr	0.4	0.3	0.5	0.3	0.5	0.7
R. Superior Parietal WM	NAA	33.2	34.1	35.7	36.0	37.4	38.9
	Cr	27.4	25.8	26.9	27.1	27.7	29.1
	Cho	4.8	4.9	5.1	5.1	5.2	5.4
	ml	14.8	15.6	15.3	15.5	15.4	16.6
	Glx	11.9	11.3	13.8	13.4	18.6	23.1
	NAA / Cr	1.2	1.3	1.3	1.3	1.4	1.4
	Cho / Cr	0.2	0.2	0.2	0.2	0.2	0.2
	ml / Cr	0.5	0.6	0.6	0.6	0.6	0.6
	Glx / Cr	0.5	0.4	0.5	0.5	0.7	0.8
R. Superior Temporal WM	NAA	30.8	30.2	30.6	30.8	29.7	26.3
	Cr	26.2	24.6	24.2	24.0	22.9	21.2
	Cho	5.9	5.6	5.9	6.0	5.8	5.1
	ml	16.0	15.4	15.6	14.6	14.2	14.3
	Glx	8.0	9.2	5.3	9.1	6.7	13.3
	NAA / Cr	1.2	1.2	1.3	1.3	1.3	1.3
	Cho / Cr	0.2	0.2	0.3	0.3	0.3	0.3
	ml / Cr	0.6	0.6	0.7	0.6	0.6	0.8
	Glx / Cr	0.3	0.4	0.3	0.5	0.3	0.7
R. Supra-Marginal WM	NAA	36.2	34.4	34.3	34.3	33.8	33.4
	Cr	29.1	24.2	23.4	23.4	23.1	22.6
	Cho	5.9	6.0	6.1	6.1	6.1	6.1
	ml	16.5	16.1	16.1	15.8	16.0	15.1
	Glx	5.4	8.3	14.1	18.6	13.2	10.3
	NAA / Cr	1.3	1.4	1.5	1.5	1.5	1.5
	Cho / Cr	0.2	0.3	0.3	0.3	0.3	0.3
	ml / Cr	0.6	0.7	0.7	0.7	0.7	0.7
	Glx / Cr	0.2	0.3	0.7	0.8	0.7	0.5
R. Thalamus	NAA	22.9	24.5	23.5	23.4	22.7	21.1
	Cr	20.9	20.5	19.6	19.7	19.9	19.0
	Cho	5.6	5.7	5.7	5.6	5.9	5.6
	ml	10.4	9.5	8.7	8.9	9.3	9.8
	Glx	2.2	7.6	8.0	11.8	6.7	5.6
	NAA / Cr	1.1	1.2	1.2	1.2	1.1	1.1
	Cho / Cr	0.3	0.3	0.3	0.3	0.3	0.3
	ml / Cr	0.5	0.5	0.5	0.5	0.5	0.5
	Glx / Cr	0.1	0.4	0.4	0.6	0.3	0.3

Table 9: Average SNR across all compartments.

Compartment	MINT 50x50x18	ROIS 50x50x18	SLIM 50x50x12	SLIM 40x40x12	SLIM 20x20x12	SLIM 16x16x12
All	25	15	13	13	11	10
Brain Stem	17	8	8	8	8	8
L. Central GM	25	17	14	14	10	9
L. Central WM	24	15	14	14	14	13
L. Cerebellum GM	35	15	15	15	15	14
L. Cerebellum WM	30	14	12	12	12	12
L. Cingulate GM	17	14	12	12	11	11
L. Cingulate WM	18	15	14	13	12	11
L. Fusiform GM	26	12	9	9	9	8
L. Fusiform WM	23	14	9	9	7	6
L. Inferior Parietal GM	27	21	18	17	15	14
L. Inferior Parietal WM	24	18	16	15	13	11
L. Inferior Temporal GM	32	15	14	13	11	10
L. Inferior Temporal WM	31	14	12	12	11	11
L. Insula GM	18	14	13	12	10	9
L. Insula WM	21	16	15	14	13	12
L. Lateral Occipital GM	32	19	18	18	14	12
L. Lateral Occipital WM	37	19	16	15	13	11
L. Lingual GM	28	17	14	13	12	10
L. Lingual WM	27	17	13	12	10	9
L. Orbito-Frontal GM	25	14	12	11	9	8
L. Orbito-Frontal WM	24	16	15	14	12	11
L. Pars GM	26	15	13	12	10	11
L. Pars WM	24	15	11	11	10	10
L. Post-Central GM	25	17	13	12	10	11
L. Post-Central WM	25	16	13	13	11	9
L. Pre-Cuneus GM	20	15	14	13	11	10
L. Pre-Cuneus WM	21	15	14	13	11	11
L. Rostral Middle Frontal GM	28	17	13	12	12	11
L. Rostral Middle Frontal WM	26	17	15	15	14	12
L. Striatum	24	12	11	10	7	7
L. Superior Frontal GM	24	13	11	11	9	7
L. Superior Frontal WM	23	15	15	14	12	12
L. Superior Parietal GM	25	15	12	11	8	7
L. Superior Parietal WM	23	16	16	15	12	11
L. Superior Temporal GM	29	13	11	11	10	9
L. Superior Temporal WM	24	13	11	10	8	7
L. Supra-Marginal GM	27	17	14	13	11	12
L. Supra-Marginal WM	24	15	13	12	12	12
L. Thalamus	16	10	9	9	8	8

Compartment	MINT 50x50x18	ROIS 50x50x18	SLIM 50x50x12	SLIM 40x40x12	SLIM 20x20x12	SLIM 16x16x12
R. Central GM	23	17	16	15	11	10
R. Central WM	23	14	14	14	13	13
R. Cerebellum GM	36	13	13	13	12	13
R. Cerebellum WM	31	13	12	12	12	11
R. Cingulate GM	17	15	13	13	11	10
R. Cingulate WM	19	16	15	15	14	13
R. Fusiform GM	27	11	8	8	8	9
R. Fusiform WM	25	14	9	9	7	7
R. Inferior Parietal GM	24	18	15	14	12	11
R. Inferior Parietal WM	24	17	17	16	14	12
R. Inferior Temporal GM	29	12	10	10	9	8
R. Inferior Temporal WM	30	13	11	11	10	11
R. Insula GM	20	13	13	12	10	9
R. Insula WM	22	18	17	16	14	13
R. Lateral Occipital GM	31	18	15	15	11	10
R. Lateral Occipital WM	31	18	15	14	12	10
R. Lingual GM	27	16	13	13	11	10
R. Lingual WM	30	16	12	11	9	8
R. Orbito-Frontal GM	26	15	12	12	10	9
R. Orbito-Frontal WM	21	16	15	14	12	12
R. Pars GM	29	14	12	12	10	10
R. Pars WM	24	16	12	11	11	10
R. Post-Central GM	23	16	13	12	10	10
R. Post-Central WM	22	16	13	12	11	9
R. Pre-Cuneus GM	20	16	14	13	12	10
R. Pre-Cuneus WM	23	15	15	14	10	10
R. Rostral Middle Frontal GM	27	17	14	14	11	12
R. Rostral Middle Frontal WM	24	18	16	15	14	12
R. Striatum	25	12	11	10	8	8
R. Superior Frontal GM	23	15	13	12	9	9
R. Superior Frontal WM	21	16	15	15	12	11
R. Superior Parietal GM	27	16	14	13	11	9
R. Superior Parietal WM	24	16	15	14	12	11
R. Superior Temporal GM	30	13	11	10	10	10
R. Superior Temporal WM	24	13	10	10	8	7
R. Supra-Marginal GM	26	16	14	13	12	11
R. Supra-Marginal WM	21	16	14	14	13	12
R. Thalamus	16	10	8	8	8	7
Ventral Diencephalon	20	8	6	6	6	6
Ventricles	19	15	13	13	11	10

Table 10: Average metabolite concentrations and standard deviations measured as a ratio of ROIS 50 x 50 x 12 over the 5 other localization runs across all compartments.

		MINT 50x50x18	SLIM 50x50x12	SLIM 40x40x12	SLIM 20x20x12	SLIM 16x16x12
All	NAA	0.97 ± 0.2	1.01 ± 0.1	1.01 ± 0.1	1.03 ± 0.2	1.03 ± 0.2
	Cr	1.05 ± 0.2	1.01 ± 0.1	1.01 ± 0.1	1.02 ± 0.2	1.03 ± 0.2
	Cho	0.98 ± 0.3	1.01 ± 0.1	1.01 ± 0.2	1.03 ± 0.2	1.04 ± 0.3
	ml	1.09 ± 1.3	1.04 ± 1.7	1.04 ± 1.7	1.06 ± 2.5	1.15 ± 5.1
	Glx	3.38 ± 11.4	2.88 ± 13.9	2.77 ± 10.3	4.19 ± 16.4	5.93 ± 28.6
	NAA / Cr	0.93 ± 0.1	1.01 ± 0.1	1.01 ± 0.1	1.02 ± 0.1	1.03 ± 0.2
	Cho / Cr	0.94 ± 0.2	1.01 ± 0.2	1.02 ± 0.2	1.03 ± 0.2	1.04 ± 0.2
	ml / Cr	1.05 ± 1.2	1.04 ± 1.6	1.03 ± 1.6	1.06 ± 2.8	1.11 ± 4.0
	Glx / Cr	3.54 ± 13.1	2.86 ± 13.5	2.78 ± 10.6	4.14 ± 16.7	6.08 ± 28.4
L. Central GM	NAA	1.06 ± 0.1	0.95 ± 0.0	0.94 ± 0.1	0.85 ± 0.1	0.82 ± 0.1
	Cr	1.12 ± 0.1	0.97 ± 0.0	0.96 ± 0.1	0.85 ± 0.1	0.77 ± 0.1
	Cho	1.09 ± 0.1	0.93 ± 0.1	0.90 ± 0.1	0.76 ± 0.1	0.79 ± 0.2
	ml	1.18 ± 0.3	0.90 ± 0.1	0.89 ± 0.2	0.81 ± 0.3	0.65 ± 0.2
	Glx	4.83 ± 10.3	1.66 ± 2.8	1.03 ± 0.4	1.05 ± 1.0	3.05 ± 6.6
	NAA / Cr	0.95 ± 0.1	0.98 ± 0.1	0.98 ± 0.0	1.01 ± 0.1	1.08 ± 0.1
	Cho / Cr	0.98 ± 0.1	0.96 ± 0.1	0.93 ± 0.1	0.90 ± 0.2	1.04 ± 0.2
	ml / Cr	1.05 ± 0.2	0.92 ± 0.2	0.92 ± 0.2	0.95 ± 0.4	0.85 ± 0.3
	Glx / Cr	4.48 ± 9.5	1.88 ± 3.2	1.02 ± 0.3	1.37 ± 1.6	4.09 ± 8.5
L. Cerebellum GM	NAA	0.85 ± 0.3	1.05 ± 0.1	1.07 ± 0.1	1.13 ± 0.1	1.11 ± 0.3
	Cr	0.80 ± 0.2	1.00 ± 0.1	1.00 ± 0.1	1.02 ± 0.1	0.98 ± 0.2
	Cho	0.69 ± 0.2	0.96 ± 0.1	0.98 ± 0.1	0.98 ± 0.1	0.91 ± 0.2
	ml	0.95 ± 0.5	1.02 ± 0.2	0.98 ± 0.2	1.08 ± 0.2	0.97 ± 0.3
	Glx	0.96 ± 0.9	1.01 ± 0.4	0.95 ± 0.4	1.27 ± 1.0	0.89 ± 0.5
	NAA / Cr	1.09 ± 0.3	1.05 ± 0.1	1.08 ± 0.1	1.11 ± 0.1	1.13 ± 0.1
	Cho / Cr	0.87 ± 0.2	0.97 ± 0.1	0.99 ± 0.1	0.97 ± 0.1	0.94 ± 0.1
	ml / Cr	1.20 ± 0.4	1.02 ± 0.2	0.99 ± 0.2	1.07 ± 0.2	1.01 ± 0.3
	Glx / Cr	1.36 ± 1.1	1.01 ± 0.4	1.00 ± 0.5	1.23 ± 0.9	0.95 ± 0.4
L. Cingulate GM	NAA	0.89 ± 0.2	1.02 ± 0.1	1.01 ± 0.1	1.08 ± 0.1	1.11 ± 0.1
	Cr	1.01 ± 0.2	1.09 ± 0.1	1.08 ± 0.1	1.15 ± 0.2	1.13 ± 0.2
	Cho	0.89 ± 0.2	1.01 ± 0.1	0.99 ± 0.1	1.05 ± 0.1	1.08 ± 0.2
	ml	0.90 ± 0.2	1.05 ± 0.2	1.04 ± 0.2	1.08 ± 0.3	1.08 ± 0.3
	Glx	1.53 ± 1.5	4.15 ± 7.7	4.97 ± 7.6	13.25 ± 32.2	4.42 ± 6.0
	NAA / Cr	0.88 ± 0.1	0.94 ± 0.1	0.94 ± 0.1	0.95 ± 0.1	1.00 ± 0.1
	Cho / Cr	0.87 ± 0.1	0.93 ± 0.1	0.92 ± 0.1	0.92 ± 0.1	0.96 ± 0.1
	ml / Cr	0.88 ± 0.2	0.96 ± 0.2	0.97 ± 0.2	0.95 ± 0.2	0.98 ± 0.3
	Glx / Cr	1.66 ± 1.6	4.94 ± 9.8	5.67 ± 9.6	10.34 ± 24.0	4.96 ± 7.0
L. Fusiform GM	NAA	0.82 ± 0.2	1.01 ± 0.1	0.99 ± 0.2	1.03 ± 0.2	0.97 ± 0.3
	Cr	0.82 ± 0.2	1.00 ± 0.1	0.99 ± 0.1	1.08 ± 0.2	1.05 ± 0.3
	Cho	0.79 ± 0.2	1.03 ± 0.2	1.03 ± 0.1	1.11 ± 0.2	1.06 ± 0.2
	ml	1.03 ± 0.7	1.14 ± 0.8	1.14 ± 0.7	1.39 ± 1.4	1.23 ± 0.9
	Glx	22.90 ± 50.1	1.32 ± 1.9	5.83 ± 14.0	38.93 ± 79.2	59.75 ± 97.0
	NAA / Cr	1.02 ± 0.2	1.01 ± 0.1	1.00 ± 0.1	0.96 ± 0.1	0.92 ± 0.2
	Cho / Cr	1.00 ± 0.3	1.04 ± 0.2	1.06 ± 0.2	1.03 ± 0.2	1.00 ± 0.3
	ml / Cr	1.32 ± 1.1	1.17 ± 0.9	1.19 ± 0.9	1.47 ± 2.1	1.52 ± 1.8
	Glx / Cr	26.96 ± 59.2	1.28 ± 1.7	5.32 ± 12.5	39.73 ± 87.0	66.10 ± 103.1

		MINT 50x50x18	SLIM 50x50x12	SLIM 40x40x12	SLIM 20x20x12	SLIM 16x16x12
Brain Stem	NAA	0.79 ± 0.4	1.03 ± 0.1	1.02 ± 0.1	1.00 ± 0.1	1.03 ± 0.1
	Cr	0.95 ± 0.4	1.03 ± 0.1	1.04 ± 0.1	1.07 ± 0.2	1.12 ± 0.3
	Cho	0.96 ± 0.5	1.05 ± 0.1	1.12 ± 0.3	1.19 ± 0.5	1.21 ± 0.6
	ml	1.06 ± 0.3	1.08 ± 0.3	1.06 ± 0.3	0.99 ± 0.3	1.23 ± 0.5
	Glx	1.45 ± 1.8	2.54 ± 2.7	0.84 ± 0.9	2.00 ± 2.0	1.02 ± 0.9
	NAA / Cr	0.84 ± 0.1	1.00 ± 0.1	1.00 ± 0.1	0.95 ± 0.1	0.95 ± 0.1
	Cho / Cr	1.08 ± 0.5	1.02 ± 0.1	1.12 ± 0.4	1.11 ± 0.4	1.09 ± 0.5
	ml / Cr	1.28 ± 0.5	1.06 ± 0.3	1.06 ± 0.3	0.93 ± 0.2	1.09 ± 0.3
	Glx / Cr	1.72 ± 2.2	2.49 ± 2.7	0.83 ± 1.0	1.90 ± 1.9	1.03 ± 0.9
L. Central WM	NAA	0.95 ± 0.1	1.04 ± 0.0	1.05 ± 0.0	1.10 ± 0.1	1.13 ± 0.1
	Cr	0.98 ± 0.1	1.02 ± 0.1	1.02 ± 0.1	1.05 ± 0.1	1.05 ± 0.1
	Cho	0.92 ± 0.1	1.07 ± 0.1	1.08 ± 0.0	1.15 ± 0.1	1.17 ± 0.1
	ml	0.96 ± 0.3	1.08 ± 0.2	1.07 ± 0.2	1.14 ± 0.3	1.11 ± 0.4
	Glx	0.62 ± 0.6	1.15 ± 1.5	0.94 ± 1.3	1.85 ± 3.4	0.55 ± 0.1
	NAA / Cr	0.97 ± 0.1	1.02 ± 0.1	1.03 ± 0.0	1.05 ± 0.1	1.09 ± 0.1
	Cho / Cr	0.94 ± 0.1	1.05 ± 0.1	1.05 ± 0.1	1.10 ± 0.1	1.13 ± 0.2
	ml / Cr	0.98 ± 0.3	1.04 ± 0.2	1.04 ± 0.2	1.06 ± 0.3	1.04 ± 0.3
	Glx / Cr	0.65 ± 0.7	1.15 ± 1.5	0.93 ± 1.3	1.75 ± 3.3	0.53 ± 0.1
L. Cerebellum WM	NAA	0.88 ± 0.2	1.07 ± 0.1	1.08 ± 0.1	1.10 ± 0.3	1.13 ± 0.2
	Cr	0.89 ± 0.2	1.05 ± 0.1	1.07 ± 0.1	1.13 ± 0.3	1.19 ± 0.3
	Cho	0.76 ± 0.2	1.06 ± 0.2	1.10 ± 0.2	1.12 ± 0.2	1.17 ± 0.3
	ml	0.81 ± 0.2	1.00 ± 0.2	0.96 ± 0.2	0.99 ± 0.2	1.00 ± 0.2
	Glx	1.67 ± 1.9	1.36 ± 1.2	1.29 ± 1.2	0.56 ± 0.3	1.24 ± 0.5
	NAA / Cr	1.01 ± 0.2	1.02 ± 0.1	1.02 ± 0.1	0.98 ± 0.1	0.96 ± 0.1
	Cho / Cr	0.86 ± 0.2	1.01 ± 0.1	1.03 ± 0.1	1.01 ± 0.2	1.00 ± 0.2
	ml / Cr	0.93 ± 0.2	0.96 ± 0.2	0.91 ± 0.2	0.90 ± 0.2	0.87 ± 0.2
	Glx / Cr	1.80 ± 1.9	1.41 ± 1.3	1.31 ± 1.3	0.52 ± 0.2	1.08 ± 0.5
L. Cingulate WM	NAA	0.81 ± 0.1	0.99 ± 0.1	0.98 ± 0.1	0.94 ± 0.1	0.90 ± 0.1
	Cr	0.97 ± 0.2	0.96 ± 0.1	0.95 ± 0.1	0.89 ± 0.1	0.84 ± 0.1
	Cho	0.95 ± 0.4	1.08 ± 0.3	1.09 ± 0.3	1.03 ± 0.2	0.97 ± 0.2
	ml	0.88 ± 0.3	1.00 ± 0.2	1.00 ± 0.2	1.01 ± 0.3	0.88 ± 0.2
	Glx	0.24 ± 0.0	0.48 ± 0.3	0.70 ± 0.3	0.88 ± 0.6	1.00 ± 0.8
	NAA / Cr	0.84 ± 0.1	1.03 ± 0.1	1.04 ± 0.1	1.07 ± 0.1	1.07 ± 0.1
	Cho / Cr	0.99 ± 0.3	1.14 ± 0.3	1.17 ± 0.5	1.17 ± 0.3	1.18 ± 0.3
	ml / Cr	0.90 ± 0.2	1.04 ± 0.2	1.06 ± 0.2	1.15 ± 0.3	1.04 ± 0.3
	Glx / Cr	0.30 ± 0.1	0.51 ± 0.3	0.73 ± 0.3	1.01 ± 0.7	1.30 ± 1.1
L. Fusiform WM	NAA	0.81 ± 0.1	0.98 ± 0.1	0.97 ± 0.1	1.06 ± 0.3	1.32 ± 0.5
	Cr	0.85 ± 0.2	0.96 ± 0.2	0.94 ± 0.1	0.99 ± 0.4	1.32 ± 0.7
	Cho	0.84 ± 0.2	1.16 ± 0.2	1.15 ± 0.2	1.21 ± 0.4	1.61 ± 0.8
	ml	1.02 ± 0.9	1.10 ± 0.7	1.06 ± 0.6	1.19 ± 1.1	1.63 ± 1.7
	Glx	2.34 ± 2.1	0.88 ± 1.2	1.03 ± 1.1	0.28 ± 0.0	N/A
	NAA / Cr	0.97 ± 0.2	1.03 ± 0.1	1.04 ± 0.1	1.13 ± 0.2	1.08 ± 0.2
	Cho / Cr	1.02 ± 0.3	1.22 ± 0.2	1.22 ± 0.2	1.26 ± 0.2	1.26 ± 0.3
	ml / Cr	1.27 ± 1.4	1.15 ± 0.7	1.13 ± 0.6	1.11 ± 0.4	1.28 ± 0.7
	Glx / Cr	2.74 ± 2.0	0.96 ± 1.3	1.08 ± 1.2	0.31 ± 0.0	N/A

		MINT 50x50x18	SLIM 50x50x12	SLIM 40x40x12	SLIM 20x20x12	SLIM 16x16x12
Ventral Diencephalon	NAA	1.02 ± 0.2	0.92 ± 0.2	0.91 ± 0.2	0.95 ± 0.1	0.93 ± 0.1
	Cr	1.07 ± 0.2	0.98 ± 0.1	0.99 ± 0.1	1.00 ± 0.1	0.99 ± 0.1
	Cho	0.98 ± 0.2	0.97 ± 0.2	0.98 ± 0.2	0.95 ± 0.1	0.98 ± 0.1
	mI	1.14 ± 0.3	1.01 ± 0.3	1.00 ± 0.3	1.22 ± 0.6	0.97 ± 0.3
	Glx	1.87 ± 2.6	2.06 ± 2.1	1.59 ± 1.4	2.98 ± 3.1	1.15 ± 1.0
	NAA / Cr	0.96 ± 0.1	0.94 ± 0.1	0.93 ± 0.1	0.95 ± 0.1	0.95 ± 0.1
	Cho / Cr	0.92 ± 0.2	0.99 ± 0.1	1.00 ± 0.2	0.95 ± 0.2	1.00 ± 0.2
	mI / Cr	1.07 ± 0.3	1.04 ± 0.3	1.02 ± 0.2	1.21 ± 0.5	0.99 ± 0.3
	Glx / Cr	1.76 ± 2.5	2.22 ± 2.4	1.55 ± 1.5	2.85 ± 2.8	1.20 ± 1.1
R. Central GM	NAA	1.07 ± 0.1	0.97 ± 0.0	0.97 ± 0.1	0.97 ± 0.1	0.93 ± 0.1
	Cr	1.16 ± 0.1	0.96 ± 0.1	0.97 ± 0.1	0.92 ± 0.1	0.88 ± 0.1
	Cho	1.21 ± 0.2	0.91 ± 0.1	0.87 ± 0.1	0.85 ± 0.3	0.81 ± 0.2
	mI	1.37 ± 0.5	1.00 ± 0.4	0.92 ± 0.2	0.80 ± 0.3	0.76 ± 0.3
	Glx	12.01 ± 22.0	7.91 ± 10.0	9.27 ± 10.3	8.41 ± 10.4	6.50 ± 12.8
	NAA / Cr	0.93 ± 0.1	1.01 ± 0.1	1.00 ± 0.1	1.06 ± 0.1	1.07 ± 0.2
	Cho / Cr	1.04 ± 0.1	0.96 ± 0.1	0.90 ± 0.1	0.93 ± 0.3	0.92 ± 0.2
	mI / Cr	1.19 ± 0.4	1.06 ± 0.5	0.95 ± 0.2	0.89 ± 0.3	0.87 ± 0.3
	Glx / Cr	13.95 ± 27.6	8.41 ± 10.6	9.91 ± 10.9	9.02 ± 10.5	8.46 ± 16.6
R. Cerebellum GM	NAA	1.16 ± 0.4	1.08 ± 0.1	1.08 ± 0.1	1.13 ± 0.1	1.12 ± 0.3
	Cr	1.11 ± 0.3	1.00 ± 0.1	1.00 ± 0.1	0.99 ± 0.1	0.97 ± 0.3
	Cho	1.06 ± 0.3	0.92 ± 0.1	0.91 ± 0.1	0.95 ± 0.2	0.90 ± 0.3
	mI	1.32 ± 0.6	1.04 ± 0.4	1.04 ± 0.4	1.01 ± 0.4	1.00 ± 0.6
	Glx	7.52 ± 20.0	6.10 ± 12.5	3.89 ± 8.4	3.64 ± 10.0	1.16 ± 0.6
	NAA / Cr	1.04 ± 0.2	1.08 ± 0.1	1.08 ± 0.1	1.14 ± 0.1	1.17 ± 0.2
	Cho / Cr	0.95 ± 0.2	0.92 ± 0.1	0.92 ± 0.1	0.97 ± 0.2	0.95 ± 0.3
	mI / Cr	1.17 ± 0.4	1.05 ± 0.4	1.04 ± 0.4	1.02 ± 0.4	1.03 ± 0.6
	Glx / Cr	6.83 ± 18.1	5.76 ± 11.6	3.80 ± 8.2	3.28 ± 8.4	1.54 ± 1.5
R. Cingulate GM	NAA	0.96 ± 0.2	1.05 ± 0.1	1.05 ± 0.1	1.03 ± 0.1	1.05 ± 0.1
	Cr	1.15 ± 0.2	1.12 ± 0.1	1.12 ± 0.1	1.08 ± 0.2	1.09 ± 0.2
	Cho	0.96 ± 0.2	1.10 ± 0.1	1.11 ± 0.1	1.07 ± 0.2	1.12 ± 0.3
	mI	0.93 ± 0.2	1.08 ± 0.2	1.10 ± 0.3	1.06 ± 0.2	1.14 ± 0.4
	Glx	0.15 ± 0.2	0.94 ± 1.1	1.19 ± 1.1	1.80 ± 1.8	2.29 ± 2.1
	NAA / Cr	0.85 ± 0.1	0.94 ± 0.1	0.95 ± 0.1	0.97 ± 0.1	0.99 ± 0.1
	Cho / Cr	0.84 ± 0.1	0.99 ± 0.1	1.00 ± 0.1	1.00 ± 0.1	1.03 ± 0.2
	mI / Cr	0.80 ± 0.1	0.98 ± 0.2	0.99 ± 0.2	1.00 ± 0.3	1.09 ± 0.4
	Glx / Cr	0.13 ± 0.1	0.88 ± 1.0	1.13 ± 1.1	2.32 ± 3.1	3.33 ± 3.6
R. Fusiform GM	NAA	1.15 ± 0.2	1.03 ± 0.1	1.01 ± 0.1	1.06 ± 0.1	1.09 ± 0.2
	Cr	1.18 ± 0.3	1.00 ± 0.1	1.03 ± 0.1	1.15 ± 0.2	1.15 ± 0.2
	Cho	1.04 ± 0.2	1.01 ± 0.2	1.00 ± 0.2	1.09 ± 0.3	1.08 ± 0.3
	mI	1.30 ± 0.6	1.03 ± 0.3	1.03 ± 0.4	1.11 ± 0.4	1.43 ± 1.4
	Glx	2.19 ± 1.6	1.45 ± 0.9	1.48 ± 1.4	1.29 ± 1.0	6.79 ± 13.5
	NAA / Cr	0.99 ± 0.1	1.03 ± 0.1	1.00 ± 0.1	0.94 ± 0.1	0.95 ± 0.1
	Cho / Cr	0.90 ± 0.2	1.02 ± 0.2	0.99 ± 0.2	0.98 ± 0.2	0.96 ± 0.3
	mI / Cr	1.12 ± 0.4	1.05 ± 0.3	1.02 ± 0.4	0.98 ± 0.3	1.38 ± 1.7
	Glx / Cr	1.94 ± 1.4	1.50 ± 0.9	1.50 ± 1.4	1.26 ± 0.9	8.20 ± 17.4

		MINT 50x50x18	SLIM 50x50x12	SLIM 40x40x12	SLIM 20x20x12	SLIM 16x16x12
Ventricles	NAA	0.90 ± 0.2	0.93 ± 0.1	0.94 ± 0.1	0.92 ± 0.1	0.96 ± 0.1
	Cr	1.03 ± 0.3	0.90 ± 0.1	0.89 ± 0.1	0.88 ± 0.1	0.93 ± 0.2
	Cho	1.08 ± 0.3	0.99 ± 0.1	1.01 ± 0.1	1.01 ± 0.1	1.05 ± 0.1
	mI	0.89 ± 0.3	0.95 ± 0.1	1.00 ± 0.1	0.90 ± 0.2	1.02 ± 0.2
	Glx	0.85 ± 0.5	0.66 ± 0.5	1.10 ± 0.4	0.60 ± 0.8	1.23 ± 1.9
	NAA / Cr	0.89 ± 0.1	1.04 ± 0.1	1.06 ± 0.1	1.06 ± 0.1	1.05 ± 0.1
	Cho / Cr	1.05 ± 0.2	1.11 ± 0.1	1.13 ± 0.1	1.18 ± 0.2	1.15 ± 0.2
	mI / Cr	0.85 ± 0.2	1.06 ± 0.1	1.12 ± 0.1	1.04 ± 0.2	1.10 ± 0.2
	Glx / Cr	0.66 ± 0.4	0.68 ± 0.5	1.18 ± 0.5	0.73 ± 0.9	1.31 ± 2.1
R. Central WM	NAA	1.04 ± 0.1	1.02 ± 0.0	1.03 ± 0.1	1.03 ± 0.1	1.03 ± 0.1
	Cr	1.11 ± 0.1	1.00 ± 0.1	1.00 ± 0.1	0.98 ± 0.1	0.98 ± 0.1
	Cho	1.10 ± 0.1	1.03 ± 0.1	1.05 ± 0.1	1.08 ± 0.1	1.08 ± 0.1
	mI	1.21 ± 0.5	0.99 ± 0.2	1.12 ± 0.3	1.27 ± 0.5	1.25 ± 0.6
	Glx	0.27 ± 0.3	1.28 ± 0.0	1.12 ± 0.2	18.18 ± 29.4	17.07 ± 24.1
	NAA / Cr	0.94 ± 0.1	1.02 ± 0.1	1.04 ± 0.1	1.06 ± 0.1	1.06 ± 0.1
	Cho / Cr	0.99 ± 0.1	1.03 ± 0.1	1.06 ± 0.1	1.10 ± 0.1	1.11 ± 0.1
	mI / Cr	1.12 ± 0.5	0.99 ± 0.3	1.13 ± 0.3	1.33 ± 0.7	1.31 ± 0.7
	Glx / Cr	0.24 ± 0.2	1.52 ± 0.0	1.23 ± 0.4	22.40 ± 36.3	20.01 ± 28.3
R. Cerebellum WM	NAA	1.05 ± 0.2	0.99 ± 0.1	0.99 ± 0.1	1.00 ± 0.1	1.04 ± 0.3
	Cr	1.12 ± 0.3	1.07 ± 0.2	1.07 ± 0.2	1.17 ± 0.5	1.15 ± 0.3
	Cho	1.01 ± 0.3	1.11 ± 0.1	1.12 ± 0.1	1.10 ± 0.1	1.15 ± 0.2
	mI	0.99 ± 0.2	1.05 ± 0.3	1.06 ± 0.3	1.09 ± 0.4	1.22 ± 0.7
	Glx	4.02 ± 9.4	1.08 ± 0.7	1.69 ± 1.8	1.80 ± 2.4	4.53 ± 9.2
	NAA / Cr	0.97 ± 0.2	0.94 ± 0.1	0.94 ± 0.1	0.91 ± 0.2	0.91 ± 0.1
	Cho / Cr	0.93 ± 0.2	1.05 ± 0.2	1.06 ± 0.2	1.05 ± 0.1	1.02 ± 0.2
	mI / Cr	0.93 ± 0.3	0.99 ± 0.2	0.99 ± 0.2	0.96 ± 0.3	1.03 ± 0.4
	Glx / Cr	6.44 ± 18.1	1.07 ± 0.7	1.67 ± 1.8	1.70 ± 2.3	4.33 ± 8.9
R. Cingulate WM	NAA	0.94 ± 0.2	0.99 ± 0.0	0.98 ± 0.0	0.96 ± 0.1	0.91 ± 0.2
	Cr	1.11 ± 0.2	0.96 ± 0.1	0.92 ± 0.1	0.91 ± 0.1	0.86 ± 0.2
	Cho	0.97 ± 0.2	1.03 ± 0.1	1.04 ± 0.1	1.00 ± 0.1	0.95 ± 0.2
	mI	0.90 ± 0.2	0.95 ± 0.2	0.94 ± 0.1	0.93 ± 0.1	0.87 ± 0.2
	Glx	0.55 ± 0.6	0.81 ± 0.7	1.00 ± 0.6	1.02 ± 0.7	1.07 ± 0.7
	NAA / Cr	0.85 ± 0.1	1.04 ± 0.1	1.07 ± 0.1	1.05 ± 0.1	1.07 ± 0.1
	Cho / Cr	0.89 ± 0.1	1.08 ± 0.1	1.14 ± 0.2	1.10 ± 0.1	1.10 ± 0.1
	mI / Cr	0.81 ± 0.1	0.99 ± 0.2	1.03 ± 0.1	1.03 ± 0.2	1.05 ± 0.3
	Glx / Cr	0.43 ± 0.4	0.88 ± 0.8	1.14 ± 0.6	1.23 ± 0.8	1.95 ± 2.4
R. Fusiform WM	NAA	1.06 ± 0.2	0.93 ± 0.1	0.93 ± 0.1	0.96 ± 0.2	1.08 ± 0.2
	Cr	1.08 ± 0.2	0.93 ± 0.1	0.93 ± 0.1	0.93 ± 0.2	1.10 ± 0.4
	Cho	1.13 ± 0.3	0.98 ± 0.1	1.02 ± 0.1	1.05 ± 0.1	1.24 ± 0.2
	mI	1.12 ± 0.4	1.05 ± 0.3	1.06 ± 0.3	1.08 ± 0.4	1.41 ± 1.2
	Glx	3.39 ± 3.6	1.51 ± 1.3	1.21 ± 1.0	1.17 ± 1.4	1.80 ± 1.2
	NAA / Cr	0.98 ± 0.1	1.00 ± 0.1	1.01 ± 0.1	1.05 ± 0.2	1.03 ± 0.2
	Cho / Cr	1.06 ± 0.2	1.06 ± 0.2	1.10 ± 0.1	1.15 ± 0.2	1.26 ± 0.2
	mI / Cr	1.05 ± 0.3	1.14 ± 0.3	1.15 ± 0.4	1.21 ± 0.5	1.40 ± 1.1
	Glx / Cr	3.23 ± 3.3	1.74 ± 1.6	1.43 ± 1.3	1.01 ± 1.1	1.75 ± 1.0

		MINT 50x50x18	SLIM 50x50x12	SLIM 40x40x12	SLIM 20x20x12	SLIM 16x16x12
L. Inferior Parietal GM	NAA	0.96 ± 0.2	1.01 ± 0.0	1.02 ± 0.1	1.07 ± 0.1	1.05 ± 0.1
	Cr	1.07 ± 0.2	1.06 ± 0.1	1.08 ± 0.1	1.17 ± 0.2	1.16 ± 0.1
	Cho	0.98 ± 0.3	1.00 ± 0.1	1.01 ± 0.1	1.00 ± 0.1	0.96 ± 0.1
	mI	0.86 ± 0.2	1.00 ± 0.1	1.00 ± 0.1	1.05 ± 0.1	1.04 ± 0.2
	Glx	13.11 ± 15.6	4.56 ± 6.6	4.89 ± 6.5	3.72 ± 6.1	5.10 ± 9.1
	NAA / Cr	0.90 ± 0.1	0.95 ± 0.1	0.95 ± 0.1	0.93 ± 0.1	0.92 ± 0.1
	Cho / Cr	0.92 ± 0.2	0.95 ± 0.1	0.94 ± 0.1	0.87 ± 0.2	0.84 ± 0.2
	mI / Cr	0.81 ± 0.1	0.94 ± 0.1	0.92 ± 0.1	0.91 ± 0.2	0.91 ± 0.2
	Glx / Cr	11.49 ± 14.4	4.06 ± 5.8	4.39 ± 5.8	3.59 ± 6.7	5.03 ± 10.0
L. Inferior Temporal GM	NAA	0.94 ± 0.2	1.08 ± 0.1	1.08 ± 0.1	1.08 ± 0.1	1.03 ± 0.1
	Cr	1.04 ± 0.2	1.11 ± 0.1	1.11 ± 0.1	1.11 ± 0.1	1.08 ± 0.2
	Cho	0.90 ± 0.2	1.04 ± 0.2	1.03 ± 0.2	1.02 ± 0.2	1.01 ± 0.2
	mI	1.15 ± 0.5	1.07 ± 0.4	1.08 ± 0.5	0.95 ± 0.3	0.89 ± 0.2
	Glx	1.39 ± 0.8	1.81 ± 1.4	1.72 ± 1.4	1.57 ± 1.6	1.00 ± 0.6
	NAA / Cr	0.90 ± 0.1	0.98 ± 0.1	0.97 ± 0.1	0.98 ± 0.1	0.97 ± 0.1
	Cho / Cr	0.87 ± 0.1	0.95 ± 0.2	0.93 ± 0.2	0.92 ± 0.2	0.95 ± 0.2
	mI / Cr	1.10 ± 0.4	0.97 ± 0.4	0.98 ± 0.4	0.87 ± 0.3	0.85 ± 0.3
	Glx / Cr	1.37 ± 0.8	1.74 ± 1.6	1.66 ± 1.6	1.53 ± 1.8	0.86 ± 0.5
L. Insula GM	NAA	0.90 ± 0.2	1.02 ± 0.1	1.03 ± 0.0	1.08 ± 0.1	1.15 ± 0.1
	Cr	0.98 ± 0.2	1.03 ± 0.0	1.05 ± 0.0	1.13 ± 0.1	1.21 ± 0.1
	Cho	0.98 ± 0.3	1.03 ± 0.1	1.04 ± 0.1	1.16 ± 0.1	1.25 ± 0.2
	mI	0.95 ± 0.3	1.01 ± 0.1	1.03 ± 0.1	1.07 ± 0.2	1.11 ± 0.2
	Glx	0.37 ± 0.1	13.44 ± 24.8	5.39 ± 8.5	2.60 ± 2.3	199.54 ± 281.2
	NAA / Cr	0.91 ± 0.2	0.99 ± 0.1	0.99 ± 0.0	0.96 ± 0.1	0.96 ± 0.1
	Cho / Cr	1.03 ± 0.3	1.00 ± 0.1	1.00 ± 0.1	1.03 ± 0.2	1.04 ± 0.2
	mI / Cr	0.98 ± 0.2	0.98 ± 0.1	0.98 ± 0.1	0.95 ± 0.2	0.92 ± 0.2
	Glx / Cr	0.36 ± 0.1	12.58 ± 23.2	4.98 ± 7.8	2.27 ± 2.0	187.52 ± 264.5
L. Lateral Occipital GM	NAA	0.81 ± 0.2	1.01 ± 0.1	1.01 ± 0.1	1.06 ± 0.2	1.12 ± 0.3
	Cr	0.84 ± 0.2	1.00 ± 0.1	1.00 ± 0.1	1.00 ± 0.1	1.04 ± 0.2
	Cho	0.76 ± 0.2	0.97 ± 0.2	0.98 ± 0.2	0.98 ± 0.2	1.03 ± 0.3
	mI	0.97 ± 0.4	0.94 ± 0.2	0.94 ± 0.2	0.96 ± 0.2	0.97 ± 0.2
	Glx	0.85 ± 0.6	0.88 ± 0.7	0.92 ± 0.8	1.48 ± 1.4	1.63 ± 1.3
	NAA / Cr	0.97 ± 0.2	1.01 ± 0.1	1.02 ± 0.1	1.05 ± 0.2	1.08 ± 0.2
	Cho / Cr	0.92 ± 0.2	0.97 ± 0.2	0.99 ± 0.2	0.98 ± 0.2	1.02 ± 0.3
	mI / Cr	1.17 ± 0.5	0.94 ± 0.2	0.96 ± 0.2	0.96 ± 0.2	0.96 ± 0.3
	Glx / Cr	0.99 ± 0.7	0.89 ± 0.8	0.94 ± 0.7	1.48 ± 1.4	1.57 ± 1.2
L. Lingual GM	NAA	0.83 ± 0.2	0.97 ± 0.1	0.96 ± 0.1	0.96 ± 0.1	0.90 ± 0.2
	Cr	0.82 ± 0.2	0.96 ± 0.1	0.96 ± 0.1	1.00 ± 0.1	0.96 ± 0.1
	Cho	0.80 ± 0.1	0.93 ± 0.1	0.92 ± 0.1	0.87 ± 0.2	0.94 ± 0.5
	mI	0.79 ± 0.2	0.91 ± 0.1	0.90 ± 0.2	0.80 ± 0.2	0.81 ± 0.2
	Glx	0.65 ± 0.2	1.33 ± 1.0	0.61 ± 0.3	0.74 ± 0.5	0.47 ± 0.2
	NAA / Cr	1.01 ± 0.2	1.01 ± 0.1	1.01 ± 0.1	0.97 ± 0.1	1.00 ± 0.1
	Cho / Cr	0.99 ± 0.1	0.98 ± 0.1	0.97 ± 0.1	0.88 ± 0.2	0.86 ± 0.2
	mI / Cr	0.99 ± 0.3	0.96 ± 0.1	0.95 ± 0.2	0.82 ± 0.3	0.86 ± 0.3
	Glx / Cr	0.86 ± 0.3	1.50 ± 1.2	0.64 ± 0.2	0.79 ± 0.5	0.52 ± 0.2

		MINT 50x50x18	SLIM 50x50x12	SLIM 40x40x12	SLIM 20x20x12	SLIM 16x16x12
L. Inferior Parietal WM	NAA	0.90 ± 0.2	1.01 ± 0.0	1.00 ± 0.0	1.00 ± 0.1	1.01 ± 0.1
	Cr	1.08 ± 0.2	1.01 ± 0.1	1.00 ± 0.1	0.94 ± 0.1	0.94 ± 0.1
	Cho	0.89 ± 0.2	1.02 ± 0.1	1.03 ± 0.1	1.10 ± 0.1	1.17 ± 0.1
	mI	0.88 ± 0.2	0.97 ± 0.1	0.95 ± 0.1	0.87 ± 0.1	0.82 ± 0.2
	Glx	2.84 ± 2.1	0.49 ± 0.5	1.25 ± 0.0	0.88 ± 0.0	N/A
	NAA / Cr	0.83 ± 0.1	1.01 ± 0.0	1.01 ± 0.0	1.06 ± 0.1	1.08 ± 0.1
	Cho / Cr	0.83 ± 0.1	1.02 ± 0.1	1.03 ± 0.1	1.17 ± 0.1	1.26 ± 0.2
	mI / Cr	0.82 ± 0.1	0.96 ± 0.1	0.95 ± 0.1	0.93 ± 0.1	0.87 ± 0.2
	Glx / Cr	2.36 ± 1.8	0.52 ± 0.5	1.12 ± 0.0	0.95 ± 0.0	N/A
L. Inferior Temporal WM	NAA	0.91 ± 0.2	0.98 ± 0.1	0.98 ± 0.0	1.03 ± 0.1	1.04 ± 0.1
	Cr	1.05 ± 0.2	0.97 ± 0.1	0.97 ± 0.1	1.01 ± 0.1	1.03 ± 0.1
	Cho	0.83 ± 0.1	1.02 ± 0.1	1.02 ± 0.1	1.07 ± 0.1	1.03 ± 0.1
	mI	1.07 ± 0.5	1.00 ± 0.2	1.02 ± 0.2	1.15 ± 0.4	0.98 ± 0.3
	Glx	4.21 ± 7.3	1.01 ± 0.3	0.83 ± 0.2	2.39 ± 3.2	N/A
	NAA / Cr	0.87 ± 0.1	1.02 ± 0.1	1.02 ± 0.1	1.02 ± 0.1	1.01 ± 0.1
	Cho / Cr	0.79 ± 0.1	1.06 ± 0.1	1.06 ± 0.1	1.07 ± 0.1	1.00 ± 0.1
	mI / Cr	0.99 ± 0.3	1.03 ± 0.1	1.05 ± 0.2	1.15 ± 0.5	0.96 ± 0.3
	Glx / Cr	3.64 ± 5.8	1.03 ± 0.4	0.85 ± 0.2	2.64 ± 3.6	N/A
L. Insula WM	NAA	0.86 ± 0.2	1.01 ± 0.0	1.00 ± 0.0	1.05 ± 0.1	1.09 ± 0.1
	Cr	0.99 ± 0.2	0.98 ± 0.1	0.96 ± 0.1	0.94 ± 0.1	0.96 ± 0.1
	Cho	0.95 ± 0.3	1.03 ± 0.1	1.02 ± 0.1	1.03 ± 0.1	1.05 ± 0.1
	mI	0.93 ± 0.3	1.00 ± 0.2	0.97 ± 0.2	0.93 ± 0.1	0.95 ± 0.1
	Glx	0.92 ± 0.0	1.37 ± 0.8	0.92 ± 0.8	0.19 ± 0.2	0.10 ± 0.0
	NAA / Cr	0.89 ± 0.1	1.03 ± 0.1	1.05 ± 0.1	1.12 ± 0.1	1.15 ± 0.1
	Cho / Cr	0.96 ± 0.1	1.06 ± 0.1	1.07 ± 0.1	1.10 ± 0.1	1.11 ± 0.1
	mI / Cr	0.97 ± 0.2	1.02 ± 0.1	1.01 ± 0.1	0.99 ± 0.1	1.00 ± 0.1
	Glx / Cr	0.88 ± 0.1	1.45 ± 1.0	0.98 ± 1.0	0.19 ± 0.2	0.11 ± 0.0
L. Lateral Occipital WM	NAA	0.81 ± 0.2	1.06 ± 0.1	1.06 ± 0.1	1.17 ± 0.1	1.18 ± 0.1
	Cr	0.87 ± 0.2	1.01 ± 0.1	1.02 ± 0.1	1.09 ± 0.1	1.07 ± 0.2
	Cho	0.72 ± 0.2	1.04 ± 0.1	1.02 ± 0.1	1.05 ± 0.1	0.99 ± 0.3
	mI	0.83 ± 0.2	0.99 ± 0.2	0.99 ± 0.2	1.01 ± 0.3	0.89 ± 0.2
	Glx	1.06 ± 0.6	1.01 ± 0.7	1.11 ± 0.4	0.82 ± 0.2	0.50 ± 0.7
	NAA / Cr	0.95 ± 0.1	1.05 ± 0.1	1.05 ± 0.1	1.08 ± 0.1	1.12 ± 0.2
	Cho / Cr	0.84 ± 0.1	1.03 ± 0.1	1.01 ± 0.1	0.98 ± 0.2	0.94 ± 0.3
	mI / Cr	0.96 ± 0.2	0.98 ± 0.2	0.98 ± 0.2	0.93 ± 0.2	0.84 ± 0.2
	Glx / Cr	1.30 ± 0.7	1.01 ± 0.7	1.14 ± 0.4	0.75 ± 0.2	0.45 ± 0.6
L. Lingual WM	NAA	0.80 ± 0.1	1.08 ± 0.1	1.09 ± 0.1	1.14 ± 0.2	1.06 ± 0.2
	Cr	0.86 ± 0.2	0.98 ± 0.1	1.00 ± 0.1	1.01 ± 0.2	0.97 ± 0.2
	Cho	0.82 ± 0.1	1.09 ± 0.1	1.11 ± 0.1	1.22 ± 0.1	1.30 ± 0.3
	mI	0.85 ± 0.2	1.06 ± 0.4	1.00 ± 0.3	1.15 ± 0.8	0.96 ± 0.3
	Glx	0.67 ± 0.7	4.22 ± 7.6	4.79 ± 8.6	10.41 ± 17.7	0.19 ± 0.2
	NAA / Cr	0.94 ± 0.1	1.10 ± 0.1	1.09 ± 0.1	1.14 ± 0.1	1.12 ± 0.2
	Cho / Cr	0.97 ± 0.1	1.13 ± 0.2	1.13 ± 0.2	1.23 ± 0.2	1.39 ± 0.4
	mI / Cr	1.01 ± 0.3	1.10 ± 0.5	1.00 ± 0.2	1.11 ± 0.5	1.06 ± 0.5
	Glx / Cr	0.81 ± 0.8	3.95 ± 7.0	4.26 ± 7.5	7.81 ± 13.2	0.19 ± 0.2

		MINT 50x50x18	SLIM 50x50x12	SLIM 40x40x12	SLIM 20x20x12	SLIM 16x16x12
R. Inferior Parietal GM	NAA	1.01 ± 0.2	1.01 ± 0.1	0.99 ± 0.3	1.11 ± 0.1	1.00 ± 0.4
	Cr	1.09 ± 0.2	1.09 ± 0.1	1.10 ± 0.1	1.13 ± 0.1	1.14 ± 0.1
	Cho	1.03 ± 0.4	1.06 ± 0.3	1.00 ± 0.1	0.95 ± 0.2	0.96 ± 0.2
	ml	1.02 ± 0.3	0.95 ± 0.1	0.92 ± 0.3	0.92 ± 0.2	0.92 ± 0.5
	Glx	5.48 ± 7.7	0.73 ± 0.5	0.99 ± 0.9	3.83 ± 2.4	3.36 ± 1.9
	NAA / Cr	0.92 ± 0.1	0.95 ± 0.1	0.96 ± 0.1	0.99 ± 0.2	0.99 ± 0.1
	Cho / Cr	0.95 ± 0.3	0.91 ± 0.1	0.91 ± 0.1	0.85 ± 0.2	0.84 ± 0.1
	ml / Cr	0.94 ± 0.2	0.88 ± 0.1	0.89 ± 0.1	0.83 ± 0.3	0.79 ± 0.2
	Glx / Cr	4.14 ± 5.5	0.63 ± 0.4	0.90 ± 0.8	3.36 ± 2.3	2.85 ± 1.7
R. Inferior Temporal GM	NAA	1.08 ± 0.2	1.02 ± 0.1	1.00 ± 0.1	1.02 ± 0.2	1.02 ± 0.2
	Cr	1.13 ± 0.2	1.02 ± 0.2	1.05 ± 0.2	1.07 ± 0.2	1.07 ± 0.2
	Cho	1.02 ± 0.1	0.91 ± 0.2	0.88 ± 0.2	0.90 ± 0.2	0.93 ± 0.3
	ml	1.30 ± 0.4	0.86 ± 0.3	0.90 ± 0.3	1.02 ± 0.3	1.07 ± 0.8
	Glx	1.68 ± 1.1	1.41 ± 1.2	1.39 ± 1.1	1.34 ± 1.2	1.10 ± 1.0
	NAA / Cr	0.97 ± 0.1	1.00 ± 0.1	0.95 ± 0.1	1.01 ± 0.2	0.96 ± 0.1
	Cho / Cr	0.92 ± 0.2	0.92 ± 0.3	0.86 ± 0.2	0.87 ± 0.3	0.87 ± 0.2
	ml / Cr	1.16 ± 0.3	0.87 ± 0.3	0.88 ± 0.3	1.00 ± 0.4	1.06 ± 0.9
	Glx / Cr	1.47 ± 0.9	1.40 ± 1.3	1.34 ± 1.2	1.06 ± 0.9	0.91 ± 0.8
R. Insula GM	NAA	0.99 ± 0.3	1.01 ± 0.1	1.02 ± 0.1	1.02 ± 0.1	1.06 ± 0.1
	Cr	1.03 ± 0.3	1.06 ± 0.1	1.08 ± 0.1	1.16 ± 0.1	1.14 ± 0.1
	Cho	1.05 ± 0.2	1.00 ± 0.2	1.04 ± 0.2	1.12 ± 0.2	1.22 ± 0.2
	ml	1.01 ± 0.5	1.02 ± 0.4	1.03 ± 0.4	1.08 ± 0.3	1.30 ± 1.0
	Glx	0.55 ± 0.0	1.58 ± 1.2	1.15 ± 1.3	1.15 ± 0.9	3.47 ± 5.3
	NAA / Cr	0.95 ± 0.2	0.95 ± 0.1	0.95 ± 0.1	0.89 ± 0.1	0.93 ± 0.1
	Cho / Cr	1.04 ± 0.2	0.96 ± 0.2	0.98 ± 0.2	0.98 ± 0.2	1.08 ± 0.2
	ml / Cr	1.01 ± 0.4	0.96 ± 0.3	0.96 ± 0.3	0.93 ± 0.2	1.15 ± 0.9
	Glx / Cr	0.47 ± 0.0	1.43 ± 1.0	1.00 ± 1.1	1.02 ± 0.9	3.14 ± 4.7
R. Lateral Occipital GM	NAA	0.94 ± 0.4	0.97 ± 0.1	0.95 ± 0.1	0.93 ± 0.1	0.93 ± 0.2
	Cr	1.02 ± 0.3	0.98 ± 0.1	0.96 ± 0.1	0.89 ± 0.2	0.87 ± 0.2
	Cho	1.01 ± 0.3	0.90 ± 0.2	0.89 ± 0.2	1.03 ± 0.3	0.90 ± 0.3
	ml	1.06 ± 0.5	0.90 ± 0.2	0.91 ± 0.2	1.01 ± 0.4	0.80 ± 0.6
	Glx	5.23 ± 8.2	1.34 ± 1.0	0.79 ± 0.6	2.55 ± 4.8	1.50 ± 1.2
	NAA / Cr	0.98 ± 0.1	1.00 ± 0.1	0.99 ± 0.1	1.06 ± 0.2	1.08 ± 0.2
	Cho / Cr	1.03 ± 0.3	0.94 ± 0.3	0.94 ± 0.2	1.17 ± 0.4	1.04 ± 0.2
	ml / Cr	1.10 ± 0.3	0.93 ± 0.2	0.96 ± 0.2	1.20 ± 0.5	0.92 ± 0.6
	Glx / Cr	4.51 ± 5.8	1.35 ± 1.0	0.89 ± 0.8	2.64 ± 4.7	2.51 ± 3.0
R. Lingual GM	NAA	1.11 ± 0.2	0.98 ± 0.1	0.98 ± 0.1	0.98 ± 0.1	0.99 ± 0.1
	Cr	1.15 ± 0.2	1.01 ± 0.1	1.00 ± 0.1	1.03 ± 0.1	1.04 ± 0.1
	Cho	0.98 ± 0.1	0.92 ± 0.1	0.92 ± 0.1	0.91 ± 0.1	0.96 ± 0.2
	ml	1.01 ± 0.3	0.90 ± 0.1	0.88 ± 0.2	0.92 ± 0.1	0.85 ± 0.2
	Glx	2.26 ± 1.2	1.54 ± 2.0	1.62 ± 2.0	1.20 ± 0.7	1.62 ± 1.7
	NAA / Cr	0.97 ± 0.1	0.97 ± 0.0	0.98 ± 0.1	0.96 ± 0.1	0.96 ± 0.1
	Cho / Cr	0.87 ± 0.1	0.92 ± 0.1	0.92 ± 0.1	0.90 ± 0.2	0.93 ± 0.2
	ml / Cr	0.88 ± 0.2	0.89 ± 0.1	0.88 ± 0.1	0.90 ± 0.1	0.83 ± 0.2
	Glx / Cr	2.11 ± 1.1	1.51 ± 1.9	1.56 ± 1.9	1.15 ± 0.6	1.46 ± 1.4

		MINT 50x50x18	SLIM 50x50x12	SLIM 40x40x12	SLIM 20x20x12	SLIM 16x16x12
R. Inferior Parietal WM	NAA	1.04 ± 0.2	1.01 ± 0.1	1.01 ± 0.1	1.00 ± 0.1	1.02 ± 0.1
	Cr	1.19 ± 0.2	1.03 ± 0.1	1.01 ± 0.1	0.98 ± 0.1	1.01 ± 0.1
	Cho	0.95 ± 0.2	1.02 ± 0.1	1.02 ± 0.1	1.03 ± 0.1	1.07 ± 0.1
	ml	0.98 ± 0.3	1.03 ± 0.1	1.02 ± 0.1	0.99 ± 0.1	0.97 ± 0.2
	Glx	0.92 ± 0.6	3.08 ± 5.1	5.19 ± 6.0	8.99 ± 13.8	12.37 ± 11.9
	NAA / Cr	0.87 ± 0.1	0.99 ± 0.1	1.01 ± 0.1	1.02 ± 0.0	1.01 ± 0.1
	Cho / Cr	0.80 ± 0.1	0.99 ± 0.1	1.02 ± 0.1	1.05 ± 0.1	1.07 ± 0.1
	ml / Cr	0.82 ± 0.1	1.01 ± 0.1	1.01 ± 0.1	1.02 ± 0.2	0.97 ± 0.2
	Glx / Cr	0.68 ± 0.4	3.16 ± 5.2	5.34 ± 6.3	9.83 ± 15.0	12.58 ± 11.7
R. Inferior Temporal WM	NAA	1.14 ± 0.2	0.99 ± 0.1	0.99 ± 0.1	1.01 ± 0.1	1.05 ± 0.1
	Cr	1.20 ± 0.3	1.01 ± 0.1	1.00 ± 0.1	1.01 ± 0.1	1.04 ± 0.2
	Cho	1.03 ± 0.2	0.99 ± 0.2	0.99 ± 0.2	0.99 ± 0.2	1.02 ± 0.2
	ml	1.18 ± 0.4	0.99 ± 0.2	1.00 ± 0.2	1.01 ± 0.3	0.90 ± 0.3
	Glx	1.78 ± 1.5	3.68 ± 10.8	0.72 ± 0.7	1.75 ± 3.6	1.03 ± 0.9
	NAA / Cr	0.97 ± 0.1	0.98 ± 0.1	1.00 ± 0.1	1.00 ± 0.1	1.02 ± 0.1
	Cho / Cr	0.87 ± 0.1	0.98 ± 0.2	0.99 ± 0.2	0.99 ± 0.2	1.01 ± 0.3
	ml / Cr	1.01 ± 0.3	0.99 ± 0.2	1.00 ± 0.2	1.00 ± 0.2	0.87 ± 0.3
	Glx / Cr	1.61 ± 1.6	3.74 ± 11.1	0.71 ± 0.6	1.69 ± 3.4	0.94 ± 0.9
R. Insula WM	NAA	0.96 ± 0.3	1.01 ± 0.0	1.01 ± 0.1	1.05 ± 0.1	1.07 ± 0.1
	Cr	1.06 ± 0.3	1.00 ± 0.1	0.99 ± 0.1	0.94 ± 0.1	0.95 ± 0.1
	Cho	1.00 ± 0.3	1.04 ± 0.1	1.02 ± 0.1	1.02 ± 0.1	1.02 ± 0.1
	ml	0.81 ± 0.3	0.97 ± 0.1	0.97 ± 0.1	0.93 ± 0.1	0.86 ± 0.2
	Glx	0.99 ± 0.9	0.87 ± 0.3	0.72 ± 0.4	0.54 ± 0.7	0.07 ± 0.0
	NAA / Cr	0.91 ± 0.1	1.01 ± 0.1	1.02 ± 0.1	1.12 ± 0.1	1.13 ± 0.1
	Cho / Cr	0.97 ± 0.1	1.04 ± 0.1	1.03 ± 0.1	1.10 ± 0.1	1.08 ± 0.1
	ml / Cr	0.78 ± 0.1	0.97 ± 0.1	0.97 ± 0.1	0.99 ± 0.1	0.91 ± 0.2
	Glx / Cr	0.93 ± 0.8	0.85 ± 0.3	0.73 ± 0.4	0.68 ± 0.9	0.07 ± 0.0
R. Lateral Occipital WM	NAA	1.00 ± 0.3	1.05 ± 0.1	1.03 ± 0.2	1.13 ± 0.2	1.18 ± 0.2
	Cr	1.02 ± 0.2	1.03 ± 0.1	1.03 ± 0.1	1.13 ± 0.2	1.20 ± 0.3
	Cho	0.99 ± 0.3	1.05 ± 0.2	1.03 ± 0.2	1.04 ± 0.1	0.99 ± 0.2
	ml	1.10 ± 0.3	0.97 ± 0.2	0.96 ± 0.1	1.03 ± 0.3	1.04 ± 0.8
	Glx	1.51 ± 1.1	1.38 ± 2.5	1.95 ± 3.0	1.97 ± 3.0	1.59 ± 2.3
	NAA / Cr	0.99 ± 0.2	1.03 ± 0.1	1.01 ± 0.2	1.01 ± 0.1	1.00 ± 0.2
	Cho / Cr	1.00 ± 0.2	1.03 ± 0.2	1.01 ± 0.2	0.95 ± 0.2	0.85 ± 0.2
	ml / Cr	1.11 ± 0.4	0.95 ± 0.2	0.93 ± 0.2	0.91 ± 0.2	0.82 ± 0.5
	Glx / Cr	1.64 ± 1.1	1.40 ± 2.6	1.97 ± 3.0	1.88 ± 3.1	1.49 ± 2.3
R. Lingual WM	NAA	1.05 ± 0.2	1.03 ± 0.1	1.02 ± 0.1	1.10 ± 0.1	1.17 ± 0.2
	Cr	1.14 ± 0.2	0.96 ± 0.1	0.95 ± 0.1	0.98 ± 0.2	1.02 ± 0.2
	Cho	0.98 ± 0.2	1.07 ± 0.2	1.06 ± 0.2	1.16 ± 0.2	1.19 ± 0.2
	ml	0.97 ± 0.2	1.03 ± 0.2	1.01 ± 0.2	0.90 ± 0.4	1.09 ± 0.7
	Glx	1.33 ± 1.5	0.39 ± 0.2	0.27 ± 0.1	0.04 ± 0.0	1.65 ± 0.0
	NAA / Cr	0.94 ± 0.1	1.08 ± 0.1	1.09 ± 0.1	1.13 ± 0.1	1.15 ± 0.1
	Cho / Cr	0.87 ± 0.1	1.13 ± 0.2	1.14 ± 0.3	1.22 ± 0.3	1.22 ± 0.4
	ml / Cr	0.87 ± 0.2	1.09 ± 0.2	1.08 ± 0.3	0.95 ± 0.4	1.09 ± 0.6
	Glx / Cr	1.27 ± 1.5	0.43 ± 0.2	0.27 ± 0.0	0.06 ± 0.0	2.03 ± 0.0

		MINT 50x50x18	SLIM 50x50x12	SLIM 40x40x12	SLIM 20x20x12	SLIM 16x16x12
L. Orbito-Frontal GM	NAA	0.99 ± 0.2	1.04 ± 0.1	1.05 ± 0.1	1.16 ± 0.2	1.20 ± 0.3
	Cr	1.09 ± 0.3	1.01 ± 0.1	1.02 ± 0.1	1.13 ± 0.2	1.15 ± 0.4
	Cho	1.00 ± 0.3	0.96 ± 0.1	0.95 ± 0.1	0.91 ± 0.2	0.88 ± 0.4
	mI	1.38 ± 1.0	1.02 ± 0.4	0.97 ± 0.5	1.11 ± 0.7	1.25 ± 1.1
	Glx	1.22 ± 1.7	2.27 ± 1.8	2.44 ± 1.8	2.08 ± 2.7	2.65 ± 2.9
	NAA / Cr	0.92 ± 0.1	1.03 ± 0.1	1.03 ± 0.1	1.05 ± 0.2	1.09 ± 0.3
	Cho / Cr	0.92 ± 0.2	0.95 ± 0.2	0.94 ± 0.2	0.82 ± 0.2	0.82 ± 0.5
	mI / Cr	1.24 ± 0.7	1.00 ± 0.4	0.95 ± 0.5	1.04 ± 0.6	1.23 ± 1.2
	Glx / Cr	1.02 ± 1.3	2.41 ± 2.0	2.55 ± 2.1	1.83 ± 2.1	2.40 ± 2.5
L. Pars GM	NAA	0.94 ± 0.2	1.04 ± 0.1	1.04 ± 0.1	1.05 ± 0.1	1.08 ± 0.2
	Cr	1.03 ± 0.2	1.07 ± 0.1	1.11 ± 0.1	1.16 ± 0.2	1.15 ± 0.2
	Cho	0.92 ± 0.3	1.04 ± 0.2	1.03 ± 0.1	1.11 ± 0.2	1.03 ± 0.3
	mI	1.04 ± 0.4	1.13 ± 0.7	1.12 ± 0.4	1.15 ± 0.4	1.02 ± 0.3
	Glx	1.27 ± 1.0	0.57 ± 0.3	1.47 ± 1.4	0.47 ± 0.1	2.02 ± 2.1
	NAA / Cr	0.90 ± 0.1	0.98 ± 0.1	0.94 ± 0.1	0.91 ± 0.1	0.94 ± 0.1
	Cho / Cr	0.90 ± 0.3	0.99 ± 0.2	0.94 ± 0.1	0.96 ± 0.1	0.89 ± 0.2
	mI / Cr	1.01 ± 0.3	1.09 ± 0.8	1.02 ± 0.3	1.01 ± 0.3	0.89 ± 0.2
	Glx / Cr	1.30 ± 1.0	0.55 ± 0.3	1.25 ± 1.1	0.43 ± 0.1	2.00 ± 2.1
L. Post-Central GM	NAA	1.09 ± 0.2	0.94 ± 0.1	0.92 ± 0.1	0.83 ± 0.1	0.91 ± 0.1
	Cr	1.14 ± 0.2	0.94 ± 0.1	0.92 ± 0.1	0.85 ± 0.1	0.96 ± 0.2
	Cho	1.11 ± 0.1	0.97 ± 0.1	0.96 ± 0.1	0.91 ± 0.2	1.01 ± 0.2
	mI	1.25 ± 0.3	0.98 ± 0.3	0.92 ± 0.2	0.82 ± 0.3	0.90 ± 0.5
	Glx	3.71 ± 5.6	3.36 ± 4.3	4.03 ± 5.1	3.81 ± 4.6	2.49 ± 3.1
	NAA / Cr	0.95 ± 0.1	1.01 ± 0.1	1.00 ± 0.1	1.01 ± 0.2	0.96 ± 0.1
	Cho / Cr	0.98 ± 0.1	1.04 ± 0.2	1.05 ± 0.2	1.09 ± 0.2	1.11 ± 0.2
	mI / Cr	1.10 ± 0.3	1.05 ± 0.3	1.00 ± 0.3	1.00 ± 0.4	0.97 ± 0.5
	Glx / Cr	4.27 ± 6.9	3.51 ± 4.3	4.41 ± 5.2	4.86 ± 5.2	2.60 ± 3.3
L. Pre-Cuneus GM	NAA	0.92 ± 0.1	1.02 ± 0.1	1.01 ± 0.0	1.03 ± 0.1	1.03 ± 0.1
	Cr	0.99 ± 0.1	1.03 ± 0.1	1.02 ± 0.1	1.02 ± 0.1	1.01 ± 0.1
	Cho	0.91 ± 0.1	0.93 ± 0.1	0.90 ± 0.1	0.83 ± 0.2	0.81 ± 0.2
	mI	0.91 ± 0.2	0.99 ± 0.2	0.93 ± 0.2	0.91 ± 0.1	0.92 ± 0.2
	Glx	6.01 ± 5.2	1.62 ± 2.2	1.99 ± 3.0	0.98 ± 0.2	23.00 ± 57.4
	NAA / Cr	0.93 ± 0.1	1.00 ± 0.1	0.99 ± 0.1	1.01 ± 0.1	1.03 ± 0.1
	Cho / Cr	0.93 ± 0.1	0.91 ± 0.1	0.88 ± 0.1	0.81 ± 0.1	0.80 ± 0.1
	mI / Cr	0.92 ± 0.2	0.96 ± 0.2	0.91 ± 0.2	0.88 ± 0.1	0.91 ± 0.2
	Glx / Cr	5.95 ± 5.1	1.60 ± 2.1	1.94 ± 2.9	0.95 ± 0.2	22.89 ± 57.0
L. Rostral Middle Frontal GM	NAA	1.01 ± 0.2	1.01 ± 0.1	1.03 ± 0.1	0.98 ± 0.3	1.06 ± 0.1
	Cr	1.07 ± 0.2	1.04 ± 0.1	1.04 ± 0.1	1.09 ± 0.1	1.06 ± 0.2
	Cho	0.99 ± 0.2	0.92 ± 0.1	0.92 ± 0.1	0.78 ± 0.2	0.84 ± 0.1
	mI	1.03 ± 0.3	1.04 ± 0.3	1.00 ± 0.3	1.00 ± 0.3	0.98 ± 0.4
	Glx	1.51 ± 1.5	3.44 ± 7.7	0.59 ± 0.8	6.78 ± 12.9	0.76 ± 0.9
	NAA / Cr	0.94 ± 0.1	0.97 ± 0.1	1.00 ± 0.1	0.96 ± 0.1	1.01 ± 0.1
	Cho / Cr	0.92 ± 0.1	0.89 ± 0.1	0.90 ± 0.2	0.77 ± 0.2	0.80 ± 0.1
	mI / Cr	0.96 ± 0.3	1.00 ± 0.2	0.97 ± 0.2	0.93 ± 0.3	0.93 ± 0.4
	Glx / Cr	1.25 ± 1.0	3.55 ± 8.1	0.54 ± 0.6	6.01 ± 11.4	0.89 ± 1.2

		MINT 50x50x18	SLIM 50x50x12	SLIM 40x40x12	SLIM 20x20x12	SLIM 16x16x12
L. Orbito-Frontal WM	NAA	0.91 ± 0.2	0.97 ± 0.1	0.98 ± 0.1	0.98 ± 0.1	0.99 ± 0.1
	Cr	0.97 ± 0.2	0.96 ± 0.1	0.94 ± 0.1	0.95 ± 0.1	0.94 ± 0.1
	Cho	0.95 ± 0.2	1.05 ± 0.1	1.08 ± 0.1	1.10 ± 0.1	1.11 ± 0.1
	mI	0.95 ± 0.4	0.97 ± 0.3	0.97 ± 0.4	0.96 ± 0.4	1.03 ± 0.6
	Glx	1.17 ± 1.2	0.97 ± 0.8	0.86 ± 1.0	0.96 ± 1.1	0.41 ± 0.5
	NAA / Cr	0.94 ± 0.1	1.01 ± 0.1	1.04 ± 0.1	1.04 ± 0.1	1.06 ± 0.1
	Cho / Cr	1.00 ± 0.2	1.10 ± 0.1	1.15 ± 0.1	1.16 ± 0.1	1.19 ± 0.2
	mI / Cr	1.00 ± 0.5	1.01 ± 0.3	1.02 ± 0.4	1.02 ± 0.4	1.10 ± 0.6
	Glx / Cr	1.10 ± 1.1	1.01 ± 0.8	0.96 ± 1.2	1.03 ± 1.1	0.42 ± 0.5
L. Pars WM	NAA	0.92 ± 0.2	1.00 ± 0.1	1.00 ± 0.1	0.96 ± 0.1	1.00 ± 0.1
	Cr	1.05 ± 0.2	1.02 ± 0.1	1.01 ± 0.1	0.94 ± 0.2	1.02 ± 0.2
	Cho	0.91 ± 0.2	1.02 ± 0.1	1.04 ± 0.1	0.97 ± 0.2	1.06 ± 0.2
	mI	0.98 ± 0.3	0.87 ± 0.2	0.85 ± 0.2	0.81 ± 0.2	0.89 ± 0.5
	Glx	1.78 ± 1.6	0.44 ± 0.5	0.76 ± 0.5	2.84 ± 3.7	0.90 ± 0.0
	NAA / Cr	0.88 ± 0.1	0.99 ± 0.1	1.01 ± 0.1	1.05 ± 0.2	1.01 ± 0.1
	Cho / Cr	0.88 ± 0.1	1.02 ± 0.1	1.05 ± 0.2	1.07 ± 0.2	1.07 ± 0.2
	mI / Cr	0.93 ± 0.2	0.88 ± 0.2	0.85 ± 0.2	0.96 ± 0.6	0.86 ± 0.3
	Glx / Cr	1.71 ± 1.7	0.44 ± 0.4	0.73 ± 0.4	2.80 ± 3.6	1.00 ± 0.0
L. Post-Central WM	NAA	0.98 ± 0.1	1.09 ± 0.1	1.14 ± 0.1	1.31 ± 0.2	1.37 ± 0.4
	Cr	1.04 ± 0.1	1.03 ± 0.1	1.04 ± 0.1	1.12 ± 0.2	1.12 ± 0.3
	Cho	0.97 ± 0.1	1.13 ± 0.1	1.19 ± 0.1	1.39 ± 0.2	1.42 ± 0.3
	mI	1.12 ± 0.4	1.05 ± 0.2	1.11 ± 0.3	1.11 ± 0.4	1.06 ± 0.5
	Glx	1.15 ± 1.0	0.53 ± 0.6	0.29 ± 0.0	2.89 ± 2.9	0.37 ± 0.4
	NAA / Cr	0.95 ± 0.1	1.07 ± 0.1	1.10 ± 0.1	1.17 ± 0.1	1.23 ± 0.1
	Cho / Cr	0.94 ± 0.1	1.10 ± 0.1	1.14 ± 0.1	1.25 ± 0.1	1.29 ± 0.2
	mI / Cr	1.08 ± 0.3	1.02 ± 0.2	1.06 ± 0.3	1.02 ± 0.4	0.97 ± 0.5
	Glx / Cr	1.22 ± 1.0	0.54 ± 0.7	0.25 ± 0.0	2.48 ± 2.4	0.35 ± 0.4
L. Pre-Cuneus WM	NAA	0.86 ± 0.1	1.00 ± 0.0	1.00 ± 0.0	0.99 ± 0.1	0.96 ± 0.1
	Cr	1.00 ± 0.1	0.98 ± 0.0	0.97 ± 0.0	0.95 ± 0.1	0.90 ± 0.1
	Cho	0.85 ± 0.1	1.02 ± 0.0	1.03 ± 0.0	1.07 ± 0.1	1.01 ± 0.1
	mI	0.85 ± 0.2	0.94 ± 0.1	0.92 ± 0.1	0.90 ± 0.2	0.89 ± 0.2
	Glx	N/A	0.69 ± 0.2	0.59 ± 0.1	0.08 ± 0.0	N/A
	NAA / Cr	0.86 ± 0.1	1.03 ± 0.0	1.03 ± 0.0	1.05 ± 0.0	1.07 ± 0.1
	Cho / Cr	0.86 ± 0.1	1.04 ± 0.0	1.06 ± 0.0	1.13 ± 0.1	1.13 ± 0.1
	mI / Cr	0.85 ± 0.2	0.96 ± 0.1	0.95 ± 0.1	0.96 ± 0.2	0.98 ± 0.2
	Glx / Cr	N/A	0.72 ± 0.2	0.63 ± 0.1	0.08 ± 0.0	N/A
L. Rostral Middle Frontal WM	NAA	0.94 ± 0.2	1.00 ± 0.1	1.00 ± 0.1	1.02 ± 0.1	0.98 ± 0.1
	Cr	1.03 ± 0.2	0.98 ± 0.1	0.98 ± 0.1	1.02 ± 0.1	0.98 ± 0.1
	Cho	0.89 ± 0.2	1.05 ± 0.1	1.06 ± 0.1	1.11 ± 0.1	1.15 ± 0.1
	mI	0.93 ± 0.2	1.00 ± 0.1	0.99 ± 0.2	0.96 ± 0.2	0.89 ± 0.3
	Glx	0.70 ± 0.4	1.35 ± 0.7	1.23 ± 0.7	1.51 ± 1.0	0.80 ± 0.7
	NAA / Cr	0.92 ± 0.1	1.02 ± 0.1	1.03 ± 0.1	1.01 ± 0.1	1.00 ± 0.1
	Cho / Cr	0.87 ± 0.1	1.07 ± 0.1	1.09 ± 0.1	1.10 ± 0.1	1.19 ± 0.2
	mI / Cr	0.90 ± 0.1	1.02 ± 0.1	1.02 ± 0.2	0.94 ± 0.2	0.91 ± 0.3
	Glx / Cr	0.65 ± 0.4	1.44 ± 0.8	1.31 ± 0.8	1.40 ± 0.9	0.80 ± 0.7

		MINT 50x50x18	SLIM 50x50x12	SLIM 40x40x12	SLIM 20x20x12	SLIM 16x16x12
R. Orbito-Frontal GM	NAA	0.97 ± 0.2	1.07 ± 0.1	1.11 ± 0.2	1.10 ± 0.2	1.13 ± 0.4
	Cr	1.02 ± 0.3	1.10 ± 0.2	1.14 ± 0.3	1.36 ± 0.7	1.51 ± 0.9
	Cho	1.19 ± 0.5	1.03 ± 0.2	1.07 ± 0.4	0.93 ± 0.2	1.01 ± 0.3
	mI	1.34 ± 0.7	1.07 ± 0.5	1.12 ± 0.4	1.04 ± 0.5	1.92 ± 3.0
	Glx	1.27 ± 1.6	1.28 ± 0.6	1.64 ± 1.2	2.98 ± 3.7	1.89 ± 1.2
	NAA / Cr	0.96 ± 0.1	0.99 ± 0.1	1.00 ± 0.1	0.93 ± 0.3	0.88 ± 0.3
	Cho / Cr	1.20 ± 0.8	1.00 ± 0.3	1.03 ± 0.4	0.86 ± 0.2	0.90 ± 0.2
	mI / Cr	1.29 ± 0.5	1.00 ± 0.2	1.01 ± 0.2	0.90 ± 0.4	1.05 ± 0.7
	Glx / Cr	1.10 ± 1.3	1.33 ± 0.7	1.74 ± 1.4	3.87 ± 6.0	1.54 ± 0.8
R. Pars GM	NAA	1.05 ± 0.3	1.04 ± 0.1	1.02 ± 0.3	1.10 ± 0.2	1.11 ± 0.2
	Cr	1.08 ± 0.3	1.07 ± 0.1	1.08 ± 0.3	1.11 ± 0.2	1.19 ± 0.3
	Cho	1.03 ± 0.3	1.03 ± 0.2	1.00 ± 0.3	1.08 ± 0.3	1.04 ± 0.3
	mI	1.06 ± 0.4	1.10 ± 0.7	1.11 ± 0.8	0.95 ± 0.4	0.94 ± 0.3
	Glx	1.82 ± 1.2	0.88 ± 0.5	1.05 ± 0.9	2.37 ± 2.1	1.34 ± 1.0
	NAA / Cr	0.98 ± 0.1	0.98 ± 0.1	0.95 ± 0.1	1.00 ± 0.2	0.96 ± 0.1
	Cho / Cr	0.97 ± 0.2	0.96 ± 0.2	0.88 ± 0.2	0.99 ± 0.2	0.93 ± 0.2
	mI / Cr	1.01 ± 0.4	1.03 ± 0.6	1.00 ± 0.7	0.88 ± 0.4	0.79 ± 0.3
	Glx / Cr	1.75 ± 1.1	0.80 ± 0.4	0.80 ± 0.5	2.19 ± 1.8	1.14 ± 0.9
R. Post-Central GM	NAA	1.10 ± 0.2	0.97 ± 0.1	0.94 ± 0.1	0.86 ± 0.1	0.90 ± 0.1
	Cr	1.17 ± 0.2	0.95 ± 0.1	0.92 ± 0.1	0.86 ± 0.1	0.90 ± 0.1
	Cho	1.20 ± 0.2	0.96 ± 0.1	0.94 ± 0.2	0.87 ± 0.2	1.01 ± 0.2
	mI	1.55 ± 0.5	0.92 ± 0.3	0.84 ± 0.4	0.72 ± 0.3	0.74 ± 0.4
	Glx	3.23 ± 4.5	66.35 ± 125.8	3.51 ± 2.3	15.67 ± 28.7	1.71 ± 2.1
	NAA / Cr	0.93 ± 0.1	1.02 ± 0.1	1.02 ± 0.1	1.00 ± 0.1	1.00 ± 0.1
	Cho / Cr	1.03 ± 0.2	1.02 ± 0.1	1.03 ± 0.2	1.00 ± 0.2	1.13 ± 0.3
	mI / Cr	1.37 ± 0.7	0.96 ± 0.4	0.90 ± 0.4	0.86 ± 0.4	0.81 ± 0.4
	Glx / Cr	3.95 ± 5.9	63.89 ± 120.2	3.61 ± 2.2	18.95 ± 34.8	1.79 ± 2.1
R. Pre-Cuneus GM	NAA	1.06 ± 0.2	1.01 ± 0.0	1.01 ± 0.0	1.04 ± 0.0	1.11 ± 0.1
	Cr	1.17 ± 0.2	1.03 ± 0.1	1.04 ± 0.1	1.07 ± 0.1	1.09 ± 0.1
	Cho	1.03 ± 0.2	0.94 ± 0.1	0.91 ± 0.1	0.86 ± 0.1	0.86 ± 0.2
	mI	1.04 ± 0.2	0.98 ± 0.2	0.96 ± 0.2	0.87 ± 0.2	0.88 ± 0.3
	Glx	0.99 ± 1.3	1.57 ± 1.6	1.04 ± 0.6	0.49 ± 0.2	6.32 ± 12.3
	NAA / Cr	0.90 ± 0.1	0.99 ± 0.1	0.97 ± 0.1	0.97 ± 0.1	1.03 ± 0.1
	Cho / Cr	0.87 ± 0.1	0.91 ± 0.1	0.87 ± 0.1	0.80 ± 0.1	0.79 ± 0.2
	mI / Cr	0.89 ± 0.1	0.95 ± 0.2	0.92 ± 0.2	0.81 ± 0.2	0.81 ± 0.3
	Glx / Cr	0.92 ± 1.2	1.61 ± 1.7	1.01 ± 0.6	0.47 ± 0.2	6.10 ± 11.9
R. Rostral Middle Frontal GM	NAA	1.02 ± 0.2	1.01 ± 0.1	1.02 ± 0.1	1.07 ± 0.1	1.08 ± 0.1
	Cr	1.04 ± 0.2	1.02 ± 0.1	1.03 ± 0.1	1.10 ± 0.2	1.11 ± 0.2
	Cho	1.01 ± 0.2	1.01 ± 0.1	0.97 ± 0.1	0.98 ± 0.2	0.90 ± 0.2
	mI	1.07 ± 0.5	1.00 ± 0.2	0.95 ± 0.2	0.93 ± 0.4	0.86 ± 0.3
	Glx	0.85 ± 0.9	0.93 ± 0.5	1.40 ± 0.9	1.09 ± 0.7	1.01 ± 0.8
	NAA / Cr	0.98 ± 0.1	1.00 ± 0.1	0.99 ± 0.1	0.98 ± 0.1	0.99 ± 0.1
	Cho / Cr	0.97 ± 0.1	1.01 ± 0.2	0.96 ± 0.2	0.90 ± 0.1	0.82 ± 0.1
	mI / Cr	1.04 ± 0.5	0.98 ± 0.2	0.92 ± 0.2	0.84 ± 0.3	0.77 ± 0.3
	Glx / Cr	0.76 ± 0.8	0.97 ± 0.5	1.50 ± 1.0	1.03 ± 0.5	0.89 ± 0.7

		MINT 50x50x18	SLIM 50x50x12	SLIM 40x40x12	SLIM 20x20x12	SLIM 16x16x12
R. Orbito-Frontal WM	NAA	0.89 ± 0.2	1.01 ± 0.1	1.01 ± 0.1	1.02 ± 0.1	1.00 ± 0.1
	Cr	0.98 ± 0.3	0.99 ± 0.1	1.00 ± 0.1	0.98 ± 0.1	0.95 ± 0.2
	Cho	0.95 ± 0.2	1.03 ± 0.1	1.04 ± 0.1	1.07 ± 0.1	1.06 ± 0.2
	mI	0.88 ± 0.2	1.01 ± 0.2	1.01 ± 0.3	1.04 ± 0.4	1.07 ± 0.5
	Glx	6.63 ± 0.0	0.92 ± 0.3	0.98 ± 0.7	0.47 ± 0.5	0.77 ± 0.6
	NAA / Cr	0.92 ± 0.1	1.03 ± 0.1	1.02 ± 0.1	1.04 ± 0.1	1.08 ± 0.1
	Cho / Cr	0.98 ± 0.1	1.05 ± 0.2	1.05 ± 0.1	1.09 ± 0.2	1.14 ± 0.2
	mI / Cr	0.91 ± 0.2	1.02 ± 0.2	1.01 ± 0.3	1.05 ± 0.3	1.10 ± 0.4
	Glx / Cr	7.77 ± 0.0	0.95 ± 0.3	1.02 ± 0.9	0.50 ± 0.5	0.87 ± 0.8
R. Pars WM	NAA	1.02 ± 0.2	1.03 ± 0.1	0.98 ± 0.1	1.00 ± 0.1	1.01 ± 0.1
	Cr	1.09 ± 0.2	1.02 ± 0.2	0.95 ± 0.3	0.97 ± 0.2	0.95 ± 0.1
	Cho	1.04 ± 0.2	1.13 ± 0.1	1.04 ± 0.2	1.14 ± 0.2	1.13 ± 0.1
	mI	0.96 ± 0.3	1.05 ± 0.4	0.96 ± 0.3	1.04 ± 0.4	0.92 ± 0.3
	Glx	0.71 ± 0.3	0.28 ± 0.2	0.14 ± 0.1	0.36 ± 0.3	0.60 ± 0.7
	NAA / Cr	0.92 ± 0.1	1.04 ± 0.1	1.20 ± 0.8	1.06 ± 0.2	1.07 ± 0.1
	Cho / Cr	0.95 ± 0.1	1.14 ± 0.2	1.31 ± 0.9	1.21 ± 0.2	1.21 ± 0.2
	mI / Cr	0.87 ± 0.2	1.06 ± 0.2	1.18 ± 0.8	1.07 ± 0.3	0.98 ± 0.3
	Glx / Cr	0.58 ± 0.2	0.32 ± 0.2	0.14 ± 0.1	0.36 ± 0.3	0.57 ± 0.6
R. Post-Central WM	NAA	1.02 ± 0.1	1.08 ± 0.1	1.12 ± 0.1	1.19 ± 0.1	1.17 ± 0.2
	Cr	1.10 ± 0.2	1.02 ± 0.1	1.04 ± 0.1	1.07 ± 0.1	1.06 ± 0.2
	Cho	1.10 ± 0.2	1.14 ± 0.1	1.15 ± 0.2	1.22 ± 0.2	1.28 ± 0.3
	mI	1.12 ± 0.2	0.97 ± 0.2	1.04 ± 0.3	1.19 ± 0.4	1.02 ± 0.3
	Glx	9.93 ± 22.6	1.41 ± 2.2	7.29 ± 9.4	9.19 ± 12.2	0.33 ± 0.3
	NAA / Cr	0.93 ± 0.1	1.06 ± 0.1	1.08 ± 0.1	1.12 ± 0.1	1.12 ± 0.1
	Cho / Cr	1.01 ± 0.1	1.12 ± 0.1	1.11 ± 0.2	1.14 ± 0.2	1.20 ± 0.2
	mI / Cr	1.03 ± 0.2	0.95 ± 0.2	1.00 ± 0.2	1.12 ± 0.4	0.97 ± 0.3
	Glx / Cr	13.16 ± 30.4	1.34 ± 2.0	6.80 ± 8.6	8.13 ± 10.4	0.31 ± 0.3
R. Pre-Cuneus WM	NAA	1.08 ± 0.3	0.98 ± 0.0	0.98 ± 0.0	0.91 ± 0.1	0.89 ± 0.1
	Cr	1.24 ± 0.2	0.97 ± 0.0	0.95 ± 0.1	0.84 ± 0.1	0.81 ± 0.1
	Cho	0.97 ± 0.2	1.01 ± 0.0	1.02 ± 0.0	1.06 ± 0.1	1.01 ± 0.1
	mI	1.00 ± 0.2	1.02 ± 0.1	1.02 ± 0.1	0.96 ± 0.2	0.94 ± 0.2
	Glx	3.56 ± 0.0	1.05 ± 0.6	1.25 ± 0.5	N/A	N/A
	NAA / Cr	0.87 ± 0.1	1.02 ± 0.0	1.03 ± 0.1	1.09 ± 0.1	1.11 ± 0.1
	Cho / Cr	0.78 ± 0.1	1.05 ± 0.1	1.07 ± 0.1	1.27 ± 0.2	1.26 ± 0.2
	mI / Cr	0.81 ± 0.1	1.06 ± 0.1	1.07 ± 0.1	1.15 ± 0.2	1.16 ± 0.2
	Glx / Cr	2.92 ± 0.0	1.15 ± 0.7	1.39 ± 0.6	N/A	N/A
R. Rostral Middle Frontal WM	NAA	0.98 ± 0.2	1.01 ± 0.1	0.99 ± 0.1	1.01 ± 0.1	0.99 ± 0.1
	Cr	1.03 ± 0.2	1.00 ± 0.1	0.99 ± 0.2	1.01 ± 0.1	1.01 ± 0.2
	Cho	0.97 ± 0.2	1.05 ± 0.1	1.04 ± 0.2	1.09 ± 0.2	1.11 ± 0.2
	mI	0.94 ± 0.4	1.06 ± 0.3	1.10 ± 0.5	1.15 ± 0.7	1.18 ± 0.7
	Glx	0.26 ± 0.0	0.87 ± 0.5	1.05 ± 0.2	0.44 ± 0.2	0.52 ± 0.3
	NAA / Cr	0.94 ± 0.1	1.01 ± 0.1	1.02 ± 0.1	1.01 ± 0.1	0.99 ± 0.1
	Cho / Cr	0.94 ± 0.2	1.04 ± 0.1	1.06 ± 0.1	1.08 ± 0.1	1.10 ± 0.2
	mI / Cr	0.89 ± 0.3	1.06 ± 0.3	1.12 ± 0.4	1.11 ± 0.4	1.13 ± 0.5
	Glx / Cr	0.29 ± 0.0	0.87 ± 0.5	1.28 ± 0.5	0.45 ± 0.2	0.56 ± 0.3

		MINT 50x50x18	SLIM 50x50x12	SLIM 40x40x12	SLIM 20x20x12	SLIM 16x16x12
L. Superior Frontal GM	NAA	1.04 ± 0.1	0.99 ± 0.1	0.95 ± 0.2	0.95 ± 0.2	0.92 ± 0.2
	Cr	1.12 ± 0.1	0.97 ± 0.1	0.95 ± 0.2	0.89 ± 0.2	0.99 ± 0.3
	Cho	1.11 ± 0.1	0.96 ± 0.1	0.92 ± 0.2	0.93 ± 0.2	0.92 ± 0.3
	mI	1.35 ± 0.9	0.97 ± 0.4	0.96 ± 0.5	1.06 ± 0.7	2.03 ± 2.0
	Glx	2.02 ± 2.6	1.83 ± 1.6	1.90 ± 1.6	2.00 ± 1.7	15.07 ± 19.9
	NAA / Cr	0.94 ± 0.1	1.04 ± 0.1	1.01 ± 0.1	1.09 ± 0.2	0.99 ± 0.2
	Cho / Cr	1.00 ± 0.1	1.00 ± 0.1	0.98 ± 0.1	1.06 ± 0.2	1.00 ± 0.4
	mI / Cr	1.20 ± 0.7	1.01 ± 0.4	1.00 ± 0.6	1.16 ± 0.7	1.83 ± 1.2
	Glx / Cr	1.91 ± 2.4	1.91 ± 1.6	1.92 ± 1.6	1.98 ± 1.4	10.83 ± 12.9
L. Superior Parietal GM	NAA	0.91 ± 0.1	0.93 ± 0.1	0.90 ± 0.1	0.80 ± 0.3	0.79 ± 0.2
	Cr	0.98 ± 0.2	0.96 ± 0.1	0.91 ± 0.2	0.80 ± 0.2	0.69 ± 0.2
	Cho	0.89 ± 0.2	0.78 ± 0.1	0.77 ± 0.2	0.73 ± 0.2	0.66 ± 0.2
	mI	0.91 ± 0.2	0.76 ± 0.2	0.77 ± 0.2	0.56 ± 0.3	0.47 ± 0.3
	Glx	1.51 ± 2.0	0.98 ± 0.8	1.00 ± 0.7	2.14 ± 2.0	2.43 ± 3.1
	NAA / Cr	0.94 ± 0.1	0.98 ± 0.1	1.00 ± 0.1	1.07 ± 0.1	1.17 ± 0.2
	Cho / Cr	0.92 ± 0.1	0.82 ± 0.2	0.86 ± 0.2	0.92 ± 0.3	0.95 ± 0.2
	mI / Cr	0.94 ± 0.2	0.80 ± 0.2	0.85 ± 0.2	0.70 ± 0.4	0.68 ± 0.4
	Glx / Cr	1.47 ± 2.0	1.00 ± 0.9	1.08 ± 0.7	2.61 ± 2.2	3.74 ± 4.9
L. Superior Temporal GM	NAA	0.99 ± 0.2	1.01 ± 0.1	1.00 ± 0.1	1.01 ± 0.1	0.98 ± 0.1
	Cr	1.05 ± 0.2	1.10 ± 0.2	1.08 ± 0.2	1.09 ± 0.2	1.01 ± 0.1
	Cho	0.98 ± 0.2	1.05 ± 0.1	1.05 ± 0.1	1.09 ± 0.1	1.05 ± 0.2
	mI	1.15 ± 0.3	1.01 ± 0.2	0.96 ± 0.2	0.93 ± 0.3	0.88 ± 0.3
	Glx	4.87 ± 5.6	2.37 ± 2.3	2.83 ± 4.0	45.54 ± 76.2	21.55 ± 49.2
	NAA / Cr	0.94 ± 0.1	0.95 ± 0.1	0.94 ± 0.1	0.95 ± 0.1	0.97 ± 0.1
	Cho / Cr	0.95 ± 0.2	0.99 ± 0.2	1.00 ± 0.2	1.05 ± 0.1	1.04 ± 0.2
	mI / Cr	1.12 ± 0.3	0.95 ± 0.2	0.91 ± 0.2	0.87 ± 0.3	0.88 ± 0.3
	Glx / Cr	5.93 ± 8.7	1.89 ± 1.7	2.71 ± 3.9	39.72 ± 66.6	19.19 ± 43.9
L. Supra-Marginal GM	NAA	1.02 ± 0.2	1.00 ± 0.0	0.99 ± 0.1	1.01 ± 0.1	1.05 ± 0.1
	Cr	1.14 ± 0.2	1.00 ± 0.1	1.00 ± 0.1	1.02 ± 0.1	1.08 ± 0.1
	Cho	1.11 ± 0.3	0.96 ± 0.1	0.95 ± 0.1	0.93 ± 0.1	0.90 ± 0.1
	mI	1.08 ± 0.3	0.98 ± 0.1	0.96 ± 0.2	0.97 ± 0.1	1.01 ± 0.2
	Glx	28.44 ± 35.1	2.31 ± 2.8	12.45 ± 26.2	3.08 ± 5.0	12.48 ± 26.6
	NAA / Cr	0.90 ± 0.1	1.00 ± 0.1	1.00 ± 0.1	0.99 ± 0.1	0.98 ± 0.1
	Cho / Cr	0.97 ± 0.2	0.97 ± 0.1	0.96 ± 0.1	0.91 ± 0.1	0.84 ± 0.1
	mI / Cr	0.94 ± 0.2	0.98 ± 0.1	0.96 ± 0.1	0.95 ± 0.1	0.93 ± 0.1
	Glx / Cr	24.31 ± 30.8	2.50 ± 3.1	11.63 ± 23.9	3.29 ± 5.5	9.52 ± 20.0
L. Striatum	NAA	1.05 ± 0.7	0.96 ± 0.1	0.96 ± 0.1	0.84 ± 0.1	0.83 ± 0.1
	Cr	1.10 ± 0.5	1.03 ± 0.1	1.04 ± 0.1	1.04 ± 0.1	1.01 ± 0.2
	Cho	1.18 ± 1.2	1.08 ± 0.1	1.09 ± 0.1	1.03 ± 0.1	1.05 ± 0.2
	mI	1.21 ± 0.4	1.07 ± 0.3	1.12 ± 0.3	0.97 ± 0.5	1.04 ± 0.5
	Glx	0.87 ± 0.7	0.97 ± 0.7	0.88 ± 0.8	1.10 ± 0.5	1.06 ± 0.7
	NAA / Cr	0.92 ± 0.1	0.94 ± 0.1	0.93 ± 0.1	0.81 ± 0.1	0.83 ± 0.1
	Cho / Cr	0.99 ± 0.3	1.05 ± 0.1	1.06 ± 0.1	1.00 ± 0.2	1.06 ± 0.2
	mI / Cr	1.17 ± 0.4	1.04 ± 0.3	1.09 ± 0.3	0.94 ± 0.5	1.07 ± 0.5
	Glx / Cr	0.85 ± 0.8	0.95 ± 0.7	0.85 ± 0.8	1.06 ± 0.5	1.13 ± 0.8

		MINT 50x50x18	SLIM 50x50x12	SLIM 40x40x12	SLIM 20x20x12	SLIM 16x16x12
L. Superior Frontal WM	NAA	0.94 ± 0.1	1.02 ± 0.1	1.03 ± 0.1	1.08 ± 0.1	1.13 ± 0.1
	Cr	0.98 ± 0.1	1.05 ± 0.1	1.05 ± 0.1	1.10 ± 0.2	1.14 ± 0.3
	Cho	0.98 ± 0.1	1.03 ± 0.1	1.04 ± 0.1	1.12 ± 0.2	1.13 ± 0.3
	mI	1.07 ± 0.4	1.11 ± 0.2	1.15 ± 0.3	1.09 ± 0.5	1.34 ± 0.5
	Glx	1.29 ± 1.1	1.14 ± 0.8	2.06 ± 3.3	0.31 ± 0.2	0.87 ± 1.0
	NAA / Cr	0.97 ± 0.1	0.97 ± 0.1	1.00 ± 0.1	1.01 ± 0.1	1.04 ± 0.2
	Cho / Cr	1.01 ± 0.1	0.98 ± 0.1	1.00 ± 0.1	1.04 ± 0.2	1.01 ± 0.2
	mI / Cr	1.09 ± 0.4	1.05 ± 0.2	1.13 ± 0.4	1.02 ± 0.5	1.20 ± 0.4
	Glx / Cr	1.48 ± 1.5	1.10 ± 0.7	2.18 ± 3.7	0.32 ± 0.2	0.98 ± 1.2
L. Superior Parietal WM	NAA	0.87 ± 0.1	1.06 ± 0.0	1.07 ± 0.0	1.17 ± 0.1	1.25 ± 0.1
	Cr	0.97 ± 0.1	1.06 ± 0.1	1.07 ± 0.1	1.18 ± 0.1	1.28 ± 0.1
	Cho	0.80 ± 0.1	1.02 ± 0.1	1.03 ± 0.1	1.11 ± 0.1	1.14 ± 0.1
	mI	0.84 ± 0.2	1.10 ± 0.3	1.10 ± 0.3	1.10 ± 0.3	1.10 ± 0.3
	Glx	1.65 ± 1.1	1.98 ± 1.8	3.40 ± 2.7	1.87 ± 2.4	2.33 ± 2.8
	NAA / Cr	0.90 ± 0.1	1.01 ± 0.1	1.00 ± 0.1	0.99 ± 0.1	0.98 ± 0.1
	Cho / Cr	0.84 ± 0.1	0.97 ± 0.1	0.97 ± 0.1	0.94 ± 0.1	0.89 ± 0.1
	mI / Cr	0.87 ± 0.2	1.05 ± 0.3	1.04 ± 0.3	0.94 ± 0.3	0.87 ± 0.2
	Glx / Cr	1.83 ± 1.1	1.92 ± 1.8	3.37 ± 2.8	1.72 ± 2.4	1.96 ± 2.5
L. Superior Temporal WM	NAA	0.92 ± 0.2	1.07 ± 0.1	1.04 ± 0.2	1.03 ± 0.2	1.13 ± 0.3
	Cr	1.07 ± 0.3	1.04 ± 0.1	1.01 ± 0.2	0.98 ± 0.2	1.13 ± 0.4
	Cho	0.89 ± 0.2	0.98 ± 0.1	1.00 ± 0.1	1.01 ± 0.2	1.05 ± 0.3
	mI	0.99 ± 0.3	0.94 ± 0.2	0.89 ± 0.2	0.88 ± 0.3	0.88 ± 0.3
	Glx	1.70 ± 1.4	1.90 ± 2.4	0.40 ± 0.3	0.08 ± 0.0	N/A
	NAA / Cr	0.86 ± 0.1	1.03 ± 0.1	1.04 ± 0.1	1.06 ± 0.1	1.03 ± 0.2
	Cho / Cr	0.84 ± 0.1	0.96 ± 0.2	1.00 ± 0.1	1.05 ± 0.2	0.99 ± 0.3
	mI / Cr	0.93 ± 0.1	0.90 ± 0.1	0.91 ± 0.4	0.92 ± 0.3	0.85 ± 0.3
	Glx / Cr	1.48 ± 1.2	1.50 ± 1.8	0.40 ± 0.3	0.13 ± 0.1	N/A
L. Supra-Marginal WM	NAA	0.90 ± 0.1	1.00 ± 0.0	1.01 ± 0.0	1.00 ± 0.0	0.97 ± 0.1
	Cr	1.08 ± 0.2	0.96 ± 0.1	0.96 ± 0.1	0.92 ± 0.1	0.89 ± 0.1
	Cho	0.91 ± 0.1	1.05 ± 0.1	1.05 ± 0.1	1.09 ± 0.1	1.07 ± 0.1
	mI	0.96 ± 0.2	0.93 ± 0.1	0.92 ± 0.1	0.94 ± 0.2	0.86 ± 0.1
	Glx	N/A	0.62 ± 0.4	0.30 ± 0.0	3.52 ± 4.6	0.79 ± 0.6
	NAA / Cr	0.84 ± 0.1	1.04 ± 0.1	1.05 ± 0.1	1.09 ± 0.1	1.09 ± 0.1
	Cho / Cr	0.86 ± 0.1	1.10 ± 0.1	1.10 ± 0.2	1.19 ± 0.1	1.21 ± 0.1
	mI / Cr	0.89 ± 0.1	0.97 ± 0.1	0.96 ± 0.1	1.02 ± 0.2	0.97 ± 0.1
	Glx / Cr	N/A	0.62 ± 0.3	0.34 ± 0.0	3.66 ± 4.8	0.88 ± 0.7
L. Thalamus	NAA	0.86 ± 0.2	0.99 ± 0.0	0.98 ± 0.0	0.97 ± 0.1	0.92 ± 0.1
	Cr	0.98 ± 0.3	1.02 ± 0.1	1.01 ± 0.1	1.04 ± 0.1	0.98 ± 0.1
	Cho	0.81 ± 0.2	1.00 ± 0.1	0.98 ± 0.1	1.00 ± 0.1	0.94 ± 0.1
	mI	1.64 ± 2.7	0.92 ± 0.1	0.93 ± 0.2	0.94 ± 0.2	1.13 ± 0.8
	Glx	1.19 ± 1.1	0.75 ± 0.4	3.06 ± 5.2	4.23 ± 5.9	2.48 ± 4.5
	NAA / Cr	0.87 ± 0.1	0.98 ± 0.0	0.98 ± 0.0	0.94 ± 0.1	0.94 ± 0.1
	Cho / Cr	0.84 ± 0.1	0.98 ± 0.1	0.97 ± 0.1	0.97 ± 0.1	0.97 ± 0.1
	mI / Cr	1.49 ± 1.9	0.91 ± 0.2	0.93 ± 0.2	0.92 ± 0.3	1.17 ± 0.8
	Glx / Cr	1.18 ± 1.1	0.71 ± 0.4	3.11 ± 5.4	4.32 ± 6.4	2.70 ± 5.1

		MINT 50x50x18	SLIM 50x50x12	SLIM 40x40x12	SLIM 20x20x12	SLIM 16x16x12
R. Superior Frontal GM	NAA	1.00 ± 0.1	0.99 ± 0.1	0.99 ± 0.1	1.00 ± 0.1	0.90 ± 0.1
	Cr	1.09 ± 0.1	0.97 ± 0.1	0.96 ± 0.1	0.93 ± 0.1	0.84 ± 0.2
	Cho	1.07 ± 0.2	0.98 ± 0.1	0.96 ± 0.1	0.89 ± 0.2	1.02 ± 0.2
	mI	3.62 ± 10.4	4.38 ± 14.8	4.46 ± 15.3	6.43 ± 22.5	15.53 ± 52.3
	Glx	3.62 ± 4.2	1.46 ± 1.1	1.85 ± 1.4	2.60 ± 2.7	11.87 ± 32.4
	NAA / Cr	0.92 ± 0.1	1.04 ± 0.1	1.04 ± 0.1	1.09 ± 0.1	1.10 ± 0.2
	Cho / Cr	0.99 ± 0.2	1.02 ± 0.2	1.01 ± 0.2	0.97 ± 0.3	1.21 ± 0.2
	mI / Cr	3.45 ± 10.1	4.17 ± 13.7	4.22 ± 14.0	7.22 ± 25.4	12.69 ± 41.1
	Glx / Cr	3.38 ± 4.2	1.56 ± 1.2	2.07 ± 1.7	2.81 ± 2.9	14.38 ± 38.7
R. Superior Parietal GM	NAA	1.01 ± 0.2	0.97 ± 0.1	0.96 ± 0.1	0.98 ± 0.1	0.83 ± 0.3
	Cr	1.09 ± 0.2	0.96 ± 0.1	0.94 ± 0.1	0.93 ± 0.1	0.87 ± 0.1
	Cho	1.13 ± 0.3	0.87 ± 0.2	0.80 ± 0.2	0.88 ± 0.3	0.74 ± 0.2
	mI	1.37 ± 1.0	0.72 ± 0.2	0.65 ± 0.3	0.54 ± 0.3	0.48 ± 0.6
	Glx	5.85 ± 6.1	26.99 ± 37.5	33.51 ± 55.5	15.61 ± 19.5	48.26 ± 83.4
	NAA / Cr	0.93 ± 0.1	1.02 ± 0.1	1.03 ± 0.1	1.05 ± 0.1	1.11 ± 0.1
	Cho / Cr	1.04 ± 0.2	0.91 ± 0.2	0.84 ± 0.2	0.93 ± 0.2	0.85 ± 0.2
	mI / Cr	1.19 ± 0.6	0.75 ± 0.2	0.70 ± 0.3	0.58 ± 0.3	0.57 ± 0.6
	Glx / Cr	5.01 ± 5.9	28.20 ± 40.2	35.65 ± 60.5	14.97 ± 18.5	63.75 ± 93.1
R. Superior Temporal GM	NAA	1.08 ± 0.1	1.06 ± 0.1	1.03 ± 0.1	1.08 ± 0.1	1.07 ± 0.1
	Cr	1.11 ± 0.1	1.07 ± 0.1	1.06 ± 0.1	1.05 ± 0.1	1.04 ± 0.1
	Cho	1.12 ± 0.2	1.07 ± 0.2	1.03 ± 0.2	1.10 ± 0.2	1.03 ± 0.2
	mI	1.35 ± 0.5	1.22 ± 0.7	1.15 ± 0.7	1.08 ± 0.5	1.05 ± 0.5
	Glx	2.89 ± 5.2	1.82 ± 2.2	0.99 ± 0.7	2.45 ± 3.8	0.69 ± 0.5
	NAA / Cr	0.98 ± 0.1	1.00 ± 0.1	0.98 ± 0.1	1.03 ± 0.1	1.03 ± 0.1
	Cho / Cr	1.01 ± 0.2	1.01 ± 0.2	0.98 ± 0.2	1.05 ± 0.2	1.00 ± 0.2
	mI / Cr	1.23 ± 0.5	1.12 ± 0.5	1.07 ± 0.5	1.03 ± 0.5	1.02 ± 0.5
	Glx / Cr	2.73 ± 5.0	1.75 ± 2.1	0.97 ± 0.7	2.39 ± 3.6	0.71 ± 0.6
R. Supra-Marginal GM	NAA	1.11 ± 0.2	1.06 ± 0.1	1.06 ± 0.1	1.12 ± 0.1	1.12 ± 0.1
	Cr	1.16 ± 0.2	1.09 ± 0.1	1.08 ± 0.1	1.12 ± 0.1	1.12 ± 0.1
	Cho	1.09 ± 0.2	0.94 ± 0.1	0.94 ± 0.1	0.95 ± 0.1	0.99 ± 0.2
	mI	1.10 ± 0.2	1.01 ± 0.2	1.03 ± 0.2	1.06 ± 0.3	1.10 ± 0.3
	Glx	0.67 ± 0.3	1.57 ± 1.1	1.83 ± 1.8	4.94 ± 7.1	4.51 ± 6.8
	NAA / Cr	0.96 ± 0.1	0.98 ± 0.1	0.99 ± 0.1	1.00 ± 0.1	1.01 ± 0.1
	Cho / Cr	0.95 ± 0.2	0.87 ± 0.1	0.88 ± 0.1	0.85 ± 0.1	0.89 ± 0.1
	mI / Cr	0.95 ± 0.1	0.94 ± 0.2	0.96 ± 0.2	0.95 ± 0.2	0.97 ± 0.3
	Glx / Cr	0.62 ± 0.2	1.47 ± 1.1	1.73 ± 1.8	4.73 ± 7.2	4.32 ± 6.9
R. Striatum	NAA	0.98 ± 0.2	0.96 ± 0.1	0.96 ± 0.1	0.90 ± 0.0	0.79 ± 0.2
	Cr	0.97 ± 0.2	1.01 ± 0.1	1.01 ± 0.1	1.03 ± 0.1	0.94 ± 0.3
	Cho	0.95 ± 0.2	1.03 ± 0.1	1.07 ± 0.2	1.11 ± 0.1	0.96 ± 0.3
	mI	0.93 ± 0.3	1.02 ± 0.2	1.01 ± 0.3	0.88 ± 0.4	0.97 ± 0.5
	Glx	1.25 ± 1.0	1.04 ± 0.7	0.70 ± 0.5	1.80 ± 1.3	2.69 ± 2.5
	NAA / Cr	1.00 ± 0.2	0.96 ± 0.1	0.96 ± 0.1	0.88 ± 0.1	0.87 ± 0.1
	Cho / Cr	0.99 ± 0.1	1.03 ± 0.1	1.07 ± 0.2	1.08 ± 0.1	1.02 ± 0.2
	mI / Cr	0.96 ± 0.2	1.01 ± 0.2	1.01 ± 0.3	0.85 ± 0.3	1.09 ± 0.5
	Glx / Cr	1.23 ± 1.1	1.04 ± 0.7	0.70 ± 0.5	1.73 ± 1.2	2.95 ± 3.0

		MINT 50x50x18	SLIM 50x50x12	SLIM 40x40x12	SLIM 20x20x12	SLIM 16x16x12
R. Superior Frontal WM	NAA	0.91 ± 0.1	1.02 ± 0.0	1.02 ± 0.0	1.06 ± 0.1	1.09 ± 0.1
	Cr	0.98 ± 0.1	1.00 ± 0.1	1.00 ± 0.1	1.03 ± 0.1	1.05 ± 0.2
	Cho	1.02 ± 0.1	1.04 ± 0.1	1.04 ± 0.1	1.06 ± 0.2	1.08 ± 0.2
	mI	1.04 ± 0.5	1.05 ± 0.2	1.01 ± 0.3	1.04 ± 0.6	0.84 ± 0.4
	Glx	1.05 ± 0.4	0.96 ± 0.6	0.72 ± 0.6	0.66 ± 0.8	1.27 ± 0.6
	NAA / Cr	0.93 ± 0.1	1.02 ± 0.1	1.02 ± 0.1	1.04 ± 0.1	1.04 ± 0.1
	Cho / Cr	1.05 ± 0.1	1.04 ± 0.1	1.04 ± 0.1	1.04 ± 0.2	1.03 ± 0.2
	mI / Cr	1.06 ± 0.5	1.05 ± 0.2	1.00 ± 0.3	1.03 ± 0.7	0.78 ± 0.4
	Glx / Cr	1.18 ± 0.6	1.00 ± 0.6	0.73 ± 0.6	0.68 ± 0.8	2.00 ± 1.6
R. Superior Parietal WM	NAA	0.99 ± 0.2	1.05 ± 0.0	1.06 ± 0.0	1.10 ± 0.1	1.15 ± 0.1
	Cr	1.07 ± 0.1	1.05 ± 0.1	1.06 ± 0.1	1.08 ± 0.1	1.13 ± 0.1
	Cho	1.01 ± 0.2	1.05 ± 0.1	1.06 ± 0.1	1.09 ± 0.2	1.13 ± 0.2
	mI	1.10 ± 0.7	1.01 ± 0.2	0.99 ± 0.2	1.00 ± 0.2	1.11 ± 0.4
	Glx	1.73 ± 1.3	5.99 ± 9.0	5.78 ± 8.8	8.28 ± 13.9	10.04 ± 12.8
	NAA / Cr	0.92 ± 0.1	1.00 ± 0.1	1.01 ± 0.1	1.03 ± 0.1	1.02 ± 0.1
	Cho / Cr	0.95 ± 0.2	1.01 ± 0.1	1.01 ± 0.1	1.01 ± 0.2	1.00 ± 0.2
	mI / Cr	1.00 ± 0.5	0.95 ± 0.1	0.94 ± 0.2	0.93 ± 0.2	0.98 ± 0.3
	Glx / Cr	1.59 ± 1.3	5.62 ± 8.6	5.61 ± 8.4	7.89 ± 12.9	9.46 ± 11.5
R. Superior Temporal WM	NAA	1.03 ± 0.1	1.01 ± 0.1	1.01 ± 0.1	0.96 ± 0.1	0.87 ± 0.2
	Cr	1.07 ± 0.1	0.98 ± 0.1	0.97 ± 0.1	0.91 ± 0.1	0.85 ± 0.2
	Cho	1.06 ± 0.2	1.05 ± 0.2	1.07 ± 0.2	1.03 ± 0.3	0.92 ± 0.3
	mI	1.09 ± 0.2	1.06 ± 0.3	1.00 ± 0.3	0.87 ± 0.2	0.94 ± 0.5
	Glx	0.60 ± 0.4	0.87 ± 0.8	2.22 ± 3.9	0.73 ± 0.2	1.99 ± 1.9
	NAA / Cr	0.96 ± 0.1	1.04 ± 0.1	1.05 ± 0.1	1.07 ± 0.2	1.06 ± 0.2
	Cho / Cr	1.00 ± 0.2	1.09 ± 0.2	1.11 ± 0.3	1.13 ± 0.2	1.09 ± 0.3
	mI / Cr	1.02 ± 0.2	1.09 ± 0.4	1.04 ± 0.4	0.95 ± 0.2	1.23 ± 0.9
	Glx / Cr	0.63 ± 0.4	0.98 ± 1.0	2.83 ± 5.3	0.79 ± 0.4	2.71 ± 2.3
R. Supra-Marginal WM	NAA	1.07 ± 0.1	1.00 ± 0.0	0.99 ± 0.0	0.98 ± 0.0	0.97 ± 0.1
	Cr	1.22 ± 0.1	0.97 ± 0.1	0.97 ± 0.1	0.96 ± 0.1	0.93 ± 0.1
	Cho	0.99 ± 0.1	1.02 ± 0.1	1.03 ± 0.1	1.03 ± 0.1	1.02 ± 0.1
	mI	1.06 ± 0.2	1.03 ± 0.2	0.99 ± 0.2	1.02 ± 0.2	0.95 ± 0.2
	Glx	0.89 ± 0.0	31.87 ± 61.5	43.11 ± 68.1	42.84 ± 73.4	0.30 ± 0.0
	NAA / Cr	0.88 ± 0.1	1.03 ± 0.1	1.03 ± 0.1	1.03 ± 0.1	1.04 ± 0.1
	Cho / Cr	0.82 ± 0.1	1.06 ± 0.1	1.07 ± 0.1	1.08 ± 0.1	1.10 ± 0.1
	mI / Cr	0.87 ± 0.1	1.07 ± 0.2	1.03 ± 0.1	1.07 ± 0.2	1.03 ± 0.2
	Glx / Cr	0.75 ± 0.0	30.25 ± 58.3	41.62 ± 65.6	41.14 ± 70.5	0.27 ± 0.0
R. Thalamus	NAA	0.97 ± 0.2	0.96 ± 0.1	0.95 ± 0.1	0.92 ± 0.1	0.86 ± 0.1
	Cr	1.07 ± 0.3	0.96 ± 0.1	0.97 ± 0.1	0.98 ± 0.1	0.93 ± 0.1
	Cho	1.01 ± 0.3	0.99 ± 0.1	0.98 ± 0.1	1.03 ± 0.1	0.98 ± 0.1
	mI	1.23 ± 0.6	0.92 ± 0.4	0.95 ± 0.4	0.97 ± 0.2	1.02 ± 0.5
	Glx	N/A	0.86 ± 0.0	0.86 ± 0.0	0.62 ± 0.2	N/A
	NAA / Cr	0.92 ± 0.1	1.00 ± 0.1	0.99 ± 0.1	0.95 ± 0.1	0.93 ± 0.1
	Cho / Cr	0.98 ± 0.2	1.03 ± 0.1	1.02 ± 0.1	1.06 ± 0.1	1.06 ± 0.1
	mI / Cr	1.15 ± 0.4	0.97 ± 0.4	0.99 ± 0.4	1.01 ± 0.2	1.13 ± 0.7
	Glx / Cr	N/A	0.84 ± 0.0	0.84 ± 0.0	0.64 ± 0.1	N/A

Table 11: Average FWHM across all compartments

Compartment	MINT 50x50x18	ROIS 50x50x18	SLIM 16x16x12	SLIM 20x20x12	SLIM 40x40x12	SLIM 50x50x12
All	0.06	0.06	0.06	0.06	0.06	0.06
Brain Stem	0.07	0.07	0.07	0.07	0.07	0.07
L. Central GM	0.06	0.05	0.06	0.06	0.05	0.05
L. Central WM	0.05	0.05	0.04	0.05	0.05	0.05
L. Cerebellum GM	0.07	0.07	0.07	0.07	0.07	0.07
L. Cerebellum WM	0.07	0.06	0.06	0.06	0.06	0.06
L. Cingulate GM	0.05	0.05	0.05	0.05	0.05	0.05
L. Cingulate WM	0.05	0.05	0.05	0.05	0.05	0.05
L. Fusiform GM	0.06	0.06	0.07	0.07	0.06	0.07
L. Fusiform WM	0.06	0.06	0.06	0.06	0.06	0.06
L. Inferior Parietal GM	0.06	0.05	0.06	0.06	0.06	0.06
L. Inferior Parietal WM	0.05	0.05	0.05	0.05	0.05	0.05
L. Inferior Temporal GM	0.06	0.06	0.07	0.07	0.07	0.07
L. Inferior Temporal WM	0.06	0.06	0.06	0.06	0.06	0.06
L. Insula GM	0.05	0.06	0.06	0.06	0.06	0.06
L. Insula WM	0.05	0.05	0.05	0.05	0.05	0.05
L. Lateral Occipital GM	0.06	0.06	0.07	0.07	0.07	0.07
L. Lateral Occipital WM	0.06	0.06	0.05	0.06	0.06	0.06
L. Lingual GM	0.06	0.06	0.06	0.06	0.06	0.06
L. Lingual WM	0.06	0.06	0.06	0.06	0.06	0.06
L. Orbito-Frontal GM	0.06	0.06	0.06	0.06	0.06	0.06
L. Orbito-Frontal WM	0.05	0.05	0.05	0.05	0.05	0.05
L. Pars GM	0.06	0.06	0.06	0.06	0.06	0.06
L. Pars WM	0.06	0.06	0.06	0.05	0.05	0.05
L. Post-Central GM	0.06	0.05	0.05	0.06	0.05	0.05
L. Post-Central WM	0.06	0.05	0.06	0.05	0.05	0.05
L. Pre-Cuneus GM	0.05	0.05	0.05	0.05	0.05	0.05
L. Pre-Cuneus WM	0.05	0.05	0.05	0.05	0.05	0.05
L. Rostral Middle Frontal GM	0.06	0.06	0.06	0.06	0.06	0.06
L. Rostral Middle Frontal WM	0.06	0.06	0.06	0.06	0.06	0.06
L. Striatum	0.06	0.06	0.08	0.07	0.07	0.07
L. Superior Frontal GM	0.06	0.06	0.07	0.06	0.06	0.06
L. Superior Frontal WM	0.06	0.06	0.05	0.05	0.05	0.05
L. Superior Parietal GM	0.05	0.06	0.07	0.07	0.06	0.06
L. Superior Parietal WM	0.05	0.05	0.05	0.05	0.05	0.05
L. Superior Temporal GM	0.06	0.06	0.07	0.06	0.06	0.06
L. Superior Temporal WM	0.05	0.05	0.05	0.05	0.05	0.05
L. Supra-Marginal GM	0.06	0.05	0.06	0.06	0.06	0.06
L. Supra-Marginal WM	0.05	0.05	0.05	0.05	0.05	0.05
L. Thalamus	0.06	0.06	0.06	0.06	0.06	0.06

Compartment	MINT 50x50x18	ROIS 50x50x18	SLIM 16x16x12	SLIM 20x20x12	SLIM 40x40x12	SLIM 50x50x12
R. Central GM	0.06	0.06	0.06	0.06	0.06	0.06
R. Central WM	0.05	0.05	0.04	0.05	0.05	0.05
R. Cerebellum GM	0.07	0.07	0.07	0.07	0.07	0.07
R. Cerebellum WM	0.07	0.06	0.06	0.06	0.07	0.06
R. Cingulate GM	0.05	0.05	0.05	0.05	0.05	0.05
R. Cingulate WM	0.05	0.05	0.05	0.05	0.05	0.05
R. Fusiform GM	0.06	0.07	0.07	0.07	0.07	0.07
R. Fusiform WM	0.06	0.06	0.06	0.06	0.06	0.06
R. Inferior Parietal GM	0.06	0.06	0.07	0.07	0.06	0.06
R. Inferior Parietal WM	0.05	0.05	0.05	0.05	0.05	0.05
R. Inferior Temporal GM	0.07	0.07	0.08	0.08	0.08	0.08
R. Inferior Temporal WM	0.06	0.06	0.06	0.06	0.06	0.06
R. Insula GM	0.06	0.06	0.06	0.06	0.06	0.06
R. Insula WM	0.05	0.05	0.05	0.05	0.05	0.05
R. Lateral Occipital GM	0.07	0.07	0.07	0.07	0.07	0.07
R. Lateral Occipital WM	0.06	0.07	0.07	0.07	0.07	0.07
R. Lingual GM	0.06	0.06	0.06	0.06	0.06	0.06
R. Lingual WM	0.06	0.06	0.06	0.06	0.05	0.05
R. Orbito-Frontal GM	0.06	0.06	0.07	0.07	0.07	0.06
R. Orbito-Frontal WM	0.05	0.05	0.05	0.05	0.05	0.05
R. Pars GM	0.06	0.07	0.07	0.07	0.07	0.07
R. Pars WM	0.06	0.06	0.06	0.06	0.06	0.06
R. Post-Central GM	0.06	0.06	0.06	0.06	0.06	0.06
R. Post-Central WM	0.05	0.05	0.06	0.05	0.05	0.05
R. Pre-Cuneus GM	0.05	0.05	0.05	0.05	0.05	0.05
R. Pre-Cuneus WM	0.05	0.05	0.04	0.04	0.05	0.05
R. Rostral Middle Frontal GM	0.06	0.06	0.06	0.06	0.06	0.06
R. Rostral Middle Frontal WM	0.06	0.06	0.06	0.06	0.06	0.06
R. Striatum	0.06	0.06	0.07	0.07	0.07	0.06
R. Superior Frontal GM	0.06	0.06	0.07	0.07	0.06	0.06
R. Superior Frontal WM	0.06	0.05	0.05	0.05	0.05	0.05
R. Superior Parietal GM	0.06	0.06	0.07	0.07	0.06	0.06
R. Superior Parietal WM	0.05	0.05	0.05	0.05	0.05	0.05
R. Superior Temporal GM	0.06	0.06	0.06	0.06	0.06	0.07
R. Superior Temporal WM	0.06	0.06	0.06	0.06	0.06	0.06
R. Supra-Marginal GM	0.05	0.06	0.06	0.06	0.06	0.06
R. Supra-Marginal WM	0.05	0.05	0.05	0.05	0.05	0.05
R. Thalamus	0.06	0.06	0.06	0.06	0.06	0.06
Ventral Diencephalon	0.07	0.07	0.07	0.07	0.07	0.07
Ventricles	0.05	0.05	0.05	0.05	0.05	0.05

Table 12: Pearson Correlation coefficients of ROIS 50 x 50 x 18 and the other 5 localization runs across all compartments.

		MINT 50x50x18	SLIM 50x50x12	SLIM 40x40x12	SLIM 20x20x12	SLIM 16x16x12
All	NAA	0.64	0.93	0.90	0.83	0.73
	Cr	0.58	0.88	0.85	0.75	0.67
	Cho	0.56	0.86	0.85	0.78	0.69
	ml	0.42	0.71	0.71	0.60	0.42
	Glx	0.07	0.24	0.22	0.12	0.10
	NAA / Cr	0.71	0.87	0.78	0.79	0.76
	Cho / Cr	0.66	0.80	0.74	0.74	0.68
	ml / Cr	0.37	0.66	0.66	0.54	0.37
	Glx / Cr	0.08	0.20	0.21	0.10	0.02
L. Central GM	NAA	0.77	0.94	0.92	0.71	0.69
	Cr	0.87	0.94	0.93	0.80	0.72
	Cho	0.81	0.86	0.86	0.71	0.83
	ml	0.67	0.81	0.81	0.54	0.71
	Glx	-0.23	-1.00	0.99	0.96	0.50
	NAA / Cr	0.43	0.88	0.87	0.63	0.49
	Cho / Cr	0.33	0.36	0.57	0.13	0.34
	ml / Cr	0.49	0.71	0.76	0.34	0.54
	Glx / Cr	-0.16	-0.92	1.00	0.95	0.50
L. Cerebellum GM	NAA	0.34	0.70	0.84	0.86	0.24
	Cr	0.42	0.87	0.86	0.84	0.82
	Cho	0.31	0.90	0.92	0.75	0.57
	ml	-0.13	0.77	0.85	0.84	0.75
	Glx	0.44	0.42	0.87	0.53	0.33
	NAA / Cr	0.10	0.88	0.96	0.88	0.83
	Cho / Cr	0.35	0.78	0.79	0.61	0.66
	ml / Cr	-0.34	0.78	0.82	0.75	0.62
	Glx / Cr	0.35	0.54	0.92	0.67	0.87
L. Cingulate GM	NAA	0.54	0.93	0.94	0.91	0.85
	Cr	0.54	0.79	0.77	0.71	0.71
	Cho	0.62	0.85	0.77	0.83	0.83
	ml	0.47	0.71	0.75	0.65	0.52
	Glx	0.50	-0.02	0.06	-0.39	-0.13
	NAA / Cr	0.52	0.68	0.68	0.53	0.54
	Cho / Cr	0.47	0.67	0.59	0.60	0.68
	ml / Cr	0.46	0.58	0.62	0.47	-0.07
	Glx / Cr	0.36	-0.15	-0.07	-0.45	-0.29
L. Fusiform GM	NAA	0.41	0.74	0.71	0.51	0.48
	Cr	0.47	0.88	0.82	0.49	0.40
	Cho	0.46	0.72	0.78	0.26	0.63
	ml	0.23	0.50	0.51	0.19	0.21
	Glx	-0.12	-0.67	-0.04	0.23	-0.30
	NAA / Cr	0.46	0.68	0.70	0.72	0.46
	Cho / Cr	-0.08	0.46	0.57	0.77	0.61
	ml / Cr	0.38	0.52	0.47	0.08	0.14
	Glx / Cr	-0.20	-0.40	-0.20	0.11	-0.24

		MINT 50x50x18	SLIM 50x50x12	SLIM 40x40x12	SLIM 20x20x12	SLIM 16x16x12
Brain Stem	NAA	-0.34	0.93	0.93	0.94	0.81
	Cr	-0.59	0.89	0.89	0.80	0.70
	Cho	-0.10	0.93	0.73	0.76	0.48
	ml	0.50	0.46	0.52	0.72	0.14
	Glx	0.58	0.26	0.20	-0.64	-0.05
	NAA / Cr	-0.03	0.74	0.60	0.53	0.55
	Cho / Cr	0.08	0.87	0.57	0.84	0.70
	ml / Cr	-0.17	0.39	0.36	0.70	0.35
	Glx / Cr	0.47	0.29	-0.14	-0.43	-0.10
L. Central WM	NAA	0.81	0.97	0.96	0.94	0.92
	Cr	0.78	0.91	0.94	0.87	0.80
	Cho	0.80	0.93	0.97	0.90	0.85
	ml	0.26	0.76	0.78	0.67	0.60
	Glx	-1.00	0.03	0.09	-0.35	0.99
	NAA / Cr	0.53	0.73	0.85	0.49	0.36
	Cho / Cr	0.38	0.57	0.79	0.33	0.11
	ml / Cr	0.29	0.76	0.73	0.65	0.62
	Glx / Cr	-1.00	0.23	0.30	-0.30	0.98
L. Cerebellum WM	NAA	0.41	0.86	0.83	0.75	0.64
	Cr	0.46	0.78	0.79	0.66	0.60
	Cho	0.42	0.69	0.68	0.62	0.21
	ml	0.31	0.69	0.58	0.31	-0.02
	Glx	-0.30	-0.05	-0.34	0.96	0.02
	NAA / Cr	0.58	0.88	0.89	0.84	0.78
	Cho / Cr	0.31	0.87	0.82	0.56	0.45
	ml / Cr	-0.06	0.31	0.28	0.63	0.47
	Glx / Cr	-0.48	-0.29	-0.33	1.00	0.00
L. Cingulate WM	NAA	0.66	0.93	0.89	0.90	0.71
	Cr	0.48	0.80	0.78	0.73	0.56
	Cho	0.30	0.70	0.64	0.85	0.76
	ml	0.43	0.57	0.62	0.47	0.57
	Glx	1.00	0.84	0.15	0.77	0.12
	NAA / Cr	0.81	0.83	0.87	0.87	0.76
	Cho / Cr	0.11	0.42	0.05	0.76	0.43
	ml / Cr	0.41	0.57	0.59	0.36	0.55
	Glx / Cr	1.00	0.76	0.29	0.83	0.39
L. Fusiform WM	NAA	0.65	0.73	0.72	0.17	0.43
	Cr	0.58	0.83	0.89	-0.17	0.51
	Cho	0.69	0.59	0.39	-0.02	0.01
	ml	0.10	0.60	0.73	-0.24	-0.22
	Glx	0.66	0.22	0.09	1.00	NaN
	NAA / Cr	0.27	0.62	0.57	0.35	0.42
	Cho / Cr	0.31	0.61	0.64	0.49	0.25
	ml / Cr	0.54	0.78	0.77	0.15	0.21
	Glx / Cr	0.49	0.20	-0.63	1.00	NaN

		MINT 50x50x18	SLIM 50x50x12	SLIM 40x40x12	SLIM 20x20x12	SLIM 16x16x12
Ventral Diencephalon	NAA	0.53	0.68	0.68	0.74	0.81
	Cr	-0.03	0.70	0.64	0.84	0.77
	Cho	0.35	0.38	0.37	0.47	0.79
	ml	0.26	0.70	0.72	0.19	0.68
	Glx	0.18	-0.21	-0.32	-0.29	-0.03
	NAA / Cr	0.63	0.69	0.68	0.67	0.66
	Cho / Cr	0.36	0.42	0.20	0.24	0.50
	ml / Cr	0.42	0.60	0.76	0.35	0.65
	Glx / Cr	0.41	-0.18	-0.21	-0.25	-0.02
R. Central GM	NAA	0.76	0.96	0.92	0.79	0.82
	Cr	0.79	0.97	0.95	0.87	0.87
	Cho	0.74	0.88	0.85	0.65	0.53
	ml	0.66	0.79	0.76	0.54	0.63
	Glx	0.41	0.39	0.31	0.48	0.53
	NAA / Cr	0.56	0.85	0.84	0.80	0.80
	Cho / Cr	0.35	0.32	0.39	0.12	-0.37
	ml / Cr	0.29	0.32	0.53	0.22	0.36
	Glx / Cr	0.46	0.29	0.04	0.77	0.67
R. Cerebellum GM	NAA	0.35	0.88	0.91	0.87	0.52
	Cr	0.50	0.88	0.91	0.85	0.50
	Cho	0.38	0.93	0.93	0.77	0.65
	ml	0.33	0.76	0.72	0.63	0.61
	Glx	-0.18	0.07	0.30	-0.24	0.76
	NAA / Cr	0.31	0.84	0.86	0.74	0.57
	Cho / Cr	0.52	0.78	0.81	0.27	0.38
	ml / Cr	0.42	0.71	0.70	0.61	0.45
	Glx / Cr	0.08	0.22	0.42	0.11	0.46
R. Cingulate GM	NAA	0.62	0.94	0.93	0.80	0.75
	Cr	0.37	0.83	0.77	0.59	0.47
	Cho	0.51	0.77	0.78	0.53	0.31
	ml	0.45	0.58	0.53	0.56	0.39
	Glx	0.96	0.03	-0.16	-0.39	-0.16
	NAA / Cr	0.38	0.77	0.69	0.43	0.47
	Cho / Cr	0.19	0.64	0.50	0.47	0.31
	ml / Cr	0.43	0.33	0.29	0.23	-0.17
	Glx / Cr	0.99	0.00	-0.08	-0.45	-0.34
R. Fusiform GM	NAA	0.65	0.93	0.94	0.76	0.74
	Cr	0.57	0.85	0.83	0.71	0.37
	Cho	0.56	0.69	0.61	0.19	-0.09
	ml	0.17	0.65	0.52	0.57	0.02
	Glx	0.09	0.34	0.09	-0.07	-0.37
	NAA / Cr	0.64	0.53	0.55	0.07	0.08
	Cho / Cr	0.40	0.35	0.34	0.31	0.02
	ml / Cr	0.15	0.64	0.55	0.66	-0.19
	Glx / Cr	0.24	0.53	0.13	-0.03	-0.34

		MINT 50x50x18	SLIM 50x50x12	SLIM 40x40x12	SLIM 20x20x12	SLIM 16x16x12
Ventricles	NAA	0.56	0.95	0.96	0.84	0.84
	Cr	0.60	0.91	0.92	0.76	0.73
	Cho	0.46	0.90	0.90	0.82	0.76
	ml	0.48	0.90	0.88	0.83	0.71
	Glx	-1.00	0.74	0.72	0.18	-0.13
	NAA / Cr	0.65	0.78	0.87	0.65	0.71
	Cho / Cr	0.38	0.68	0.75	0.65	0.66
	ml / Cr	0.45	0.85	0.86	0.72	0.50
	Glx / Cr	-1.00	0.57	0.59	-0.15	-0.22
R. Central WM	NAA	0.79	0.95	0.93	0.87	0.81
	Cr	0.81	0.96	0.95	0.85	0.84
	Cho	0.83	0.93	0.89	0.85	0.88
	ml	0.27	0.77	0.71	0.48	-0.07
	Glx	1.00	1.00	1.00	0.77	-1.00
	NAA / Cr	0.63	0.85	0.85	0.83	0.70
	Cho / Cr	0.31	0.84	0.85	0.74	0.64
	ml / Cr	-0.21	0.76	0.71	0.31	-0.28
	Glx / Cr	1.00	1.00	-1.00	0.30	-1.00
R. Cerebellum WM	NAA	0.66	0.83	0.84	0.96	0.65
	Cr	0.53	0.69	0.69	0.44	0.51
	Cho	0.47	0.85	0.87	0.91	0.69
	ml	0.60	0.48	0.48	0.43	0.00
	Glx	0.33	0.08	-0.23	-0.10	-0.28
	NAA / Cr	0.22	0.68	0.66	0.38	0.59
	Cho / Cr	0.09	0.66	0.71	0.76	0.58
	ml / Cr	0.33	0.71	0.69	0.58	0.28
	Glx / Cr	0.17	0.36	0.28	0.23	0.28
R. Cingulate WM	NAA	0.52	0.97	0.97	0.94	0.70
	Cr	0.39	0.88	0.81	0.70	0.55
	Cho	0.60	0.89	0.87	0.86	0.45
	ml	0.51	0.74	0.83	0.70	0.69
	Glx	0.09	0.66	0.43	0.12	0.65
	NAA / Cr	0.74	0.78	0.73	0.77	0.82
	Cho / Cr	0.10	0.54	0.41	0.50	0.35
	ml / Cr	0.48	0.75	0.83	0.65	0.54
	Glx / Cr	0.37	0.66	0.27	-0.21	0.40
R. Fusiform WM	NAA	0.48	0.88	0.84	0.56	0.49
	Cr	0.67	0.92	0.90	0.70	0.52
	Cho	0.40	0.81	0.82	0.46	0.50
	ml	0.34	0.30	0.24	0.04	0.08
	Glx	-0.50	0.87	0.85	-1.00	-1.00
	NAA / Cr	0.66	0.78	0.76	0.64	0.41
	Cho / Cr	0.35	0.75	0.80	0.66	0.62
	ml / Cr	0.11	0.53	0.49	0.19	-0.16
	Glx / Cr	-0.26	0.82	0.82	-1.00	1.00

		MINT 50x50x18	SLIM 50x50x12	SLIM 40x40x12	SLIM 20x20x12	SLIM 16x16x12
L. Inferior Parietal GM	NAA	0.43	0.97	0.92	0.84	0.89
	Cr	0.53	0.85	0.74	0.38	0.46
	Cho	0.46	0.85	0.78	0.80	0.78
	mI	0.43	0.95	0.86	0.88	0.88
	Glx	-0.75	0.10	0.26	0.89	0.82
	NAA / Cr	0.30	0.80	0.77	0.22	0.55
	Cho / Cr	0.18	0.39	0.34	0.18	0.18
	mI / Cr	0.53	0.91	0.81	0.56	0.64
	Glx / Cr	-0.71	0.11	0.17	0.83	0.76
L. Inferior Temporal GM	NAA	0.53	0.87	0.84	0.78	0.82
	Cr	0.61	0.80	0.86	0.89	0.79
	Cho	0.42	0.41	0.44	0.60	0.66
	mI	0.08	0.54	0.42	0.59	0.65
	Glx	0.42	0.24	0.45	-0.41	0.15
	NAA / Cr	0.65	0.73	0.68	0.57	0.58
	Cho / Cr	0.49	0.10	0.16	0.35	0.60
	mI / Cr	0.17	0.48	0.34	0.50	0.69
	Glx / Cr	0.17	-0.07	0.11	-0.34	0.34
L. Insula GM	NAA	0.57	0.95	0.96	0.93	0.89
	Cr	0.64	0.98	0.98	0.90	0.87
	Cho	0.32	0.91	0.93	0.75	0.69
	mI	0.44	0.89	0.83	0.67	0.69
	Glx	1.00	0.80	0.95	0.24	-1.00
	NAA / Cr	-0.08	0.91	0.91	0.85	0.67
	Cho / Cr	0.07	0.96	0.96	0.74	0.73
	mI / Cr	0.24	0.75	0.70	0.49	0.38
	Glx / Cr	1.00	0.75	0.98	0.20	-1.00
L. Lateral Occipital GM	NAA	0.43	0.79	0.70	0.56	0.39
	Cr	0.31	0.85	0.74	0.85	0.38
	Cho	0.19	0.59	0.66	0.53	0.15
	mI	0.11	0.56	0.79	0.52	0.46
	Glx	0.18	-0.16	-0.10	-0.16	-0.42
	NAA / Cr	0.09	0.64	0.58	0.34	0.08
	Cho / Cr	0.16	0.58	0.34	0.30	-0.41
	mI / Cr	0.26	0.31	0.77	0.54	0.26
	Glx / Cr	0.00	-0.36	-0.21	-0.17	-0.43
L. Lingual GM	NAA	0.43	0.93	0.88	0.89	0.38
	Cr	0.63	0.90	0.89	0.85	0.79
	Cho	0.73	0.80	0.80	0.59	0.05
	mI	0.31	0.87	0.80	0.64	0.64
	Glx	0.90	0.85	0.84	0.49	0.94
	NAA / Cr	0.30	0.88	0.86	0.76	0.69
	Cho / Cr	0.68	0.81	0.78	0.25	0.34
	mI / Cr	0.31	0.83	0.60	0.25	0.30
	Glx / Cr	0.85	0.87	0.97	0.33	1.00

		MINT 50x50x18	SLIM 50x50x12	SLIM 40x40x12	SLIM 20x20x12	SLIM 16x16x12
L. Inferior Parietal WM	NAA	0.38	0.95	0.94	0.92	0.82
	Cr	0.43	0.91	0.89	0.88	0.82
	Cho	0.39	0.90	0.84	0.83	0.66
	mI	0.30	0.92	0.83	0.69	0.36
	Glx	0.34	-1.00	1.00	1.00	NaN
	NAA / Cr	0.47	0.95	0.90	0.87	0.81
	Cho / Cr	0.52	0.89	0.81	0.67	0.61
	mI / Cr	0.55	0.85	0.80	0.77	0.61
	Glx / Cr	0.32	-1.00	1.00	1.00	NaN
L. Inferior Temporal WM	NAA	0.50	0.94	0.97	0.92	0.86
	Cr	0.50	0.85	0.88	0.81	0.81
	Cho	0.57	0.89	0.90	0.81	0.67
	mI	0.11	0.84	0.78	0.54	0.74
	Glx	-0.02	0.99	0.94	-0.24	NaN
	NAA / Cr	0.50	0.72	0.77	0.76	0.64
	Cho / Cr	0.34	0.59	0.59	0.59	0.70
	mI / Cr	0.26	0.84	0.80	0.14	0.57
	Glx / Cr	-0.07	0.98	0.94	-0.29	NaN
L. Insula WM	NAA	0.67	0.97	0.96	0.91	0.93
	Cr	0.54	0.93	0.89	0.83	0.79
	Cho	0.43	0.88	0.84	0.79	0.74
	mI	0.41	0.74	0.76	0.84	0.76
	Glx	1.00	-1.00	-0.75	-0.28	1.00
	NAA / Cr	0.42	0.81	0.80	0.77	0.74
	Cho / Cr	0.36	0.61	0.58	0.58	0.54
	mI / Cr	0.43	0.76	0.78	0.86	0.85
	Glx / Cr	1.00	-1.00	-0.96	-0.34	1.00
L. Lateral Occipital WM	NAA	0.53	0.90	0.89	0.77	0.68
	Cr	0.22	0.89	0.87	0.74	0.74
	Cho	0.51	0.76	0.84	0.68	0.14
	mI	0.12	0.48	0.55	0.40	0.73
	Glx	0.39	0.14	0.57	-1.00	-1.00
	NAA / Cr	0.65	0.82	0.79	0.73	0.60
	Cho / Cr	0.38	0.66	0.62	0.49	0.03
	mI / Cr	0.26	0.49	0.50	0.51	0.73
	Glx / Cr	0.42	0.22	0.61	-1.00	1.00
L. Lingual WM	NAA	0.67	0.67	0.62	0.18	0.68
	Cr	0.63	0.75	0.75	0.54	0.44
	Cho	0.76	0.88	0.91	0.78	0.43
	mI	0.35	0.02	0.32	-0.19	0.16
	Glx	-0.77	-0.71	-0.76	-0.90	-0.30
	NAA / Cr	0.58	0.68	0.75	0.62	0.39
	Cho / Cr	0.73	0.74	0.72	0.64	0.09
	mI / Cr	0.17	-0.09	0.43	0.06	-0.20
	Glx / Cr	-0.74	-0.70	-0.74	-0.91	-0.26

		MINT 50x50x18	SLIM 50x50x12	SLIM 40x40x12	SLIM 20x20x12	SLIM 16x16x12
R. Inferior Parietal GM	NAA	0.30	0.91	0.80	0.83	0.37
	Cr	0.48	0.91	0.92	0.76	0.83
	Cho	0.38	0.30	0.73	0.59	0.67
	mI	0.22	0.79	0.22	0.67	0.25
	Glx	0.77	-0.04	0.30	0.54	0.53
	NAA / Cr	0.61	0.86	0.85	0.42	0.65
	Cho / Cr	0.37	0.68	0.56	0.19	0.62
	mI / Cr	0.43	0.71	0.63	0.52	0.47
	Glx / Cr	0.79	0.02	0.26	0.37	0.57
R. Inferior Temporal GM	NAA	0.57	0.86	0.86	0.82	0.68
	Cr	0.71	0.85	0.85	0.81	0.78
	Cho	0.64	-0.02	0.04	0.22	0.77
	mI	0.28	0.72	0.63	0.49	-0.21
	Glx	0.09	-0.05	0.17	0.48	0.38
	NAA / Cr	0.11	-0.05	0.15	0.05	0.23
	Cho / Cr	0.28	0.09	0.17	0.32	0.62
	mI / Cr	0.30	0.71	0.60	0.50	-0.02
	Glx / Cr	0.05	-0.23	0.01	0.42	0.41
R. Insula GM	NAA	0.51	0.96	0.95	0.89	0.82
	Cr	0.54	0.91	0.91	0.91	0.91
	Cho	0.41	0.27	0.22	0.25	0.43
	mI	0.15	0.18	0.20	0.60	-0.05
	Glx	1.00	-0.25	-0.26	0.38	-0.68
	NAA / Cr	0.25	0.84	0.81	0.85	0.63
	Cho / Cr	0.29	0.35	0.34	0.48	0.38
	mI / Cr	-0.10	0.65	0.68	0.71	0.06
	Glx / Cr	1.00	0.34	0.10	-0.47	-0.42
R. Lateral Occipital GM	NAA	0.27	0.91	0.85	0.74	0.49
	Cr	0.08	0.86	0.74	0.50	0.03
	Cho	0.40	0.75	0.78	0.49	0.63
	mI	-0.20	0.86	0.71	0.37	0.08
	Glx	0.30	0.36	0.45	0.44	-0.43
	NAA / Cr	0.66	0.61	0.75	0.47	0.49
	Cho / Cr	0.31	0.45	0.48	-0.23	0.60
	mI / Cr	0.42	0.61	0.38	-0.43	-0.02
	Glx / Cr	0.31	0.64	0.62	0.34	-0.75
R. Lingual GM	NAA	0.50	0.96	0.95	0.89	0.84
	Cr	0.67	0.93	0.89	0.90	0.82
	Cho	0.63	0.83	0.81	0.75	0.54
	mI	0.34	0.89	0.85	0.80	0.77
	Glx	0.25	0.61	-0.03	0.28	-0.03
	NAA / Cr	0.53	0.93	0.89	0.79	0.69
	Cho / Cr	0.73	0.81	0.78	0.77	0.56
	mI / Cr	0.33	0.86	0.77	0.83	0.54
	Glx / Cr	0.31	0.52	0.00	0.47	0.34

		MINT 50x50x18	SLIM 50x50x12	SLIM 40x40x12	SLIM 20x20x12	SLIM 16x16x12
R. Inferior Parietal WM	NAA	0.47	0.95	0.95	0.91	0.88
	Cr	0.45	0.86	0.81	0.85	0.78
	Cho	0.58	0.90	0.88	0.86	0.84
	mI	0.44	0.92	0.91	0.86	0.78
	Glx	0.73	0.82	-0.43	-0.21	-0.43
	NAA / Cr	0.62	0.85	0.82	0.92	0.87
	Cho / Cr	0.33	0.68	0.63	0.63	0.53
	mI / Cr	0.60	0.87	0.85	0.74	0.67
	Glx / Cr	0.85	0.81	-0.39	-0.35	-0.41
R. Inferior Temporal WM	NAA	0.54	0.90	0.90	0.91	0.84
	Cr	0.45	0.93	0.93	0.88	0.64
	Cho	0.15	0.62	0.61	0.53	0.51
	mI	0.12	0.85	0.83	0.64	0.39
	Glx	-0.10	0.16	-0.05	0.60	0.40
	NAA / Cr	0.41	0.76	0.65	0.78	0.47
	Cho / Cr	0.30	0.38	0.32	0.31	-0.36
	mI / Cr	0.23	0.79	0.72	0.59	0.54
	Glx / Cr	-0.21	0.00	0.01	0.68	0.48
R. Insula WM	NAA	0.35	0.98	0.96	0.96	0.95
	Cr	0.36	0.94	0.95	0.87	0.86
	Cho	0.27	0.90	0.89	0.85	0.75
	mI	0.30	0.93	0.93	0.82	0.63
	Glx	-0.31	0.66	0.76	-0.88	1.00
	NAA / Cr	0.38	0.73	0.75	0.65	0.58
	Cho / Cr	0.36	0.74	0.75	0.58	0.51
	mI / Cr	0.72	0.86	0.85	0.88	0.74
	Glx / Cr	-0.70	0.76	0.80	-0.83	1.00
R. Lateral Occipital WM	NAA	0.29	0.95	0.92	0.79	0.67
	Cr	0.27	0.82	0.84	0.60	0.21
	Cho	0.28	0.70	0.73	0.84	0.76
	mI	-0.16	0.69	0.79	0.44	0.13
	Glx	-0.27	0.38	0.60	-0.67	-0.64
	NAA / Cr	0.44	0.85	0.80	0.69	0.47
	Cho / Cr	0.17	0.35	0.45	0.36	0.44
	mI / Cr	0.26	0.75	0.86	0.76	0.42
	Glx / Cr	-0.17	0.30	0.62	-0.79	-0.69
R. Lingual WM	NAA	0.53	0.95	0.95	0.63	0.43
	Cr	0.52	0.90	0.84	0.65	0.39
	Cho	0.48	0.93	0.88	0.30	0.34
	mI	0.49	0.84	0.59	0.52	0.07
	Glx	-0.75	0.87	-1.00	1.00	1.00
	NAA / Cr	0.56	0.81	0.70	0.78	0.64
	Cho / Cr	0.71	0.67	0.52	0.20	0.11
	mI / Cr	0.44	0.68	0.42	0.38	-0.01
	Glx / Cr	-0.52	0.88	1.00	1.00	1.00

		MINT 50x50x18	SLIM 50x50x12	SLIM 40x40x12	SLIM 20x20x12	SLIM 16x16x12
L. Orbito-Frontal GM	NAA	0.68	0.94	0.94	0.72	0.59
	Cr	0.48	0.95	0.94	0.86	0.70
	Cho	0.26	0.86	0.85	0.77	0.65
	mI	0.24	0.62	0.65	0.56	0.38
	Glx	-0.59	0.51	0.45	-0.03	-0.09
	NAA / Cr	0.64	0.79	0.74	0.70	0.58
	Cho / Cr	0.42	0.57	0.54	0.59	0.62
	mI / Cr	0.13	0.51	0.57	0.52	0.31
	Glx / Cr	-0.57	0.38	0.27	0.08	-0.02
L. Orbito-Frontal WM	NAA	0.66	0.94	0.92	0.84	0.78
	Cr	0.64	0.82	0.79	0.75	0.60
	Cho	0.56	0.95	0.95	0.91	0.76
	mI	0.42	0.69	0.59	0.65	0.45
	Glx	0.17	0.86	0.67	-0.52	-0.41
	NAA / Cr	0.48	0.86	0.81	0.70	0.66
	Cho / Cr	0.02	0.66	0.69	0.67	0.57
	mI / Cr	0.37	0.68	0.59	0.49	0.38
	Glx / Cr	0.15	0.87	0.64	-0.55	-0.49
L. Pars GM	NAA	0.52	0.74	0.79	0.78	0.71
	Cr	0.43	0.78	0.76	0.66	0.73
	Cho	0.35	0.69	0.84	0.76	0.70
	mI	0.35	0.57	0.64	0.49	0.40
	Glx	-0.57	0.27	-0.51	-1.00	-0.28
	NAA / Cr	0.78	0.51	0.72	0.48	0.45
	Cho / Cr	0.01	0.44	0.57	0.58	0.37
	mI / Cr	0.08	0.62	0.69	0.33	0.51
	Glx / Cr	-0.59	0.65	-0.23	1.00	-0.21
L. Pars WM	NAA	0.47	0.90	0.92	0.55	0.70
	Cr	0.38	0.62	0.62	-0.01	0.71
	Cho	0.61	0.80	0.75	0.27	0.54
	mI	0.39	0.74	0.82	0.85	0.72
	Glx	-1.00	0.59	0.85	0.64	1.00
	NAA / Cr	0.62	0.58	0.59	0.29	0.57
	Cho / Cr	0.15	0.47	0.44	0.11	0.45
	mI / Cr	0.34	0.61	0.70	0.40	0.63
	Glx / Cr	-1.00	0.67	0.88	0.67	1.00
L. Post-Central GM	NAA	0.61	0.91	0.87	0.82	0.70
	Cr	0.65	0.91	0.87	0.80	0.70
	Cho	0.71	0.87	0.82	0.73	0.71
	mI	0.74	0.80	0.79	0.50	0.33
	Glx	-0.27	-0.24	-0.26	-0.31	0.21
	NAA / Cr	0.21	0.75	0.68	0.38	0.59
	Cho / Cr	0.20	0.63	0.53	0.50	0.48
	mI / Cr	0.50	0.72	0.76	0.38	0.33
	Glx / Cr	-0.71	-0.13	-0.05	0.21	0.35
L. Post-Central WM	NAA	0.71	0.90	0.88	0.65	0.47
	Cr	0.65	0.90	0.88	0.73	0.71
	Cho	0.76	0.89	0.90	0.76	0.71
	mI	0.51	0.71	0.68	0.81	0.65
	Glx	-0.10	-0.70	1.00	1.00	1.00
	NAA / Cr	0.08	0.66	0.59	0.56	0.53
	Cho / Cr	0.00	0.73	0.70	0.66	0.29
	mI / Cr	0.38	0.71	0.53	0.67	0.49
	Glx / Cr	0.20	-0.49	1.00	1.00	1.00
L. Pre-Cuneus GM	NAA	0.79	0.94	0.97	0.93	0.86
	Cr	0.67	0.89	0.91	0.91	0.84
	Cho	0.80	0.92	0.93	0.89	0.82
	mI	0.66	0.74	0.84	0.60	0.74
	Glx	1.00	0.15	0.05	1.00	0.70
	NAA / Cr	0.46	0.73	0.76	0.76	0.68
	Cho / Cr	0.42	0.67	0.66	0.62	0.46
	mI / Cr	0.46	0.59	0.76	0.60	0.62
	Glx / Cr	1.00	0.06	-0.03	1.00	0.74
L. Pre-Cuneus WM	NAA	0.71	0.99	0.99	0.95	0.79
	Cr	0.64	0.98	0.97	0.89	0.68
	Cho	0.69	0.97	0.96	0.89	0.66
	mI	0.59	0.92	0.91	0.77	0.50
	Glx	NaN	1.00	1.00	1.00	NaN
	NAA / Cr	0.68	0.93	0.93	0.89	0.81
	Cho / Cr	0.50	0.92	0.90	0.80	0.84
	mI / Cr	0.67	0.92	0.92	0.68	0.71
	Glx / Cr	NaN	-1.00	-1.00	1.00	NaN
L. Rostral Middle Frontal GM	NAA	0.60	0.91	0.89	0.72	0.81
	Cr	0.53	0.78	0.69	0.58	0.73
	Cho	0.29	0.80	0.73	0.74	0.78
	mI	0.44	0.58	0.53	0.33	0.46
	Glx	0.38	0.23	0.55	-0.62	-0.16
	NAA / Cr	0.51	0.70	0.62	0.67	0.58
	Cho / Cr	0.19	0.25	0.11	0.19	0.15
	mI / Cr	0.05	0.53	0.54	0.43	0.49
	Glx / Cr	0.54	0.02	0.46	-0.62	-0.39
L. Rostral Middle Frontal WM	NAA	0.32	0.91	0.91	0.81	0.88
	Cr	0.18	0.89	0.85	0.79	0.79
	Cho	0.53	0.74	0.72	0.52	0.67
	mI	0.35	0.78	0.78	0.57	0.43
	Glx	0.88	0.64	0.71	0.64	-0.61
	NAA / Cr	0.57	0.80	0.77	0.80	0.82
	Cho / Cr	0.47	0.45	0.34	0.35	0.23
	mI / Cr	0.43	0.73	0.65	0.65	0.47
	Glx / Cr	0.88	0.01	0.05	0.53	-0.41

		MINT 50x50x18	SLIM 50x50x12	SLIM 40x40x12	SLIM 20x20x12	SLIM 16x16x12
R. Orbito-Frontal GM	NAA	0.56	0.81	0.76	0.80	0.72
	Cr	0.38	0.79	0.74	0.52	0.45
	Cho	-0.24	0.48	0.25	0.56	0.52
	mI	0.38	0.81	0.76	0.69	-0.16
	Glx	-0.20	0.72	0.83	0.16	0.54
	NAA / Cr	0.61	0.77	0.76	0.45	0.46
	Cho / Cr	-0.10	0.41	0.22	0.74	0.79
	mI / Cr	0.29	0.85	0.76	0.66	0.25
	Glx / Cr	0.16	0.67	0.75	-0.10	0.71
R. Pars GM	NAA	0.38	0.92	0.42	0.80	0.65
	Cr	0.21	0.85	0.57	0.62	0.47
	Cho	0.25	0.63	0.75	0.71	0.77
	mI	-0.26	-0.14	-0.20	0.24	0.58
	Glx	-0.28	0.52	0.04	-0.44	0.17
	NAA / Cr	0.46	0.13	0.46	0.22	0.21
	Cho / Cr	0.40	0.15	0.61	0.34	0.46
	mI / Cr	-0.43	-0.26	-0.11	0.03	0.57
	Glx / Cr	-0.26	0.61	0.39	-0.42	0.36
R. Post-Central GM	NAA	0.63	0.85	0.90	0.66	0.81
	Cr	0.74	0.94	0.90	0.64	0.86
	Cho	0.68	0.75	0.62	0.34	0.53
	mI	0.84	0.55	0.43	0.32	0.22
	Glx	-0.32	-0.59	1.00	0.69	0.77
	NAA / Cr	0.37	0.53	0.70	0.44	0.31
	Cho / Cr	0.05	0.16	0.07	0.21	-0.14
	mI / Cr	0.19	0.39	0.26	0.15	-0.09
	Glx / Cr	-0.31	-0.56	1.00	0.51	0.59
R. Pre-Cuneus GM	NAA	0.59	0.98	0.97	0.96	0.93
	Cr	0.59	0.94	0.91	0.90	0.85
	Cho	0.49	0.88	0.86	0.78	0.77
	mI	0.65	0.72	0.60	0.49	-0.01
	Glx	1.00	0.33	-1.00	0.80	-0.91
	NAA / Cr	0.34	0.71	0.62	0.50	0.48
	Cho / Cr	-0.07	0.43	0.40	0.36	0.18
	mI / Cr	0.67	0.62	0.57	0.29	-0.10
	Glx / Cr	1.00	0.25	-1.00	0.76	-0.85
R. Rostral Middle Frontal GM	NAA	0.39	0.94	0.94	0.85	0.85
	Cr	0.40	0.73	0.79	0.71	0.70
	Cho	0.33	0.83	0.89	0.87	0.88
	mI	0.17	0.79	0.73	0.66	0.70
	Glx	-0.47	0.46	0.02	0.54	0.17
	NAA / Cr	0.57	0.70	0.74	0.52	0.45
	Cho / Cr	0.43	0.27	0.37	0.61	0.61
	mI / Cr	0.02	0.79	0.72	0.64	0.71
	Glx / Cr	-0.40	0.37	-0.36	0.60	0.13

		MINT 50x50x18	SLIM 50x50x12	SLIM 40x40x12	SLIM 20x20x12	SLIM 16x16x12
R. Orbito-Frontal WM	NAA	0.54	0.95	0.94	0.90	0.82
	Cr	0.34	0.72	0.75	0.72	0.41
	Cho	0.36	0.89	0.91	0.74	0.55
	mI	0.44	0.54	0.54	0.30	0.03
	Glx	1.00	0.76	-0.03	-0.55	0.02
	NAA / Cr	0.53	0.71	0.74	0.63	0.64
	Cho / Cr	0.41	0.43	0.56	0.46	0.43
	mI / Cr	0.40	0.41	0.22	0.08	-0.04
	Glx / Cr	1.00	0.67	-0.07	-0.37	-0.50
R. Pars WM	NAA	0.51	0.87	0.65	0.90	0.81
	Cr	0.51	0.56	0.38	0.57	0.54
	Cho	0.10	0.74	0.65	0.68	0.74
	mI	0.33	0.08	0.23	0.10	0.49
	Glx	1.00	1.00	1.00	-1.00	-0.32
	NAA / Cr	0.48	0.52	0.26	0.54	0.53
	Cho / Cr	0.63	0.40	-0.15	0.41	0.38
	mI / Cr	0.52	0.44	0.14	0.34	0.63
	Glx / Cr	1.00	1.00	1.00	-1.00	-0.32
R. Post-Central WM	NAA	0.63	0.93	0.94	0.82	0.62
	Cr	0.66	0.93	0.91	0.89	0.52
	Cho	0.68	0.88	0.72	0.75	0.53
	mI	0.67	0.83	0.78	0.39	0.45
	Glx	-0.42	-0.05	-0.07	-0.13	0.36
	NAA / Cr	0.60	0.71	0.75	0.69	0.51
	Cho / Cr	0.41	0.57	0.18	0.71	0.26
	mI / Cr	0.26	0.48	0.46	0.31	0.56
	Glx / Cr	-0.49	0.02	0.06	-0.17	0.22
R. Pre-Cuneus WM	NAA	0.41	0.99	0.99	0.95	0.74
	Cr	0.62	0.95	0.91	0.74	0.46
	Cho	0.52	0.98	0.96	0.80	0.77
	mI	0.71	0.91	0.86	0.69	0.57
	Glx	1.00	0.82	0.44	NaN	NaN
	NAA / Cr	0.08	0.87	0.82	0.71	0.69
	Cho / Cr	-0.23	0.89	0.87	0.36	0.37
	mI / Cr	0.72	0.88	0.87	0.81	0.79
	Glx / Cr	1.00	0.70	0.27	NaN	NaN
R. Rostral Middle Frontal WM	NAA	0.12	0.88	0.76	0.83	0.69
	Cr	0.20	0.73	0.74	0.49	0.46
	Cho	0.32	0.75	0.50	0.66	0.44
	mI	0.02	0.57	0.37	0.31	0.20
	Glx	1.00	0.05	0.68	-0.01	0.00
	NAA / Cr	0.25	0.68	0.82	0.74	0.77
	Cho / Cr	0.47	0.71	0.88	0.74	0.73
	mI / Cr	0.18	0.61	0.45	0.47	0.38
	Glx / Cr	1.00	0.22	0.85	-0.73	0.17

		MINT 50x50x18	SLIM 50x50x12	SLIM 40x40x12	SLIM 20x20x12	SLIM 16x16x12
L. Superior Frontal GM	NAA	0.79	0.79	0.29	0.41	0.49
	Cr	0.80	0.67	-0.04	0.31	0.30
	Cho	0.86	0.77	0.49	0.64	0.57
	mI	0.56	0.73	0.36	0.52	0.09
	Glx	-0.21	-0.48	-0.33	0.04	0.93
	NAA / Cr	0.54	0.85	0.72	0.40	0.03
	Cho / Cr	0.77	0.80	0.82	0.65	0.24
	mI / Cr	0.33	0.75	0.48	0.69	0.47
	Glx / Cr	-0.17	-0.45	-0.46	0.13	0.98
L. Superior Parietal GM	NAA	0.77	0.91	0.81	0.82	0.45
	Cr	0.75	0.89	0.82	0.61	0.70
	Cho	0.80	0.92	0.91	0.85	0.50
	mI	0.47	0.73	0.79	0.69	0.31
	Glx	-0.80	0.00	0.17	-0.23	-0.79
	NAA / Cr	0.43	0.89	0.89	0.62	0.68
	Cho / Cr	0.44	0.68	0.71	0.66	0.25
	mI / Cr	0.60	0.62	0.66	0.60	-0.16
	Glx / Cr	-0.80	-0.06	0.19	-0.09	-0.70
L. Superior Temporal GM	NAA	0.40	0.92	0.92	0.88	0.76
	Cr	0.38	0.53	0.66	0.61	0.80
	Cho	0.14	0.74	0.76	0.69	0.49
	mI	0.41	0.72	0.79	0.75	0.53
	Glx	0.11	0.90	0.77	0.59	0.49
	NAA / Cr	0.45	0.54	0.59	0.63	0.66
	Cho / Cr	0.31	0.53	0.48	0.47	0.12
	mI / Cr	0.08	0.23	0.42	0.49	0.32
	Glx / Cr	0.19	0.81	0.81	0.53	0.55
L. Supra-Marginal GM	NAA	0.55	0.95	0.90	0.83	0.84
	Cr	0.55	0.86	0.82	0.83	0.77
	Cho	0.38	0.87	0.88	0.87	0.87
	mI	0.44	0.92	0.90	0.89	0.83
	Glx	-0.66	0.33	-0.71	-0.99	-0.39
	NAA / Cr	0.29	0.90	0.84	0.79	0.83
	Cho / Cr	-0.03	0.54	0.63	0.80	0.70
	mI / Cr	0.34	0.91	0.91	0.92	0.83
	Glx / Cr	-0.77	0.33	-0.68	-0.97	0.05
L. Striatum	NAA	0.43	0.90	0.87	0.92	0.65
	Cr	0.49	0.84	0.83	0.81	0.36
	Cho	0.34	0.93	0.91	0.84	0.58
	mI	0.12	0.62	0.67	0.47	0.36
	Glx	0.51	0.09	0.12	0.30	-0.02
	NAA / Cr	0.35	0.73	0.77	0.61	0.28
	Cho / Cr	0.39	0.79	0.74	0.61	0.14
	mI / Cr	0.18	0.43	0.51	0.29	0.15
	Glx / Cr	0.43	0.01	0.02	0.21	-0.40

		MINT 50x50x18	SLIM 50x50x12	SLIM 40x40x12	SLIM 20x20x12	SLIM 16x16x12
L. Superior Frontal WM	NAA	0.81	0.88	0.92	0.82	0.79
	Cr	0.77	0.88	0.81	0.62	0.58
	Cho	0.89	0.85	0.87	0.71	0.61
	mI	0.63	0.72	0.90	0.52	0.63
	Glx	0.12	0.47	0.40	0.79	0.12
	NAA / Cr	0.22	0.77	0.71	0.59	0.67
	Cho / Cr	0.40	0.83	0.77	0.51	0.36
	mI / Cr	0.29	0.62	0.38	0.30	0.44
	Glx / Cr	-0.16	0.18	0.02	0.69	0.00
L. Superior Parietal WM	NAA	0.58	0.97	0.96	0.91	0.84
	Cr	0.60	0.93	0.91	0.87	0.86
	Cho	0.73	0.95	0.95	0.92	0.86
	mI	0.47	0.76	0.63	0.53	0.66
	Glx	0.91	0.75	-0.46	0.04	0.78
	NAA / Cr	0.48	0.82	0.66	0.84	0.79
	Cho / Cr	0.68	0.71	0.71	0.80	0.83
	mI / Cr	0.26	0.49	0.11	0.33	0.56
	Glx / Cr	0.86	0.72	-0.66	0.05	0.79
L. Superior Temporal WM	NAA	0.42	0.84	0.80	0.65	0.45
	Cr	0.42	0.73	0.75	0.64	0.29
	Cho	0.18	0.84	0.84	0.71	0.13
	mI	0.44	0.61	0.61	0.47	0.57
	Glx	-0.07	0.01	0.80	1.00	NaN
	NAA / Cr	0.49	0.75	0.64	0.69	0.33
	Cho / Cr	0.28	-0.04	0.23	0.44	-0.05
	mI / Cr	0.52	0.78	0.52	0.62	0.47
	Glx / Cr	-0.48	0.17	0.96	1.00	NaN
L. Supra-Marginal WM	NAA	0.67	0.97	0.97	0.94	0.93
	Cr	0.40	0.92	0.88	0.90	0.92
	Cho	0.57	0.74	0.69	0.70	0.62
	mI	0.51	0.82	0.87	0.74	0.87
	Glx	NaN	-1.00	1.00	-0.03	-0.81
	NAA / Cr	0.57	0.87	0.84	0.86	0.88
	Cho / Cr	0.27	0.56	0.45	0.62	0.58
	mI / Cr	0.63	0.84	0.91	0.68	0.88
	Glx / Cr	NaN	-1.00	1.00	-0.35	-0.45
L. Thalamus	NAA	0.64	0.98	0.92	0.89	0.63
	Cr	0.66	0.91	0.85	0.66	0.38
	Cho	0.67	0.82	0.59	0.74	0.53
	mI	0.00	0.92	0.85	0.87	0.68
	Glx	-0.55	0.82	-0.12	-0.55	-0.10
	NAA / Cr	0.48	0.91	0.89	0.72	0.76
	Cho / Cr	0.51	0.66	0.72	0.55	0.48
	mI / Cr	0.10	0.88	0.81	0.81	0.65
	Glx / Cr	0.98	0.64	-0.43	-0.63	-0.42

		MINT 50x50x18	SLIM 50x50x12	SLIM 40x40x12	SLIM 20x20x12	SLIM 16x16x12
R. Superior Frontal GM	NAA	0.77	0.91	0.87	0.86	0.49
	Cr	0.84	0.78	0.79	0.79	-0.04
	Cho	0.54	0.91	0.91	0.84	0.57
	mI	0.60	0.66	0.66	0.28	-0.22
	Glx	0.31	0.23	-0.15	-0.21	-0.04
	NAA / Cr	0.66	0.57	0.65	0.65	-0.08
	Cho / Cr	-0.01	0.69	0.76	0.60	0.81
	mI / Cr	0.50	0.50	0.51	0.08	-0.24
	Glx / Cr	0.38	0.10	-0.23	-0.15	-0.06
R. Superior Parietal GM	NAA	0.49	0.81	0.84	0.65	0.39
	Cr	0.60	0.92	0.94	0.85	0.82
	Cho	0.54	0.72	0.83	0.55	0.51
	mI	0.41	0.76	0.75	0.47	0.02
	Glx	0.39	-0.04	0.32	-0.50	-0.39
	NAA / Cr	0.40	0.75	0.80	0.67	0.72
	Cho / Cr	0.35	0.33	0.35	0.20	0.01
	mI / Cr	0.31	0.73	0.63	0.37	-0.08
	Glx / Cr	-0.17	0.04	0.10	-0.48	-0.49
R. Superior Temporal GM	NAA	0.71	0.89	0.94	0.84	0.87
	Cr	0.68	0.89	0.91	0.85	0.84
	Cho	0.48	0.28	0.35	0.36	0.54
	mI	0.34	0.28	0.26	0.37	0.49
	Glx	0.33	0.78	0.77	0.17	0.80
	NAA / Cr	0.41	0.71	0.74	0.81	0.71
	Cho / Cr	0.44	0.23	0.34	0.32	0.38
	mI / Cr	0.02	0.33	0.34	0.12	0.29
	Glx / Cr	0.45	0.81	0.78	0.31	0.83
R. Supra-Marginal GM	NAA	0.46	0.95	0.95	0.89	0.89
	Cr	0.56	0.80	0.83	0.78	0.78
	Cho	0.54	0.85	0.88	0.88	0.77
	mI	0.63	0.80	0.77	0.72	0.57
	Glx	0.91	-0.12	-0.32	0.23	0.25
	NAA / Cr	0.25	0.64	0.70	0.71	0.71
	Cho / Cr	0.16	0.40	0.60	0.80	0.65
	mI / Cr	0.54	0.59	0.61	0.65	0.53
	Glx / Cr	0.93	-0.14	-0.33	0.30	0.33
R. Striatum	NAA	0.61	0.95	0.90	0.98	0.61
	Cr	0.64	0.95	0.94	0.98	0.41
	Cho	0.59	0.89	0.82	0.88	0.84
	mI	0.16	0.65	0.83	0.38	-0.02
	Glx	-0.30	0.48	0.40	0.00	-0.31
	NAA / Cr	0.24	0.76	0.39	0.85	0.33
	Cho / Cr	0.53	0.56	0.34	0.72	0.67
	mI / Cr	0.10	0.60	0.73	0.51	0.60
	Glx / Cr	-0.28	0.51	0.37	-0.08	-0.50

		MINT 50x50x18	SLIM 50x50x12	SLIM 40x40x12	SLIM 20x20x12	SLIM 16x16x12
R. Superior Frontal WM	NAA	0.88	0.95	0.94	0.87	0.74
	Cr	0.74	0.92	0.89	0.79	0.69
	Cho	0.83	0.95	0.95	0.85	0.76
	mI	0.76	0.85	0.78	0.67	0.52
	Glx	0.73	0.65	0.47	1.00	-1.00
	NAA / Cr	0.48	0.84	0.90	0.70	0.71
	Cho / Cr	0.33	0.79	0.79	0.51	0.55
	mI / Cr	0.38	0.85	0.77	0.53	0.54
	Glx / Cr	0.59	0.59	0.30	1.00	-1.00
R. Superior Parietal WM	NAA	0.54	0.98	0.96	0.87	0.88
	Cr	0.75	0.89	0.93	0.87	0.89
	Cho	0.53	0.93	0.91	0.67	0.67
	mI	0.76	0.76	0.81	0.76	0.44
	Glx	0.28	-0.62	-0.28	-0.68	-0.42
	NAA / Cr	0.30	0.70	0.72	0.66	0.69
	Cho / Cr	-0.01	0.59	0.66	0.31	0.20
	mI / Cr	0.46	0.81	0.84	0.74	0.47
	Glx / Cr	0.48	-0.69	-0.19	-0.57	-0.39
R. Superior Temporal WM	NAA	0.73	0.87	0.90	0.76	0.77
	Cr	0.80	0.84	0.85	0.36	0.67
	Cho	0.42	0.49	0.42	-0.04	0.15
	mI	0.66	0.33	0.38	0.44	0.32
	Glx	0.04	0.34	0.11	0.94	0.36
	NAA / Cr	0.67	0.53	0.65	0.35	0.25
	Cho / Cr	0.37	0.44	0.25	0.34	-0.11
	mI / Cr	0.50	0.14	0.13	0.39	0.06
	Glx / Cr	0.63	0.39	0.07	0.48	0.51
R. Supra-Marginal WM	NAA	0.77	0.96	0.97	0.97	0.96
	Cr	0.83	0.88	0.89	0.84	0.86
	Cho	0.75	0.92	0.91	0.85	0.79
	mI	0.71	0.66	0.76	0.74	0.76
	Glx	1.00	-0.97	-0.22	-0.10	1.00
	NAA / Cr	0.63	0.80	0.83	0.64	0.80
	Cho / Cr	0.38	0.79	0.75	0.42	0.63
	mI / Cr	0.62	0.63	0.79	0.65	0.72
	Glx / Cr	1.00	-0.97	-0.19	-0.08	1.00
R. Thalamus	NAA	0.30	0.83	0.88	0.89	0.84
	Cr	0.23	0.65	0.73	0.70	0.51
	Cho	0.44	0.82	0.85	0.91	0.63
	mI	0.25	0.57	0.59	0.86	0.66
	Glx	NaN	1.00	1.00	1.00	NaN
	NAA / Cr	0.46	0.86	0.86	0.78	0.65
	Cho / Cr	-0.22	0.90	0.84	0.85	0.55
	mI / Cr	0.34	0.58	0.59	0.72	0.35
	Glx / Cr	NaN	1.00	1.00	1.00	NaN

Table 13: Percentage of non-zero data obtained after processing in LCModel and passing post-filtration parameters

% data obtained by compartment							
L. Central GM	85%	R. Central GM	85%	L. Central WM	85%	R. Central WM	85%
L. Cerebellum GM	96%	R. Cerebellum GM	90%	L. Cerebellum WM	86%	R. Cerebellum WM	90%
L. Cingulate GM	89%	R. Cingulate GM	89%	L. Cingulate WM	85%	R. Cingulate WM	88%
L. Fusiform GM	89%	R. Fusiform GM	89%	L. Fusiform WM	78%	R. Fusiform WM	79%
L. Inferior Parietal GM	88%	R. Inferior Parietal GM	79%	L. Inferior Parietal WM	81%	R. Inferior Parietal WM	85%
L. Inferior Temporal GM	90%	R. Inferior Temporal GM	77%	L. Inferior Temporal WM	86%	R. Inferior Temporal WM	91%
L. Insula GM	85%	R. Insula GM	86%	L. Insula WM	84%	R. Insula WM	86%
L. Lateral Occipital GM	87%	R. Lateral Occipital GM	73%	L. Lateral Occipital WM	80%	R. Lateral Occipital WM	87%
L. Lingual GM	86%	R. Lingual GM	88%	L. Lingual WM	82%	R. Lingual WM	81%
L. Orbito-Frontal GM	80%	R. Orbito-Frontal GM	71%	L. Orbito-Frontal WM	86%	R. Orbito-Frontal WM	86%
L. Pars GM	80%	R. Pars GM	82%	L. Pars WM	81%	R. Pars WM	83%
L. Post-Central GM	84%	R. Post-Central GM	78%	L. Post-Central WM	85%	R. Post-Central WM	86%
L. Pre-Cuneus GM	89%	R. Pre-Cuneus GM	85%	L. Pre-Cuneus WM	80%	R. Pre-Cuneus WM	82%
L. Rostral Middle Frontal GM	84%	R. Rostral Middle Frontal GM	81%	L. Rostral Middle Frontal WM	83%	R. Rostral Middle Frontal WM	82%
L. Superior Frontal GM	79%	R. Superior Frontal GM	82%	L. Superior Frontal WM	89%	R. Superior Frontal WM	86%
L. Superior Parietal GM	76%	R. Superior Parietal GM	73%	L. Superior Parietal WM	87%	R. Superior Parietal WM	86%
L. Superior Temporal GM	83%	R. Superior Temporal GM	85%	L. Superior Temporal WM	81%	R. Superior Temporal WM	85%
L. Supra-Marginal GM	88%	R. Supra-Marginal GM	91%	L. Supra-Marginal WM	82%	R. Supra-Marginal WM	84%
L. Striatum	90%	R. Striatum	89%	L. Thalamus	84%	R. Thalamus	81%
Brain Stem	83%	Ventral Diencephalon	73%	Ventricles	85%	All	84%
% data obtained by metabolite							
NAA	95%	NAA / Cr	95%	Cho	95%	Cho / Cr	95%
mI	94%	mI / Cr	94%	Glx	46%	Glx / Cr	45%
Cr	95%						
% data obtained by localization type							
SLIM 16x16x12	79%	SLIM 20x20x12	82%	SLIM 40x40x12	85%	SLIM 50x50x12	85%
MINT 50x50x18	86%	ROIS 50x50x18	88%				
% data obtained by subject							
Subject 008	88%	Subject 009	82%	Subject 010	85%	Subject 012	84%
Subject 013	77%	Subject 014	88%	Subject 015	82%	Subject 016	85%
Subject 017	80%	Subject 018	87%	Subject 019	85%	Subject 020	78%
Subject 021	86%	Subject 022	89%	Subject 023	86%	Subject 024	85%
Subject 025	86%	Subject 026	85%	Subject 027	85%	Subject 028	78%